R009-01
B 会場 ：9/26　AM1 （9:00-10:30）
9:00〜9:15

#村上　豪[1)],Benkhoff　Johannes[2)]
([1)]ISAS/JAXA,[(2)]ESA

Mercury's dynamic magnetosphere: updates from the BepiColombo cruise observations

#Go Murakami[1)],Johannes Benkhoff[2)]
([1)]Institute of Space and Astronautical Science, Japan Aerospace Exploration Agency,[(2)]ESA

Mercury is the innermost planet in the Solar System and has a unique space environment. Mercury possesses a weak global magnetic field and is subject to the intense solar wind due to its proximity to the Sun (0.31-0.47 AU). In such conditions, Mercury formed a small but highly dynamic magnetosphere. Because of its small size and its proximity to the Sun, Mercury was unable to retain the bulk of its atmosphere and ionosphere. These conditions make Mercury's space environment unique and an excellent science target for comparative study with Earth. The first Mercury orbiter, MESSENGER (MErcury Surface, Space ENvironment, GEochemistry, and Ranging), explored this innermost region of the Solar System during 2011 – 2015 and provided a number of new findings. For example, Mercury's magnetosphere is much more dynamic than had been predicted. Magnetic field measurements indicated Dungey cycles on Mercury with a period of a few minutes. MESSENGER detected many energetic electron events with periodicities of a few minutes and electron precipitations at the nightside. These outstanding discoveries still remain as open issues due to some limitations of instruments onboard MESSENGER and its extended elliptical orbit with apherm in southern hemisphere. The ESA-JAXA joint mission BepiColombo is now on the track to Mercury. After the successful launch of the two spacecraft for BepiColombo, Mio (Mercury Magnetospheric Orbiter: MMO) and Mercury Planetary Orbiter (MPO), commissioning operations of the spacecraft and their science payloads were completed. BepiColombo will arrive at Mercury in the end of 2025, and it has 7-years cruise with the heliocentric distance range of 0.3-1.2 AU. Even before arrival, we already obtained fruitful science data from Mercury during three Mercury flybys completed on 1 October 2021, 23 June 2022, and 19 June 2023. We performed science observations with almost all the instruments onboard Mio and successfully obtained comprehensive data of Mercury's magnetosphere such as magnetic fields, plasma particles, and waves. Here we present the updated status of BepiColombo mission, initial results of the science observations during the Mercury flybys, and the upcoming observation plans.

R009-02
B 会場 ：9/26　AM1 （9:00-10:30）
9:15〜9:30

#原田　裕己 [1)], 齋藤　義文 [2)], 相澤　紗絵 [3)],Andre　Nicolas[4)],Hadid　Lina[5)],Delcourt　Dominique[5)], パーショ
ン　ムーア [6)],Fraenz　Markus[7)], 横田　勝一郎 [8)],Fedorov　Andrei[4)], 三宅　亙 [9)],Penou　Emmanuel[4)],Barthe
Alain[4)],Sauvaud　Jean-Andre[4)],Katra　Bruno[5)], 松田　昇也 [10)], 村上　豪 [11)]
[(1] 京大・理,[(2] 宇宙研,[(3] 宇宙研／ピサ大学,[(4]IRAP, CNRS-UPS-CNES,[(5]LPP-CNRS-Sorbonne Université-Ecole
Polytechnique,[(6] 東大,[(7]Max-Planck-Institute for Solar System Research,[(8] 大阪大,[(9] 東海大・工,[(10] 金沢大学,[(11]ISAS/JAXA

Low-Energy Ions and Electrons in Mercury's Magnetosphere: Initial Reports of Mio's Third Flyby

#Yuki Harada[1)],Yoshifumi Saito[2)],Sae Aizawa[3)],Nicolas Andre[4)],Lina Hadid[5)],Dominique Delcourt[5)],Moa Persson[6)],Markus
Fraenz[7)],Shoichiro Yokota[8)],Andrei Fedorov[4)],Wataru Miyake[9)],Emmanuel Penou[4)],Alain Barthe[4)],Jean-Andre Sauvaud[4)],Bruno
Katra[5)],Shoya Matsuda[10)],Go Murakami[11)]
[(1]Graduate School of Science, Kyoto University,[(2]Institute of Space and Astronautical Science, Japan Aerospace Exploration Agency,[(3]ISAS/JAXA, University of Pisa,[(4]IRAP, CNRS-UPS-CNES,[(5]LPP-CNRS-Sorbonne Universite-Ecole Polytechnique,[(6]The University of Tokyo,[(7]Max-Planck-Institute for Solar System Research,[(8]Osaka University,[(9]Tokai University,[(10]Kanazawa University,[(11]Institute of Space and Astronautical Science, Japan Aerospace Exploration Agency

We report on the initial analyses of low-energy ion and electron data obtained during Mio's third Mercury flyby. The first and second flybys demonstrated the highly variable nature of Mercury's magnetosphere in response to varying upstream solar wind conditions. Specifically, magnetospheric ions measured during the second flyby are characterized by a factor of $>$10 higher energies near the closest approach than those of the first flyby, and cold dense ions detected around midnight during the first flyby were completely absent during the second flyby. Dynamic electron signatures were observed during both flybys and characteristic "inverted-V" electrons were identified in the second flyby data. We will discuss the latest third flyby results in comparison to the past two flybys with a particular focus on low-energy ion and electron signatures in Mercury's magnetosphere.

R009-03
B 会場 ：9/26　AM1 （9:00-10:30）
9:30〜9:45

無水鉱物への水素イオン照射実験による水星表層における太陽風起源 H2O 生成過程の解明

#北野　智大 [1)], 木村　智樹 [1)], 大槻　美沙子 [1)], 星野　亮 [1)], 仲内　悠祐 [2)]
([1] 東京理科大,([2] 立命館大

Water molecule creation by the solar wind on Mercury's surface modeled by the hydrogen irradiation to the anhydrous mineral

#Tomohiro Kitano[1)],Tomoki Kimura[1)],Misako Otsuki[1)],Ryo Hoshino[1)],Yusuke Nakauchi[2)]
([1]Tokyo University of Science,([2]Ritsumeikan Univ.

At Mercury and Moon, water molecules are created from surface minerals through the thermal and non-thermal chemical processes driven by the solar photon and solar wind irradiations. Recent studies suggested that there is water ice in the polar permanent shadowed regions of Mercury based on the neutron spectroscopies onboard the MESSENGER spacecraft (Lawrence et al., 2013) and of Moon based on the near-infrared spectrometer onboard the Chandrayaan-1 spacecraft (Li et al., 2018). Although the source of polar ice is still unknown, the recent numerical simulations of water transport on Mercury (Jones et al., 2020) suggested the water creation process by the solar wind hydrogen irradiation to the surface material as a potential source of polar ice. However, the water creation on Mercury's surface with the real solar wind condition has not yet been directly confirmed by either the observations or experiment. This study demonstrates the water creation on Mercury's surface by the solar wind based on the hydrogen ion and electron irradiation experiments to an anhydrous silicate mineral, Enstatite, which is a candidate for Mercury's surface material. The hydrogen ion and electron were irradiated with a flux of 1e+14-1e+15$cm^{-2}s^{-1}$ and fluence of 1e+18-1e+19cm^{-2}. Temporally stable water vapor release was confirmed for a long time (approximately 1e+4s) only during the hydrogen ion irradiation. The yield of water molecules by the hydrogen ion irradiation was estimated after removing the adhering water from the sample surface to be 0.37-0.38/incident ion. For the electron irradiation after the hydrogen irradiation, it was found that the electron irradiation enhance degassing of the water vapor, which was created by the hydrogen irradiation. If we assume that the water molecules are released from Mercury's cusp region, the experimentally estimated yield corresponds to a water creation rate of 2.6-2.8e+6kg/year. With the rate of ice accumulation on the surface to the water creation from the surface estimated by the water transfer simulation by Jones et al.(2020), the total amount of ice accumulated on Mercury's surface through 3 billion years was estimated to be 7.8-8.3e+13kg from our experiment. This is a significant amount compared to the total ice estimation of 1e+14-1e+15kg by the previous radar observations (Eke et al., 2017; Deutsch et al., 2018; Susorney et al., 2019). This result suggests that the water created by solar wind irradiation is a possibly essential source of the polar ice on Mercury. We are going to conduct the deuterium irradiation experiment to demonstrate the water creation and removing effects of the water adhering to the sample surface.

水星や月において、表層の鉱物は太陽光や太陽風の照射による熱的、非熱的な化学過程を経て、水分子を生成する。MESSENGER 探査機搭載の中性子分光計や Chandrayaan-1 探査機搭載の赤外分光器の観測に基づいた近年の研究によって、水星や月の極域の永久影での水氷の存在が示唆されている (Lawrence et al., 2013; Li et al., 2018)。その起源は未解明であるが、水星表面では太陽風水素イオン照射による表層鉱物における水生成が有力な候補の１つであることが、近年の水輸送の数値シミュレーションから示唆された (Jones et al.,2020)。しかし、実際の太陽風プラズマの組成 (電子、陽子) やエネルギー (keV 帯) の条件を満たしたプラズマ照射による、水星表層鉱物の水生成は観測的・実験的には未実証である。本研究は水星表層組成に類似した無水ケイ酸塩鉱物である Enstatite 試料への水素イオン、電子照射実験に基づき、太陽風による水星表層の水生成の実証を試みた。水素イオンや電子を、1e+14-1e+15$cm^{-2}s^{-1}$ の flux、1e+18-1e+19cm^{-2} の fluence で照射した。水素照射時のみ長時間 (約 1e+4s) 安定してサンプルからの水分子の放出が確認された。サンプルに元々付着していた水の影響が無いと思われる時間帯において、水素イオン照射に対する水分子の yield を見積もった結果、0.37-0.38/incident ion と推定された。水素イオンを照射した後に、電子を照射した場合、水素照射で生成された鉱物中の水分子の放出を促進する傾向がみられた。水素照射で推定した yield を用いて、水星のカスプ領域から水分子が放出されると仮定すると、2.6-2.8e+6kg/year の水生成率に相当する。Jones et al. (2020) の水輸送シミュレーションにおける水の生成に対する氷の堆積効率と、本実験で得られた水生成率に基づき、水星表層に堆積する氷の総量を見積もると、30 億年で 7.8-8.3e+13kg になることが示唆された。これは先行研究のレーダー観測に基づく推定総量 1e+14-1e+15kg(Eke et al., 2017; Deutsch et al., 2018; Susorney et al., 2019) と比較して、有意な量である。この結果から、太陽風照射による水生成が極域氷の供給過程として有力であることが示唆される。今後はサンプルの付着水の影響を除去した水生成の再現を狙い、重水素照射実験等の検証実験を行う予定である。

R009-04
B 会場 ：9/26　AM1 （9:00-10:30）
9:45〜10:00

BepiColombo/PHEBUS による第 2, 3 回水星スイングバイ時の Mg 大気分布の観測結果の比較

#鈴木　雄大 [1)],Quémerais　Eric[2)],Robidel　Rozenn[2)],Chaufray　Jean-Yves[2)], 村上　豪 [1)], 吉岡　和夫 [3)],Yoshikawa Ichiro[3)]
(1 宇宙科学研究所,(2LATMOS-OVSQ,(3 東京大学

Comparison of exospheric Mg distributions observed by BepiColombo/PHEBUS during the 2nd and 3rd Mercury swing-bys

#Yudai Suzuki[1)],Eric Quemerais[2)],Rozenn Robidel[2)],Jean-Yves Chaufray[2)],Go Murakami[1)],Kazuo Yoshioka[3)],Ichiro Yoshikawa[3)]
(1JAXA/ISAS,(2LATMOS-OVSQ,(3University of Tokyo

Mercury's exospheric atoms are mainly ejected from the surface through several processes such as thermal input, UV irradiation, solar wind particle sputtering, and micro-meteoroid impact. Observations by the MESSENGER spacecraft have shown that Mercury magnesium (Mg) exosphere is related to its surface abundance. Additionally, Mg is an interesting species as its surface abundance reflects the non-uniformity of magma compositions. However, spatial distribution (especially in the latitude direction) and seasonal variability of Mg exosphere is not well understood due to its dark brightness and the geometry of MESSENGER.

BepiColombo, the Mercury orbiting mission led by ESA and JAXA, is on its way to the planet. The 2nd and 3rd Mercury swing-bys were conducted on 22/06/2022 and 19/06/2023 (UTC), respectively, and many instruments observed the Mercury environments then. In this study, we analyzed Mg exosphere data from PHEBUS, the UV spectrometer onboard BepiColombo, to deduce temperature and production rate of Mg exosphere during each swing-by.

As a result, similar signals were obtained through both swing-bys. Season, local time, and longitude of Mercury during both observations were similar, but boresights of PHEBUS were different (2nd: northward, 3rd: southward). These results show that Mg production rates have little year-to-year variability, which is consistent with the fact that Mg is mainly ejected by micro-meteoroid impact. Besides, these results mean that dust impact flux has little north-south asymmetry.

In this talk, we introduce the results obtained by observations of the spectrometer onboard BepiColombo, PHEBUS, during the 2nd and 3rd swing-bys.

水星大気中の原子は、主に熱入力、紫外線照射、太陽風粒子の衝突、ダストの衝突等の宇宙空間環境の影響による表層からの原子の脱離によって供給される。MESSENGER 探査機の観測結果から、特に Mg 大気の分布は表層の Mg 分布と強く結びついていることが明らかになった。加えて、表層の Mg 分布はマグマ組成の不均一性を反映している可能性が高く、地質学の観点からも興味深い原子種である。しかし、その発光強度の小ささや MESSENGER の軌道の問題から、Mg 大気の空間分布 (特に緯度依存性) および放出機構の季節変動性の詳細は明らかになっていない。

現在、日欧共同水星探査計画 BepiColombo が進行中である。2022 年 6 月 22 日には 2 回目の、2023 年 6 月 20 日には 3 回目の水星スイングバイが行われ、様々な観測装置によって水星の観測が行われた。本研究では、BepiColombo 搭載分光器 PHEBUS による中性 Mg 大気の観測データを解析し、各スイングバイ時の大気の温度および放出量を算出した。

結果、2 回のスイングバイで類似した値が得られた。両観測時の水星の季節・地方時・経度は類似しているが、PHEBUS の視線方向が異なる (第 2 回は北向き、第 3 回は南向き)。これらの観測結果から Mg 大気放出量に年々変動性が無いと考えられ、Mg が主にダスト衝突によって放出されると考えられていることと整合的である。また、今回の結果はダストの衝突フラックスに南北非対称性が無いことを意味している。

本発表では、BepiColombo 搭載分光器 PHEBUS による第 2, 3 回水星スイングバイ時の Mg 大気分布の観測結果について紹介する。

R009-05
B 会場 ：9/26　AM1 （9:00-10:30）
10:00〜10:15

磁気圏ローブにおける昼側月面電位のマッピングに向けたかぐやと ARTEMIS 観測を用いた初期解析

#加藤　正久 [1)], 原田　裕己 [1)], 西野　真木 [2)], 齋藤　義文 [2)], 横田　勝一郎 [3)], 高橋　太 [4)], 清水　久芳 [5)],Shaosui Xu[6)],Andrew R　Poppe[6)],Jasper S　Halekas[7)]
[(1] 京大・理,[(2] 宇宙研,[(3] 大阪大,[(4] 九大・理・地惑,[(5] 東大・地震研,[(6] カリフォルニア大学バークレー校,[(7] アイオワ大学

Mapping the dayside lunar surface potential in the magnetotail lobes: A preliminary analysis of Kaguya and ARTEMIS observations

#Masahisa Kato[1)],Yuki Harada[1)],Masaki N Nishino[2)],Yoshifumi Saito[2)],Shoichiro Yokota[3)],Futoshi Takahashi[4)],Hisayoshi Shimizu[5)],Shaosui Xu[6)],Andrew R Poppe[6)],Jasper S Halekas[7)]
[(1]Department of Geophysics, Graduate School of Science, Kyoto University,[(2]Institute of Space and Astronautical Science, Japan Aerospace Exploration Agency,[(3]Osaka University,[(4]Department of Earth and Planetary Sciences, Faculty of Sciences, Kyushu University,[(5]Earthquake Research Institute, University of Tokyo,[(6]Space Sciences Laboratory, University of California, Berkeley, US,[(7]Department of Physics and Astronomy, University of Iowa, US

Since the Moon does not have a dense atmosphere, the lunar surface is exposed to the ambient plasma and interacts with the charged particles directly. Surface charging is one of the phenomena caused by the interaction. Although the study of lunar surface charging has been conducted for a long time, the global spatial distribution of the lunar surface potential has not been fully characterized. In this study, we compare the energy spectra model of photoelectrons from the lunar surface that we developed recently with observations obtained in the terrestrial magnetotail lobes by Acceleration, Reconnection, Turbulence and Electrodynamics of the Moon's Interaction with the Sun (ARTEMIS) and Kaguya. We aim to map the dayside lunar surface potential by analyzing the electrostatic acceleration and deceleration of lunar photoelectrons between the spacecraft and the lunar surface. We report the preliminary results of the analysis.

月は濃密な大気を持たないため、月面は周辺のプラズマにさらされており荷電粒子との直接的な相互作用が発生している。月面帯電はこの相互作用の結果生じる現象の一つである。月面帯電についての研究はこれまで長い間にわたり行われてきたが、月面電位の全球的な分布については詳細な描像が得られているわけではない。本研究では、我々が開発した数値モデルで計算した月面から放出された光電子のエネルギースペクトルと、地球磁気圏ローブでの ARTEMIS とかぐやにより観測されたエネルギースペクトルを比較する。月面と探査機の間の光電子の静電的な加減速を解析することで、月面昼側電位のマッピングを行うことを目指す。今回は、解析の初期的な結果を報告する。

R009-06
B 会場 ：9/26　AM1 （9:00-10:30）
10:15〜10:30

太陽風プラズマ駆動の月微小空洞の局所的な表面帯電による静電的イオン散乱

#中園　仁 [1)], 三宅　洋平 [2)]
([1] 神戸大学大学院システム情報学研究科,[2] 神戸大学大学院システム情報学研究科

Ion scattering by localized surface charging of solar wind plasma-driven lunar microcavities

#JIn Nakazono[1)],Yohei Miyake[2)]
([1]Graduate School of System Informatics, Kobe University,[2]Graduate School of System Informatics, Kobe University

Space plasma such as solar wind plasma and sunlight directly fall on the surface of solid celestial bodies such as the Moon, which have a thin atmosphere and no intrinsic magnetic field, creating an electrostatic environment near the surface with the accumulation of electric charge on the celestial body surface due to colliding plasma and photoelectron generation by the photoelectric effect. Orbital observations by lunar explorers have suggested that the lunar dayside surface is positively charged. In general, space plasma has the ability to negatively charge solid surfaces, and it has been believed that electron emission processes such as the photoelectric effect are essential to maintain the lunar surface at a positive floating potential. On the other hand, the lunar surface has various spatial-scale cavities ranging from topographic features such as craters, vertical holes, and boulders to rock and regolith layers. Several simulation results have shown that these cavities restrict free plasma motion in space and create a unique electrostatic environment due to the surface topography.

We have conducted simulations of a cavity with an aperture equal to or smaller than the Debye length on the lunar surface, with solar wind plasma pouring down from the sky. We found that the solar wind plasma flow forms a positive potential in a simple rectangular cavity and can positively charge the cavity up to several hundred volts, which is equivalent to the kinetic energy of solar wind ion particles, as the width-depth ratio of the cavity increases. This result suggests the formation of localized positive potentials in microcavities formed by the deposition of rocks and regolith particles on the diurnal lunar surface where solar wind plasma is blown. The KAGUYA satellite observations also suggest that some solar wind ions are reflected and scattered by the lunar surface on the diurnal side of the Moon. It has been reported that most of these scattered ions are composed of protons. We report here on the relationship between the solar wind ions reflected by the local positive potential inside the microcavity and the scattered ions observed by the satellite.

月を始めとする大気が希薄で固有磁場を持たない固体天体表面には、太陽風プラズマなどの宇宙プラズマや太陽光が直接表層に降り注ぎ、衝突プラズマによる天体表面への電荷の蓄積や光電効果による光電子の発生とともに表面近傍での静電気環境を形成する。月探査機による軌道上観測では月昼側表面は正に帯電していることが示唆されてきた。一般に宇宙プラズマは固体表面を負に帯電させる能力を持っており、月面を正の浮遊電位に保つためには光電効果などの電子放出過程が不可欠であると考えられてきた。一方、月面はクレーターや縦孔、ボルダーなどの地形から岩石・レゴリス層にいたるまで様々な空間スケールの凹凸を持つ。こうした凹凸は宇宙空間中の自由なプラズマ運動を制限し、表面形状により特有の静電気環境を作り出すことがいくつかのシミュレーション結果によって明らかにされている。

私達はこれまでに、月面上のデバイ長と同等かそれより小さい開口部を持つ空洞に対し、上空から太陽風プラズマが降り注ぐ状況を想定しシミュレーションを実施した。その結果、太陽風プラズマ流は単純な直方体空洞内に正電位を形成し、空洞の幅深さ比の増大に伴い太陽風イオン粒子の運動エネルギーと同程度の数 100V まで正に帯電させ得ることが判明した。この結果は、太陽風プラズマが吹き付けられる昼側月面の岩石やレゴリス粒子の堆積により形成される微小空洞における局所的な正電位形成を示唆している。また、かぐや衛星観測では、昼側月面において太陽風イオンの一部が月面により反射・散乱されることが示唆されている。こうした散乱イオンの殆どはプロトンで構成されていることが報告されている。今回、私達は微小空洞内部の局所的な正電位により反射される太陽風イオンと衛星観測に現れる散乱イオンの関連について報告する。

R009-07
B 会場 ：9/26　AM2 （10:45-12:30）
10:45〜11:00

彗星コマ中の D/H 観測を目的とした共鳴吸収型フィルタの開発

#山崎　朝 [1)], 鈴木　雄大 [2)], 田口　真 [3)], 桑原　正輝 [4)], 吉岡　和夫 [5)]
([1] 東大,[2]JAXA/ISAS,[3] 立教大・理・物理,[4]Rikkyo Univ.,[5] 東大・新領域

Development of Absorption Cell Filters for D/H Observations in Cometary Comae

#Ashita Yamazaki[1)],Yudai Suzuki[2)],Makoto Taguchi[3)],Masaki Kuwabara[4)],Kazuo Yoshioka[5)]
([1]University of Tokyo,[2]Institute of Space and Astronautical Science, Japan Aerospace Exploration Agency,[3]Department of Physics, College of Science, Rikkyo University,[4]Rikkyo University,[5]Graduate School of Frontier Sciences, The University of Tokyo,

The deuterium to hydrogen abundance ratio (D/H ratio) within hydrogen corona of planets and small celestial bodies is essential for understanding their formation processes and atmospheric escape processes. We conducted experiments aimed at improving the measurement accuracy and lifetime of absorption cell filters; these are developed for spectroscopic observations of hydrogen coronae from spacecrafts.

The absorption cell is a filter that absorbs the hydrogen Lyman-alpha line (H Ly-α) emitted by hydrogen atoms through resonant scattering. It is a cylindrical glass cell of which both bottom surfaces are made of MgF_2, and hydrogen gas is filled within. When tungsten filaments that are attached in the cell are tuned on, the hydrogen gas thermally dissociates into atoms, which resonantly scatter H Ly-α that enters the cell; the resonant scattering results in the absorption of H Ly-α in the line of sight. Since there is a 33 pm difference in wavelengths of H and D Ly-α, H and D cells selectively absorb these emissions respectively. This allows separate measurement of hydrogen and deuterium densities in the corona.

However, there are mainly two issues with the absorption cell: 1) absorption of H Ly-α by the D cell, and 2) instability in absorption due to filament lifetime. Regarding 1), a small contamination of H_2 gas mixing into the D cell causes apparent increase in the brightness of D Ly-α. Filament oxidation due to introduction of water and oxygen into the cell causes 2). The oxidation would also lead to an increase in filament resistance; therefore, the temperature rises, giving the need to consider its impact on the dissociation rate of hydrogen molecules.

To address these issues, we developed a system using getters and cold traps to ensure the enclosure of pure H_2 and D_2 gases within the cells. Getters were introduced to remove H_2 gas from the vacuum line before enclosing D_2 gas, as a measure against 1). Cold traps, on the other hand, were introduced to remove water and oxygen from the vacuum line, as a preventive measure against 2). Species dependence of these adsorption effects was quantitatively evaluated in an experiment using a quadrupole mass spectrometer.

The absorption cell filter will be integrated into an ultraviolet spectroscopic imaging device; this will be installed on the Comet Interceptor spacecraft to observe cometary coma of a long-period comet. Numerical evaluations were conducted to determine the conditions for ensuring the measurement accuracy of D/H observations that will be necessary for achieving mission objectives: specifically, the upper limit of the abundance ratio of H_2 gas relative to D_2 gas enclosed within the D cell. Furthermore, the filament lifetime was evaluated through an experiment by varying power supplied to the filament to ensure fulfillment of the mission purposes. Additionally, the absorptance of H Ly-α by the D cell will be measured to quantitatively discuss the achievable accuracy of D/H observations.

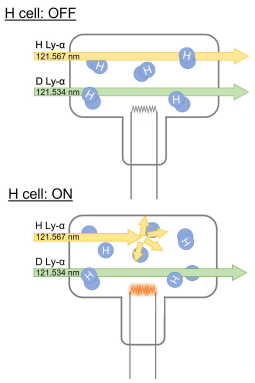

R009-08
B 会場 ：9/26　AM2 （10:45-12:30）
11:00〜11:15

塩化ナトリウムへのプラズマ照射実験と物理化学モデリングによるエウロパの希薄大気生成と表層組成の解明

#星野　亮 [1)], 木村　智樹 [1)], 大槻　美沙子 [1)], 北野　智大 [1)], 仲内　悠祐 [2)], 土屋　史紀 [3)], 木村　淳 [4)], 丹　秀也 [5)]
([1] 東京理科大,[2] 立命館大,[3] 東北大・理・惑星プラズマ大気,[4] 阪大,[5] 海洋研究開発機構

Europa's surface composition uncovered by the plasma irradiation experiment for NaCl samples

#Ryo Hoshino[1)],Tomoki Kimura[1)],Misako Otsuki[1)],Tomohiro Kitano[1)],Yusuke Nakauchi[2)],Fuminori Tsuchiya[3)],Jun Kimura[4)],Shuya Tan[5)]
([1]Tokyo University of Science,[2]Ritsumeikan University,[3]Planetary Plasma and Atmospheric Research Center, Graduate School of Science, Tohoku University,[4]Osaka University,[5]JAMSTEC

Jupiter's icy moon Europa potentially has an interior water ocean with a habitable environment for life. Elemental and molecular compositions of Europa's surface materials tell us that of the interior ocean because the materials may be exchanged between the ocean and the surface. Europa's surface materials are continuously irradiated with Jovian plasmas, UV, and micrometeorites from space. The irradiated energy drives the space weathering process. In particular, Jovian plasmas are dominant energy sources of space weathering at Europa. Europa's materials are sputtered from the surface by plasma irradiation, creating a tenuous atmosphere. The residual un-sputtered surface material may change in the elemental and molecular compositions by irradiation. However, since this process comprises complex physics and chemistries that are difficult to be theoretically estimated, it has been a big unsolved problem to quantitatively associate the tenuous atmosphere with the surface compositions accompanying the space weathering.

Here we present the laboratory experiment that irradiates a potential surface material NaCl with energetic H_2^+, O_2^+ ions, and electrons under the same condition (10 keV particle energy with a fluence of 5e+18 /cm^2) to simultaneously model Europa's surface material alteration and atmospheric sputtering. We found that the electron more efficiently sputters Europa's surface than the ions under Europa's environment. For example, the total Na production rate by the hydrogen and oxygen ion irradiations is estimated to be 1.1e+6 /cm^2/s, while that by the electron irradiation is to be 2.7e+5 /cm^2/s. We also found that the yield of Cl (8.7e-1 /incident particle) is greater than that of Na (2.8e-2 /incident particle). These results suggest that the surface NaCl is decomposed predominantly by electron irradiation and forms the resultant tenuous atmosphere, while on Europa's surface, Na is concentrated more effectively than Cl because of the small volatility of Na.

We numerically modeled the 3-dimensional structure of the Na tenuous atmosphere, subject to constraints from experimental Na yields. The total mass of the Na tenuous atmosphere is estimated to be about 700 kg, which is comparable to estimates obtained from previous ground-based telescope observations [Brown and Hill 1996]. The NaCl sample used in the irradiation experiment was found to have a concentration of 85%, consistent with telescope observations, indicating the possibility of a high concentration of NaCl on Europa's surface. This observation suggests that NaCl originating from the subsurface ocean may have been concentrated on the surface by the upwelling process from the subsurface ocean to the surface or by space weathering after the eruption.

In the future, we plan to conduct similar irradiation experiments and modeling on saltwater ice to further constrain the surface concentration and to more realistically reproduce Europa's surface environment.

木星の氷衛星であるエウロパは、内部海を持つことから生命の存在可能性が示唆されている天体の 1 つである。その内部海と表層の間では水や塩などの物質の輸送が行われている可能性があり、エウロパ表層の物質組成等の理解は内部海環境の理解につながる。エウロパでは、宇宙空間からのプラズマや紫外線などが表層物質に照射され、宇宙風化が起こる。木星氷衛星で宇宙風化の主要因とされるプラズマは表層でスパッタリングを引き起こし、それにより弾き出された粒子はエウロパの希薄大気を生成する一方、表層物質の組成は変化すると考えられる。しかし、その一連の生成過程は物理・化学的に複雑で、プラズマスパッタリングによる希薄大気生成と表層風化に伴う組成の変化について、定量的な関連付けは未だなされていない。

そこで、本研究では、エウロパ表層候補物質である NaCl に H_2^+,O_2^+, 電子を同条件 (10 keV, 5e+18 /cm^2) で照射し、初めてエウロパ環境におけるスパッタリングと表層物質の組成変化を同時に再現した。 その結果、エウロパ環境下ではイオンに比べ、電子の方が効率的に Na のスパッタリングを起こすことが明らかになった。例えば、 水素イオンと酸素イオンの照射による Na 大気の生成率の合計が 2.7e+5 /cm^2/s である一方、電子照射による生成率は 1.1e+6 /cm^2/s であった。また、塩素原子は Na 原子よりも効率的にスパッタリングされることがわかった。例えば、水素イオンと酸素イオンの照射による Na 大気の yield の合計は 2.8e-2 /incident particle であり、同照射による Cl 大気の生成率は 8.7e-1 /incident particle であった。上記より、エウロパ環境下では、NaCl 中の Na は主に電子照射により乖離し希薄大気を生成する一方、Na よりも Cl が効率よく揮発することで Na が表層に濃縮されることが示唆された。

実験で得た Na の yield を制約条件とした 3 次元希薄大気モデリング [Leblanc et al., 2002] を行い、エウロパ周囲の Na 希薄大気の総量を計算した。その結果、地上望遠鏡観測による大気総量の見積もり [Brown and Hill 1996] と同程度の

約 700 kg となった。照射実験に用いたサンプルの NaCl 濃度は 85 %であり、このサンプルから得られた yield による希薄大気生成が、観測と整合していることから、表層の NaCl は高濃度で存在している可能性がある。これは内部海中に溶解している NaCl が内部海から表層に湧昇する過程、もしくは表層へ噴出した後の宇宙風化により濃縮されていることを示唆している。

今後は、食塩水の氷に対して同様の照射実験とモデリングを行い、よりエウロパ環境に近い条件での表層濃度の制約を行う。

R009-09
B 会場 ：9/26　AM2 （10:45-12:30）
11:15〜11:30

30.4 nm における SiC/Mo/Si 多層膜反射鏡の反射率とその耐熱性について

#寺本　駿一郎 [2)], 井上　和輝 [1)], 吉岡　和夫 [1,2)], 吉川　一朗 [1,2)]
[(1] 東京大学,[(2] 東大・新領域

The reflectance and heat resistance of SiC/Mo/Si multilayer mirrors at 30.4 nm

#Shunichiro Teramoto[2)],Kazuki Inoue[1)],Kazuo Yoshioka[1,2)],Ichiro Yoshikawa[1,2)]
[(1]The University of Tokyo,[(2]Graduate School of Frontier Sciences, The University of Tokyo

In planetary science missions such as Nozomi [1], Kaguya, and EQQULEUS [2], a technology using periodic multilayers in the EUV wavelength range for normal incidence optics developed. Grazing incidence optics can't have a large numerical aperture and have significant limitations in resolution due to diffraction. Therefore, normal incidence optics are necessary to understand the distribution of plasma. However, the problem is that normal incidence optics has low reflectance. We can solve this problem by using multilayer mirrors.

Multilayer mirrors can dramatically improve reflectance due to the interference of reflected light at each interface. In particular, the development of high-reflectance multilayer mirrors for He II radiation at 30.4 nm is progressing. A Mo/Si mirror is widely used due to its high stability. However, the low reflectivity of around 15-20% is a challenge.

Previously, we demonstrated the performance of a new multilayer mirror consisting of 40 pairs of Mg and SiC, achieving a maximum reflectivity of over 30%. However, it was found that the Mg/SiC mirror had a critical flaw. The reflectivity decreases in high-temperature and high-humidity environments. In actual observations, multilayer mirrors are exposed to high-temperature and humid environments before launch and extremely cold environments in space. Therefore, it is necessary to develop observation equipment that is resistant to such environmental changes.

Since a combination of Mo/Si is stable [L.Yunpeng et al., 2014], we designed a new multilayer mirror (SiC/Mo/Si). The new mirror is manufactured by depositing the three different materials periodically. To evaluate its resistance to high-temperature environments, we conducted a heat environment test in a constant-temperature oven (50 degrees Celsius for 24 hours) and compared the reflectances of the mirrors before and after heating. We irradiated EUV light onto multilayer mirrors and evaluated its wavelength dependence.

In this presentation, we discuss the reflectivity and thermal stability of SiC/Mo/Si mirrors. Additionally, we will also share the measurement results of reflectances for other new multilayer mirrors, B4C/Mg2Si and SiC/Mg2Si mirrors. We will discuss the requirements for the mirrors that should be integrated into the next-generation artificial satellite.

[1] I. Yoshikawa, et al., Telescope of extreme ultraviolet (TEX) onboard SELENE, Earth Planets Space, 60, 2008, 407 – 416.
[2] M. Kuwabara, et al., JAXA Research and Development Report, 2019.

のぞみ衛星 [1]、EQQULEUS [2] などの探査ミッションでは、EUV 波長域の直入射光学系に多層膜を用いる技術が採用された。斜入射光学系は開口面積を大きくできず、回折による解像力の制限が大きい。よって、プラズマの分布を把握するためには、直入射光学系が必要であるが、低反射率が問題となる。この問題を解決するために、多層膜反射鏡を用いる。多層膜鏡は、各界面で反射する光が干渉することにより、反射率を向上することができる。特に、30.4 nm の He II の輝線に対応した高い反射率を持つ多層膜反射鏡の開発が進んでいる。主に現在使われている Mo/Si 反射鏡は安定性が高いが、反射率は 15〜20% 程度と低いことが課題である。

従来、われわれのチームは 40 組の Mg と SiC からなる新しい多層膜反射鏡の性能を評価し、最大反射率 30% 以上を達成したが、この Mg/SiC 反射鏡には致命的な欠陥があることが判明した。高温・高湿の環境下では反射率が低下するという問題である。多層膜反射鏡は打ち上げ前の高温多湿環境や宇宙での極寒環境にさらされる。そのため、こうした環境変化に強い観測装置を開発する必要がある。

以上の問題点から新しい多層膜反射鏡（SiC/Mo/Si）を開発した。この新しい鏡は、3 つの異なる材料を周期的な蒸着により製造されている。高温環境に対する耐性を評価するため、恒温槽（50 ℃、24 時間）で熱環境試験を行い、加熱前後の鏡の反射率を比較した。EUV 光を多層膜反射鏡に照射し、波長依存性を評価した。

本発表では、SiC/Mo/Si 鏡の反射率と耐熱性について議論する。また、ほかの新しい多層膜反射鏡である B4C/Mg2Si、SiC/Mg2Si に関する反射率の測定結果にもふれ、次期人工衛星に搭載するべき鏡の条件について議論する。

[1] I. Yoshikawa, et al., Telescope of extreme ultraviolet (TEX) onboard SELENE, Earth Planets Space, 60, 2008, 407 – 416.
[2] M. Kuwabara, et al., JAXA Research and Development Report, 2019.

R009-10
B 会場 ：9/26　AM2 （10:45-12:30）
11:30〜11:45

#安田　陸人 [1)], 木村　智樹 [2)], 三澤　浩昭 [1)], 土屋　史紀 [1)], 佐藤　晋之祐 [1)], 笠羽　康正 [1)], 堺　正太朗 [1)], 熊本　篤志 [3)]
([1] 東北大・理・惑星プラズマ大気研究センター,([2]Tokyo University of Science,([3] 東北大・理・地球物理,([4] 東北大・理・惑星プラズマ大気,([5] 東北大学 惑星プラズマ・大気研究センター,([6] 東北大・理,([7] 東北大・理・地球物理,([8] 東北大・理・地球物理

Feasibility study of ionospheric explorations at Jupiter's icy moons using Faraday rotation effect

#Rikuto Yasuda[1)],Tomoki Kimura[2)],Hiroaki Misawa[1)],Fuminori Tsuchiya[1)],Shinnosuke Satoh[1)],Yasumasa Kasaba[1)],Shotaro Sakai[1)],Atsushi Kumamoto[3)]
([1]Planetary Plasma and Atmospheric Research Center, Graduate School of Science, Tohoku Univeristy,([2]Tokyo University of Science,([3]Department of Geophysics, Graduate School of Science, Tohoku University,([4]Planetary Plasma and Atmospheric Research Center, Graduate School of Science, Tohoku University,([5]Tohoku University,([6]Planetary Plasma and Atmospheric Research Center（PPARC), Graduate School of Science, Tohoku University,([7]Department of Geophysics/Planetary Plasma and Atmospheric Research Center, Graduate School of Science, Tohoku University,([8]Department of Geophysics, Graduate School of Science, Tohoku University

Jupiter's icy moons such as Europa, Ganymede, and Callisto may harbor subsurface liquid water oceans. While only Earth has oceans on the surface in the current solar system, multiple icy bodies like the icy moons of giant planets potentially have oceans under the icy crust. These icy bodies are candidates for more universal habitable bodies than Earth-type bodies. For keeping habitability, energy supplies to the bodies are necessary. Ionospheres of icy moons are formed by external energy supplies. The ionospheres therefore contain essential information for understanding the habitability of each icy moon. The ionospheric electron density distribution is key for narrowing down the candidates of dominant ionospheric formation processes driven by the energy supplies, e.g., photoionization, electron impact ionization, sputtering, and sublimation. However, the density distribution is still unclear because previous observation methods, radio science and in-situ observations using upper hybrid resonance emissions, were limited in the spatial range of observations.

Propagating paths of Jovian radio emissions across the icy moons' ionosphere have information on the ionospheric electron density distribution. We have developed a numerical calculation tool that simulates the propagating paths based on ray tracing and estimates occultation timing. In Yasuda et al., in prep., we compared this simulation with the occultation observed with the Galileo PWS and estimated the maximum electron density at the surface. However, we couldn't restrict the ionospheric scale height because the propagation paths with some different input parameters degenerated, which led to the difficulty in resolving the ionospheric scale height.

In addition to the propagation paths of Jovian radio emissions, changes in the polarization angle associated with the Faraday rotation effect also have information on the electron densities along the ray path. We conducted a feasibility study of electron density distribution estimation from the rotation angle measurement. With ionospheric models constrained by Yasuda et al., in prep., we found that the polarization of Jupiter's hectometric radiation in the MHz range rotates at least 2 π. For Jupiter's decametric radiation, we found the polarization angle rotation to be at most about 5 degrees at 10 MHz. We are going to examine the integration time and resolution required for reliable detection of polarization angle rotation by simulating upcoming JUICE/RPWI data in its orbit around Jupiter. Combining these simulations with the RPWI data, we will uncover the energy supply system to the icy moons to understand the habitability of the icy moons.

R009-11
B 会場 ：9/26　AM2 （10:45-12:30）
11:45〜12:00

#今 井　雅 文 [1)],Kurth William S.[2)],Kolmasova Ivana[3)],Santolik Ondrej[3)],Wong Michael H.[4,5)],Brown Shannon T.[6)],Hospodarsky George B.[2)],Bolton Scott J.[7)],Levin Steven M.[6)]
([1] 新居浜高専,([2]University of Iowa,([3]The Czech Academy of Sciences,([4]SETI Institute,([5]Center for Integrative Planetary Science, University of California, Berkeley,([6]Jet Propulsion Laboratory, California Institute of Technology,([7]Southwest Research Institute, Sa

Statistical study of Jupiter dispersed pulses observed by Juno

#Masafumi Imai[1)],William S. Kurth[2)],Ivana Kolmasova[3)],Ondrej Santolik[3)],Michael H. Wong[4,5)],Shannon T. Brown[6)],George B. Hospodarsky[2)],Scott J. Bolton[7)],Steven M. Levin[6)]
([1]National Institute of Technology, Niihama College,([2]University of Iowa,([3]The Czech Academy of Sciences,([4]SETI Institute,([5]Center for Integrative Planetary Science, University of California, Berkeley,([6]Jet Propulsion Laboratory, California Institute of Technology,([7]Southwest Research Institute, San Antonio

Jupiter's lightning produces strong pulses at radio wavelengths. One type of lightning-induced electromagnetic waves are dispersed millisecond pulses called Jupiter dispersed pulses (JDPs) found at frequencies below 150 kHz. During the polar perijove passes of Juno through 33 orbits, we found over three thousand 16-ms burst snapshots that included one or more JDPs observed by the radio and plasma wave (Waves) instrument. Assuming that JDPs propagate in the free left-hand ordinary (L-O) mode, we proposed an O mode propagation model in which low-density plasma irregularities are located between Juno and lightning strokes. These irregularities take the form of ionospheric holes with densities below 250 cm^{-3}. By taking account of the group delay of L-O mode waves, we estimate the length of these irregularities from a fraction of a km to a few times 10^5 km. Also, we compare the JDP locations with the cloud features captured by the Hubble Space Telescope. In this presentation, we show the statistical characteristics of JDPs and the related ionospheric holes using Juno data.

R009-12
B 会場 ：9/26　AM2 （10:45-12:30）
12:00〜12:15

#笠羽　康正 [1)], 土屋　史紀 [1)], 三澤　浩昭 [1)], 加藤　雄人 [1)], 北　元 [2)], 木村　智樹 [3)], 熊本　篤志 [1)], 安田　陸人 [1)], 佐藤　晋之祐 [1)], 堺　正太朗 [1)], 三好　由純 [4)], 笠原　禎也 [5)], 松田　昇也 [5)], 八木谷　聡 [5)], 尾崎　光紀 [5)], 小嶋　浩嗣 [6)], 栗田　怜 [6)],Cecconi　Baptiste[7)],Wahlund　Jan-Erik[8)],JUICE　RPWI team[1)]
[1) 東北大・理,[2) 東北工業大,[3) 東京理科大,[4) 名大 ISEE,[5) 金沢大,[6) 京都大 生存研,[7)LESIA, Obs de Paris, France,[8)IRF Uppsala, Sweden

Radio & Plasma Wave Investigation (RPWI) aboard JUICE: The first half year of the long travel to Jupiter and Icy Moons

#Yasumasa Kasaba[1)],Fuminori Tsuchiya[1)],Hiroaki Misawa[1)],Yuto Katoh[1)],Hajime Kita[2)],Tomoki Kimura[3)],Atsushi Kumamoto[1)],Rikuto Yasuda[1)],Shinnosuke Satoh[1)],Shotaro Sakai[1)],Yoshizumi Miyoshi[4)],Yoshiya Kasahara[5)],Shoya Matsuda[5)],Satoshi Yagitani[5)],Mitsunori Ozaki[5)],Hirotsugu Kojima[6)],Satoshi Kurita[6)],Cecconi Baptiste[7)],Wahlund Jan-Erik[8)],JUICE RPWI team[1)]
[1)Graduate School of Science, Tohoku University,[2)Tohoku Institute of Technology,[3)Tokyo University of Science,[4)ISEE, Nagoya University,[5)Kanazawa University,[6)RISH, Kyoto University,[7)LESIA, Obs de Paris, France,[8)IRF Uppsala, Sweden

JUpiter ICy moons Explorer (JUICE), ESA's first L-class mission, was launched in 14 April 2023 and started the long travel toward Jupiter and Icy Moons. This talk provides the initial operation results of last half year as a view of Radio & Plasma Wave Investigation (RPWI), especially the view from Japanese contributors.

RPWI provides a unique and first opportunity in this huge mission. The RPWI will investigate electromagnetic fields and plasma environment around Jupiter and icy moons with passive and active soundings by 4 Langmuir probes (LP-PWI) and a search coil magnetometer (SCM) + a tri-dipole antenna (RWI) on the long MAG-Boom with JMAG.

For lower frequency side (LP and LF), RPWI enables to investigate electric field and electromagnetic interactions governing Jupiter - moon systems, cold plasmas in the ionospheres of icy moons for investigations of surfaces and salty conductive sub-surface oceans., and cold micrometeorite impacts. The high frequency part (HF), i.e., Preamp of RWI and its High Frequency Receiver HF is procured by the RPWI Japan team, with the colleagues in Austria, France, Poland, and Sweden. This part will enable the characterization of Jovian radio emissions (including gonio-polarimetry), passive radio sounding of the ionospheric densities of icy moons, and passive sub-surface radar measurements.

April, May, and June was Near Earth Commission Period, and JUICE initially executed the deployment operations. We saw some troubles, but 10.7-m MAG-Boom was deployed within 1-week from the launch, and the deployment of 3-dipole antennas of RWI on the MAG Boom also succeeded during the JpGU meeting in May. Now (June 2023) we are checking the performance of whole RPWI system including its high frequency part. This talk will provide a summary of this result. This talk will also show planned activities in commissioning and cruise phases, and the full observations around Jupiter and icy moon system.

Potentially, the HF part of RPWI has an enough capability to detect Jovian radio emissions from magnetosphere (aurora etc.), atmosphere (lightning), and icy moons. Direction and polarization capabilities are first enabled in the Jovian system, to identify their source locations and characteristics. RPWI with other instruments covers the survey of harsh environment around Jupiter, environments and interaction with icy moons, and their surface and subsurface characteristics.

The most key parts of the HF part is the sensing of the ionospheres, surface, and subsurface of icy moons during the flybys and on the orbit around Ganymede. We will do unique remote observations of the ionospheres below the spacecraft orbit by the radio occultation and reflection of Jovian radio signals. It has a capability to detect the ionospheric density not only in usual status but also episodic plume ejections triggered by expected crustal activities. The sensing of surface and subsurface are more challenging. We try the passive subsurface radar (PSSR) concept which sounds the icy crusts of Galilean satellites by the reflections of penetrated Jovian radio emissions (HOM/DAM).

R009-13
B 会場 ：9/26　AM2 （10:45-12:30）
12:15〜12:30

近赤外撮像装置 TOPICS 開発と名寄ピリカ望遠鏡でのファーストライト

#坂野井　健 [1)], 永田　和也 [1)], 大友　綾 [1)], 鍵谷　将人 [1,2)], 木下　凌太 [1)], 平原　靖大 [2)], 齊藤　大晶 [3)], 高木　聖子 [3)], 内藤　博之 [4)]
([1] 東北大学・理・PPARC,[2] 名古屋大学・環境科学,[3] 北海道大学・理,[4] なよろ市立天文台

First light of a near-infrared imager TOPICS at the Nayoro Observatory

#Takeshi Sakanoi[1)],Kazuya Nagata[1)],Aya Otomo[1)],Masato Kagitani[1,2)],Ryota Kinoshita[1)],Yasuhiro Hirahara[2)],Hiroaki Saito[3)],Seiko Takagi[3)],Hiroyuki Naito[4)]
([1]Planetary Plasma and Atmospheric Research Center, Graduate School of Science, Tohoku University,[2]Graduate School of Environmental Studies, Nagoya University,[3]Graduate School of Science, Hokkaido University,[4]Naoyoro Observatory

We are developing a near-infrared imager TOPICS (Tohoku Planetary near-Infrared Camera System) for continuous monitoring of planetary atmospheric emission in the near-infrared range, such as Jupiter's H3+ aurora and Io volcanic eruption. In this presentation, we report on the recent development and validation of TOPICS, and the results of the first light at the 1.6m Pirka telescope of Hokkaido University.

For the development of TOPICS, we fabricated the driving electrics and improved the vacuum cooling system for safe operation of the infrared detector and for remote operation from Japan during future observation at Haleakala, Hawaii (Kambara, 2020, Nagata, 2022). Details are as follows. (1) Current measurement circuit: We developed the current measurement circuit for each of the bias and clock voltages driving the detector. This enabled the remote monitoring of nominal operation of the detector. (2) Power-on voltage control circuit: We developed a power-on voltage control circuit with a logic IC and an analog switch for each of bias and clock lines. As a result of an electrical test, we found an unexpected undershoot when the bias voltage was turned on. Thus, we improved the feedback section of the voltage follower circuit. (3) Vacuum cooling system: In the previous experiment, the detector temperature was about 20K higher than the optimum value (30-35K). We succeeded to cool the detector temperature down to 29.8 K by improving the thermal path, and obtained the small thermal noise (1.9 e/s/pix). (4) Calibration using a blackbody: We verified the fullwell (161800 e/pix) and the quantum efficiency (0.89), as expected, by experiments with a blackbody. On the other hand, the readout noise was found to be about 870 e-rms, indicating that further improvement of electronics is necessary to obtain a better S/N.

Since the performance of TOPICS was verified from the indoor experiment, we visited Nayoro Observatory from February 14 to 27, 2023, installed TOPICS at the Nasmyth focus of the 1.6-m Pirka Telescope of Hokkaido University to observe Jupiter and Venus. During this period, Jupiter and Venus were limited to low elevations of the western sky in the evening time, and the weather was not stable. However, we carried out first light of TOPICS by observing the Moon on February 23, and succeeded to obtain 883 images on consecutive four nights until February 26. On the evening of February 26, the K-band (2.2 μ m and 2.3 μ m) and L-band (3.4 μ m and 3.9 μ m) images of Venus (Vmag = -3.9) and Jupiter (Vmag = -2.0) were observed. As a result, Jupiter and Europa were imaged in the K-band, and the counts of Venus were saturated, as estimated, at the shortest exposure time (0.6s) of TOPICS. On the other hand, sky background emission was high in the L-band (about 6,000 counts with a 10-second exposure of TOPICS 3.4 μ m narrow-band filter observation). Therefore, although Betelgeuse imaging (exposure time of 0.7-1 s) was successful, we could not obtain Jupiter's H3+ auroral emission from the image data integrating for 10 minutes. In addition, oblique noise in the image, which was not seen in the Tohoku University laboratory, appeared, suggesting that noise countermeasures are necessary.

We now plan to conduct observation using TOPICS with the Pirka telescope in the summer of 2023 to observe Jupiter's infrared aurora, and install it on the T60 telescope in Haleakala, Hawaii, in the winter of 2023. In parallel, we develop a near-infrared spectrograph ESPRIT (R˜20,000) which adopts a common detector and driving electronics. We expect new results from combined infrared and visible observations with the Haleakala telescope dedicated to monitoring of planetary atmosphere, such as Jupiter's H3+ aurora, Io volcanic activity and gasses originated from Io.

我々は、木星 H3+ オーロラやイオ火山噴火変動など惑星大気発光の近赤外連続モニタリングのために、これまで近赤外撮像装置 TOPICS(Tohoku Planetary near-Infrared Camera System) 開発をしてきた。本発表では、TOPICS の最近の開発と性能評価、および北海道大学口径 1.6m ピリカ望遠鏡でのファーストライトの成果を報告する。

TOPICS の開発について、赤外検出器の安全な動作、および今後のハレアカラ観測時における日本からの遠隔運用にむけて、駆動電気回路系の製作および真空冷却系の改良を行ってきた（Kambara,2020, Nagata,2022）。この具体的な内容を以下に示す。(1）電流計測回路の開発：検出器駆動に必要なバイアス電圧とクロック電圧それぞれについて電流値を計測する回路を開発し、正常動作を確認した。これにより、検出器の正常動作を常時モニターすることが可能となった。(2）電源電圧投入制御回路の開発：ロジック IC とアナログスイッチ用いて、検出器駆動各電源の投入シーケンス制御を可能とした。この単体電気試験の結果、バイアス電圧投入時に想定外のアンダーシュートが発生する問題が判明した。これに対してボルテージフォロワ回路の帰還部の改良を施した。(3）真空冷却系の改良：従来の実験では、検出器温度が最適値（30-35K）よりも約 20K 高かった。これに対し熱パスの改良を施し、検出器温度を 29.8K まで冷却させた。実験の

結果、熱雑音が 1.9e/s/pix と十分小さい事が確認された。(4) 黒体炉を用いた較正：黒体炉を用いた実験から、フルウェルが 161800e/pix、量子効率が約 0.89 と期待通りの性能を有していることが確認された。一方で、読み出しノイズが約 870erms であり、改良の余地があることが分かった。

以上の室内実験から TOPICS 動作が検証できたので、2023 年 2 月 14-27 日までなよろ市立天文台を訪問し、北大 1.6m ピリカ望遠鏡ナスミス焦点に TOPICS を設置してファーストライト観測を実施した。この期間、観測対象の木星と金星は、夕方の西側の低いエレベーションに限られ、また天候も安定しなかったため、観測条件を満たすことが難しかった。しかしながら、2 月 23 日に月の撮像に成功し、この後 26 日まで 4 晩連続して合計 883 枚の画像を取得した。特に 26 日の晩では、金星（Vmag=-3.9）と木星（Vmag=-2.0）の K バンド（2.2μm、2.3μm）、および L バンド（3.4μm、3.9 μm）の観測に成功した。この結果、 K バンドで木星およびエウロパが撮像され、金星では TOPICS の最短露出時間（0.6s）でカウントが飽和する（見積もり通り）など、国内でも十分に観測可能なことが分かった。一方 L バンドでは、TOPICS の 3.4μm 狭帯域フィルター観測の場合、背景スカイ発光が 10 秒露出で約 6000 カウントあった。このため、ベテルギウス撮像（露出時間 0.7-1s）には成功したものの、木星観測では露出約 10 分の画像の解析では H3+ オーロラは検出されなかった。加えて、東北大の実験室では見られなかった画像中の斜めノイズが確認され、駆動回路系のノイズ対策が必要であることがわかった。

今後、TOPICS は、2023 年夏にピリカ望遠鏡による木星赤外観測を再度実施し、2023 年冬にハワイ・ハレアカラの T60 望遠鏡に設置する計画である。また、これと並行して、検出器と駆動回路が共通の近赤外分光器 ESPRIT（波長分解能 20,000）の開発を進める計画である。ハレアカラの専有望遠鏡による赤外と可視を組み合わせた観測から、木星 H3+ オーロラとイオ火山活動および噴出ガス変動のモニタリング観測から、新しい成果が期待される。

R009-14
B 会場 ：9/27　AM1 （9:00-10:30）
9:00〜9:15

#寺田　直樹[1)], 横田　勝一郎[2)], 松岡　彩子[3)], 村田　直史[4)], 桂華　邦裕[5)], 原田　裕己[3)], 益永　圭[4)], 中川　広務[1)], 今城　峻[3)], 齋藤　義文[4)], デルクール　ドミニク[6,7)], ハディッド　リナ[7)], 二穴　喜文[8)], 関　華奈子[5)], 浅村　和史[4)], 笠原　慧[5)], 西野　真木[4)], 野村　麗子[4)], 原　拓也[9)], デービッド　ブレイン[10)], ルブラン　フランソワ[11)], 堺　正太朗[1)], キムラ　トモキ[12)], 三宅　洋平[13)], 臼井　英之[13)]
([1 東北大学,([2 大阪大学,([3 京都大学,([4JAXA,([5 東京大学,([6LPC2E/CNRS,([7LPP/CNRS,([8Swedish Institute of Space Physics,([9University of California,([10University of Colorado Boulder,([11LATMOS/CNRS,([12 東京理科大学,([13 神戸大学

Ion and magnetic field observations planned by Martian Moons eXploration (MMX)

#Naoki Terada[1)],Shoichiro Yokota[2)],Ayako Matsuoka[3)],Naofumi Murata[4)],Kunihiro Keika[5)],Yuki Harada[3)],Kei Masunaga[4)],Hiromu Nakagawa[1)],Shun Imajo[3)],Yoshifumi Saito[4)],Dominique Delcourt[6,7)],Lina Hadid[7)],Yoshifumi Futaana[8)],Kanako Seki[5)],Kazushi Asamura[4)],Satoshi Kasahara[5)],Masaki N Nishino[4)],Reiko Nomura[4)],Takuya Hara[9)],David Brain[10)],Francois Leblanc[11)],Shotaro Sakai[1)],Tomoki Kimura[12)],Yohei Miyake[13)],Hideyuki Usui[13)]
([1Tohoku University,([2Osaka University,([3Kyoto University,([4JAXA,([5The University of Tokyo,([6LPC2E/CNRS,([7LPP/CNRS,([8Swedish Institute of Space Physics,([9University of California,([10University of Colorado Boulder,([11LATMOS/CNRS,([12Tokyo University of Science,([13Kobe University

Martian Moons eXploration (MMX) is a sample return mission planned by JAXA, targeting the Martian moons (Kuramoto et al., 2022). The MMX spacecraft is scheduled to be launched in 2024, inserted into Mars orbit in 2025, carry out close-up observations of Phobos and multiple flybys of Deimos, collect samples from Phobos, and return to the Earth in 2029. In addition, during the 3-year Mars orbiting phase, MMX will perform remote observations of the Martian atmosphere and in situ measurements of ions escaping from Mars (Ogohara et al., 2022).

Mass Spectrum Analyzer (MSA) (Yokota et al., 2021) aboard MMX will perform in situ measurements of ions and magnetic fields around the Martian moons to investigate the origin of the two moons as well as the evolutionary processes of both moons and the Martian surface environment. MSA consists of an ion energy mass spectrometer and two magnetometers, which will measure mass/charge and velocity distributions of low-energy ions and magnetic field vectors, respectively. To achieve a high mass resolution of m/dm $>$100, the TOF chamber of MSA for MMX is designed to be longer than previous analyzers such as IMA for Kaguya and MSA for BepiColombo/MIO.

MSA observations correspond to three of the six medium objectives of MMX: (MO1.1) Reveal whether Phobos originated as a captured asteroid or resulted from a giant impact, (MO2.1) obtain a basic description of the elementary processes of surface evolution for moons in the circum-Martian environment, and (MO2.2) add new findings and constraints on the history of changes in the Martian surface. To accomplish these medium objectives, MSA has four observation targets: For MO1.1, (1) measure refractory ions (Si+, Ca+, Fe+, etc.) emitted from the Phobos surface and (2) measure water-related ions (O+, OH+, H2O+, etc.) originating from inside Phobos (if they exist); for MO2.1, (3) measure incident ions to Phobos (H+ and He++ of the solar wind and O+ and O2+, etc. of the escaping ions from the Martian atmosphere), scattered ions, and emitted ions with monitoring the surrounding magnetic field; and for MO2.2, (4) measure O+, C+, N+, Ar+, and their key isotopes in the escaping ions from the Martian atmosphere. In this presentation, these planned observations will be explained, along with possible collaborations with other MMX instruments, sample analyses, and plasma observations by MAVEN, MEx, and ESCAPADE.

R009-15
B 会場 ：9/27　AM1 （9:00-10:30）
9:15〜9:30

#やん　まおどん [1,2],Lei Jiuhou[2], 寺田　直樹 [1],Zhang BinZheng[3],Dang Tong[2], 堺　正太朗 [1], 坂田　遼弥 [1]
([1] 東北大・理・地球物理,[2] 中国科学技術大学,[3] 香港大学,[4] 東北大・理・地球物理,[5] 東北大・理・地球物理,[6] 東北大・理・地球物理学専攻,[7] 東北大・理・地球物理

Kelvin－ Helmholtz Instability at Mars by a Newly-developed Multifluid Model

#Maodong Yan[1,2],Jiuhou Lei[2],Naoki Terada[1],BinZheng Zhang[3],Tong Dang[2],Shotaro Sakai[1],Ryoya Sakata[1]
([1]Department of Geophysics, Graduate School of Science, Tohoku University,[2]University of Science and Techonology of China,[3]The University of Hong Kong,[4]Department of Geophysics, Graduate School of Science, Tohoku University,[5]Department of Geophysics/Planetary Plasma and Atmospheric Research Center, Graduate School of Science, Tohoku University,[6]Department of Geophysics, Graduate School of Science, Tohoku University,[7]Department of Geophysics, Graduate School of Science, Tohoku University

Shear-driven Kelvin-Helmholtz (K-H) instability can form along the boundary of the solar wind interaction with non-magnetic planets (such as Mars and Venus) and detach the plasma clouds to contribute the ion escape process. Previous studies reported partially and fully developed K-H vortices at Martian ionopause. In this work, we develop a new multifluid model, which solves the continuity, momentum and energy equations for four species (Hˆ+, Oˆ+, O_2ˆ+, CO_2ˆ+) separately, to study the K-H instability at Mars. The simulation results show that the K-H instability prominently occurs in the − E hemisphere, due to the effect of convective electric field. The K-H instability is generated in the region with a solar zenith angle of ˜45 degrees, and propagates downstream along the boundary with a period of 1-2 minutes. The hemispherical asymmetry and period are well consistent with the observations.

R009-16
B 会場 ：9/27　AM1 （9:00-10:30）
9:30〜9:45

MAVEN と MEX の多点観測に基づく上流プロトンサイクロトロン波動が火星電離圏に圧縮性の ULF 磁気音波を駆動するプロセスの統計的研究

#今田　馨 [1)], 原田　裕己 [1)],Fowler Christopher M.[2)],Collinson Glyn[3)],Halekas Jasper S.[4)],Ruhunusiri Suranga[4)],DiBraccio Gina A.[3)],Romanelli Norberto[3)]
[(1] 京大・理,[(2] ウエストバージニア大学,[(3]NASA ゴダードスペースフライトセンター,[(4] アイオワ大学

Statistical Study of Processes of Upstream PCW Driving ULF Waves in the Martian Ionosphere: MAVEN and MEX Multi-Point Observations

#Kaworu Imada[1)],Yuki Harada[1)],Christopher M. Fowler[2)],Glyn Collinson[3)],Jasper S. Halekas[4)],Suranga Ruhunusiri[4)],Gina A. DiBraccio[3)],Norberto Romanelli[3)]
[(1]Graduate School of Science, Kyoto University,[(2]Department of Physics and Astronomy, West Virginia University,[(3]NASA Goddard Space Flight Center,[(4]Department of Physics and Astronomy, University of Iowa

Proton cyclotron waves (PCWs) generated upstream of the Martian Bow shock (BS) have been studied in detail in terms of Mars-solar wind interactions since the first observation by Phobos-2 (Riedler et al., 1989; Russell et al., 1990, 1992) because they could have a significant impact on the ionosphere. In the presence of newborn pickup protons resulting from Mars' hydrogen corona extended beyond the BS and solar wind protons, the resultant proton velocity distribution function is often unstable to drive the electromagnetic ion/ion right-hand (RH) and left-hand (LH) resonant instabilities (Gary, 1991, 1993; Romeo et al., 2021). The dominant mode of the two depends on the angle between the solar wind velocity and the interplanetary magnetic field (cone angle), among other plasma parameters. For instance, the LH (RH) instability is predominant for large (small to moderate) cone angles (Gary, 1991). When the excited waves are observed in the spacecraft reference frame, their frequencies are Doppler-shifted due to the relative motion between the spacecraft and the solar wind, and these waves resulting from both instabilities are left-hand and elliptically polarized with a frequency close to the local proton gyrofrequency (Romanelli et al., 2013; Romeo et al., 2021). Case studies based on Mars Atmosphere and Volatile EvolutioN (MAVEN) revealed that the PCWs are advected back to the BS by the solar wind flow, and "ring" the induced magnetosphere as the associated pressure pulses drive compressive magnetosonic waves in the ionosphere at an ultralow frequency (ULF) similar to that of the upstream PCW (Collinson et al, 2018; Fowler et al., 2018, 2021). Furthermore, if the waves propagate to altitudes at which planetary heavy ions (mainly O^+, $O_2{}^+$) are dominant components, the waves are thought to be capable of heating these ions via wave-particle interactions (Andersson et al., 2010; Ergun et al., 2006). Indeed, Fowler et al. (2018, 2021) reported some events in which MAVEN presumably observed wave-heated ions.

However, since there have been few analyses based on multi-point observations of the upstream of the BS and the ionosphere, the probability at which the upstream PCWs drive the new ULF magnetosonic waves in the ionosphere (defined as ringing probability in this study) has not been derived yet. Accordingly, it has been also unclear how much the ringing process contributes to long-term Mars' atmospheric loss.

In this study, we estimate the ringing probability by analyzing multi-point observations of local magnetic fields based on MAVEN and Mars Express (MEX) obtained between October 2014 and December 2018. First, we identify a number of events in which the Mars Advanced Radar for Subsurface and Ionosphere Sounding (MARSIS) instrument on board MEX operated in the ionosphere while MAVEN confirmed the PCWs with its magnetometers in the upstream region. Then, we estimate the local magnetic field magnitude at MEX for each event from ionograms obtained by MARSIS (Akalin et al., 2010; Gurnett et al., 2005), and automatically identify whether compressional fluctuations were detected in the ionosphere at frequencies close to those of the upstream PCWs, thereby estimating the ringing probability.

As of this writing, we have completed analyses for 99 orbits of MEX and the results show that the ringing probability is about 30% on the dayside (SZA<80 [degree]) and about 23% just above 200 – 300 km on the dayside, at which the ULF waves can heat planetary ions (Ergun et al., 2006; Fowler et al., 2018). In this presentation, we will report the results of the analysis with an increase in the number of orbits to about 130. In addition, we will discuss the global ion escape rate possibly driven by the ringing process in the context of previous studies such as Andersson et al. (2010), Ergun et al. (2006), Fowler et al. (2018, 2021), and Romeo et al. (2021).

火星のバウショック上流で発生するプロトンサイクロトロン波動 (PCW) は、惑星電離圏にまで影響を与えうることが知られている現象であり、Phobos-2 による初観測 (Riedler et al., 1989; Russell et al., 1990, 1992) 以降、火星-太陽風相互作用の観点から詳しく研究されてきた。火星が近日点付近に位置するときにバウショック上流を超えて広がる水素外圏コロナ由来の新生ピックアッププロトンと、太陽風プロトンによって構成される速度分布は不安定であり、electromagnetic ion/ion right-hand (RH) および left-hand (LH) resonant instabilities を駆動する (Gary, 1991, 1993; Romeo et al., 2021)。どちらのモードが支配的かは惑星間空間磁場 (IMF) コーン角に依存しており、大きい場合は LH が支配的となり、小–中程度ではもう一方のモードが支配的になる (Gary, 1991)。これらのモードの波動を衛星系で観測すると、波動はドップラーシフトの影響を受け、どちらも局所的なプロトンサイクロトロン周波数にピークを持つ左回りの楕円偏波として観測さ

れる (Romanelli et al., 2013; Romeo et al., 2021)。Mars Atmosphere and Volatile EvolutioN (MAVEN) の観測に基づく事例解析によって、上流 PCW はその特性を変化させながら太陽風によって吹き流されていき、圧力パルスとして誘導磁気圏を打ち鳴らすことによって電離圏内に PCW と近い周波数にピークを持つ圧縮性の ULF 磁気音波を駆動することが明らかにされた (Collinson et al., 2018; Fowler et al., 2018)。さらに、惑星重イオン (主に O^+,$O_2{}^+$) が支配的な高度まで波動が伝播すると、波動-粒子相互作用によってイオンの加熱に寄与しうると考えられており (Andersson et al., 2009; Ergun et al., 2006)、実際に MAVEN が波動によるイオン加熱を観測したと考えられるイベントも報告されている (Fowler et al., 2018, 2021)。

しかし、これまでの研究では太陽風領域と電離圏の多点観測に基づく解析が少なかったため、PCW が電離圏に ULF 波動を駆動する確率 (本研究で ringing probability と定義) が明らかにされてこなかった。それに伴い、一連のプロセスが長期的にどの程度火星の大気散逸に寄与しているのかも十分に議論されてこなかった。

本研究ではこれらの課題に対して、Mars Express (MEX) と MAVEN による波動の多点観測によってアプローチした。まず、2 つの探査機が同時に運用されていた 2014 年 10 月から 2018 年 12 月までの期間において、MEX が電離圏に位置していた時間帯に、MAVEN が磁力計観測によってバウショック上流に PCW が存在していることを確認しているイベントを多数同定した。その後、MEX に搭載されている観測装置 Mars Advanced Radar for Subsurface and Ionosphere Sounding (MARSIS) の観測データから MEX の局所的な磁場強度を推定し (Akalin et al., 2010; Gurnett et al., 2005)、電離圏に上流 PCW の周波数に近いピークを持つ磁場強度の変動が存在するかどうかを、アルゴリズムを開発することによって各時刻で自動判定した。この判定結果を統計解析することで ringing probability とそのパラメータ依存性を推定した。予稿投稿時点までに、MEX の 99 軌道に対して解析を完了させており、昼側 (SZA<80°) では約 3 割の確率で ringing が検出されることや、惑星重イオンの加熱に寄与しうる高度である 200 – 300 km(Ergun et al., 2006; Fowler et al., 2018) の直上 (300 – 350 km) では、昼側で約 23% の確率で ringing が検出されることが結果として得られた。本講演では、対象とする軌道を 130 個程度に増やした解析結果を報告する。さらに、得られた ringing probability と先行研究 (Andersson et al., 2009; Ergun et al., 2006; Fowler et al., 2018; Romeo et al.,2021) の結果や議論を組み合わせることで、一連のプロセスの長期的な大気散逸への寄与について議論する。

R009-17
B 会場 ：9/27　AM1 （9:00-10:30）
9:45〜10:00

#坂田　遼弥 [1)],Sun　Wenyi[2)],Ma　Yingjuan[2)], 関　華奈子 [3)],Russell　Christopher T.[2)], 寺田　直樹 [1)], 堺　正太朗 [1,4)], 品川　裕之 [5)]
([1] 東北大・理・地球物理学専攻,[2] カリフォルニア大学ロサンゼルス校,[3] 東大理・地球惑星科学専攻,[4] 東北大・理・惑星プラズマ・大気研究センター,[5] 情報通信研究機構

Comparison study of two global multispecies MHD models of Mars

#Ryoya Sakata[1)],Wenyi Sun[2)],Yingjuan Ma[2)],Kanako Seki[3)],Christopher T. Russell[2)],Naoki Terada[1)],Shotaro Sakai[1,4)],Hiroyuki Shinagawa[5)]
([1]Department of Geophysics, Graduate School of Science, Tohoku University,[2]University of California, Los Angeles, CA, USA,[3]Department of Earth and Planetary Science, Graduate School of Science, University of Tokyo,[4]Planetary Plasma and Atmospheric Research Center, Graduate School of Science, Tohoku University,[5]National Institute of Information and Communications Technology

Atmospheric escape to space has played a key role in atmospheric evolution and climate change on Mars. As direct and global interactions occur between the solar wind and the upper atmosphere due to lack of a global intrinsic magnetic field, the global configuration of the plasma environment around Mars is required for understanding of atmospheric escape. The spacecraft observations in recent decades have revealed the plasma dynamics significantly, but the global picture cannot be fully captured by only in-situ observations due to temporal and spatial limitations. The global simulation is another important tool to study the solar-wind Mars interactions. Various plasma phenomena have been investigated based on numerical simulations. However, there are still discrepancies not only between simulations and observations, but also among different simulation models. In a comparative study of several numerical models for Mars, the simulation results showed large differences in plasma distributions and ion escape rates, although the models used the same upstream inputs and the neutral atmosphere (Brain et al., 2010). The differences can arise from various factors. The extent to which physical processes are taken into account is a model-dependent issue. Simulations can also be affected by model assumptions (e.g., magnetohydrodynamics, MHD, or hybrid) and numerical implementations (e.g., numerical scheme and grid system).

The purpose of this study is to understand how numerical simulation can be affected by considered physical processes and numerical implementations. We compared two global multispecies MHD models: the “Sun model” based on the BATS-R-US (Sun et al., 2023) and the “Sakata model” based on a newly developed multifluid model (Sakata et al., in prep). Both models consider five ion species (planetary H^+, O^+, $O_2{}^+$, $CO_2{}^+$, and solar wind H^+). We used the typical upstream conditions and neutral atmosphere on present Mars and adopted the same chemical reactions, collision frequencies, and inner boundary conditions. Crustal magnetic fields were not included. In addition to the comparison, we also surveyed the effects of two physical processes: electric resistivity and photoelectron heating. Two types of simulation were performed for the effects of resistivity: simulations with resistivity and those without resistivity. For photoelectron heating, we assumed three heating rates: 0.3 eV, 1 eV, and 5 eV per photoelectron. The baseline case includes the resistivity and assumed 1 eV photoelectron heating.

In the baseline case, the simulation results show good agreement between the two models. The 1D profiles along the subsolar line are nearly identical, including the shock location, the magnetic pileup, and the ionospheric composition, indicating the consistency of the two models. However, there are some discrepancies in the trans-terminator and nightside dynamics. The escape rates of planetary ions are also in good agreement. Both resistivity and photoelectron heating affect the ionosphere. The inclusion of resistivity changes the magnetic configuration in the ionosphere via magnetic diffusion. Photoelectron heating is an important energy source and increases the plasma temperature. These effects change the escape rates of molecular ions largely. We will report the detailed analysis on the differences between the two models' results and the effects of resistivity and photoelectron heating.

References

Brain, D., Barabash, S., Boesswetter, A., Bougher, S., Brecht, S., Chanteur, G., et al. (2010). A comparison of global models for the solar wind interaction with Mars. Icarus, 206(1), 139 – 151. https://doi.org/10.1016/j.icarus.2009.06.030

Sun, W., Ma, Y., Russell, C. T., Luhmann, J., Nagy, A., & Brain, D. (2023). 5-Species MHD study of Martian proton loss and source. Journal of Geophysical Research: Space Physics, 128, e2023JA031301. https://doi.org/10.1029/2023JA031301

R009-18
B 会場 ：9/27　AM1 （9:00-10:30）
10:00〜10:15

#堺　正太朗 [1,2], 中山　陽史 [3], 関　華奈子 [4], 寺田　直樹 [1], 品川　裕之 [5], 坂田　遼弥 [1],Leblanc　François[6],Brain David[7], 田中　高史 [8]
([1] 東北大・理・地球物理,[2] 東北大・理・PPARC,[3] 立教大・理・物理,[4] 東大・理・地球惑星,[5] 情報通信研究機構,[6]LATMOS/CNRS, Sorbonne Université,[7]LASP, University of Colorado Boulder,[8] 九州大・i-SPES

Effects of stellar XUV spectra on atmospheric escape from a Mars-like planet orbiting inactive low-mass stars

#Shotaro Sakai[1,2],Akifumi Nakayama[3],Kanako Seki[4],Naoki Terada[1],Hiroyuki Shinagawa[5],Ryoya Sakata[1],Leblanc Francois[6],David A. Brain[7],Takashi Tanaka[8]
([1]Department of Geophysics, Graduate School of Science, Tohoku University,[2]Planetary Plasma and Atmospheric Research Center, Graduate School of Science, Tohoku University,[3]Department of Physics, Graduate School of Science, Rikkyo University,[4]Department of Earth and Planetary Science, Graduate School of Science, University of Tokyo,[5]National Institute of Information and Communications Technology,[6]LATMOS/CNRS, Sorbonne University,[7]Laboratory for Atmospheric and Space Physics, University of Colorado Boulder,[8]International Research Center for Space and Planetary Environmental Science, Kyushu University

Atmospheric evolution is one of the key parameters in answering the question of how Earth was able to maintain a thick atmosphere and yield a habitable environment. A universal understanding of atmospheric evolution, including that of exoplanetary systems, is essential to explain how planets have evolved to their current state. In particular, atmospheric escape is strongly linked to atmospheric evolution. It is dependent on the planetary size, the existence of an intrinsic magnetic field, its intensity, the stellar activity, and stellar wind conditions. The variation in stellar activity affects both thermal escape and nonthermal escape. Ancient Mars, when the solar activity was more active than at present, had a very high atmospheric escape rate, the magnitude of the X-ray and extreme ultraviolet (XUV) irradiance being one of the parameters to determine the ion escape rate.

Many exoplanets have been discovered in recent years, and among them, M and K dwarfs are of particular interest because they might have habitable environments. The habitable zones of these stars are located very close to the main stars within 0.1 AU. Exoplanets in the habitable zones of these stars must therefore be exposed to intense XUV radiation and stellar winds. Numerical simulations suggested that the ion escape rate from Proxima Centauri b, orbiting at 0.049 AU, is three orders of magnitude greater than at the present Mars, with a value of ~10^{27} s^{-1} (Dong et al., 2017). The previous study assumed an XUV intensity several tens of times that of the Sun to determine the ion escape rate, but in fact, the shape of the XUV spectrum determines the thermospheric profile, controlling the ion escape rate.

The XUV spectrum is quite important in determining the thermospheric profile, controlling the ion escape as well as the ionospheric distribution. The current study focuses on the stellar XUV spectrum, and after investigating thermospheric profiles under various XUV spectra using a thermosphere model, the impact of the stellar XUV spectrum on ion escape is presented using a multispecies magnetohydrodynamic model (REPPU-Planets). The target stellar systems are Sun, HD85512, and GJ581. Note that these stars are somewhat inactive XUV environments compared to Proxima Centauri. The planets are of Mars type and located at 1.52, 0.622, and 0.174 AU, respectively, in order to keep the same irradiance as that of the Martian orbit in the present solar system. Mars under 10 times XUV irradiance at 1.52 AU is also investigated to understand the effects of the shape of the XUV spectrum on ion escape. According to the thermosphere model, the thermosphere of the HD85512 system is the most extended, followed by the GJ581 system. The ion escape rates are estimated by REPPU-Planets simulations using these thermospheric profiles as input. Ion escape is also the most intense for the HD85512 system, followed by the GJ581 system. The XUV irradiances between 40 and 100 nm are one of the most important parameters to determine the atomic ion escape rate. The $O_2{}^+$ escape rate is smaller in the high XUV environments because of the larger dissociative recombination, associated with decreasing the $O_2{}^+$ density. The C^+ escape rate, meanwhile, is higher in high XUV environments due to greater photodissociation of CO_2 and CO, and the associated charge exchange.

Reference:
Dong, C., et al. (2017). Is Proxima Centauri b habitable? A study of atmospheric loss. ApJL, 837, L26.

R009-19
B 会場 ：9/27　AM1 （9:00-10:30）
10:15〜10:30

ひさき衛星観測結果と比較したジオコロナモデルの妥当性の検証

#古賀　亮一[1)], 土屋　史紀[2)], 村上　豪[3)], 桑原　正輝[4)], 堺　正太朗[2,9)], 木村　智樹[5)], 吉岡　和夫[6)], 木村　淳[7)], 高木　聖子[8)], 亀田　真吾[4)]
([1] 名古屋大,[2] 東北大・理・惑星プラズマ大気,[3]ISAS/JAXA,[4] 立教大,[5] 東京理科大,[6] 東大・新領域,[7] 大阪大,[8] 北海道大,[9] 東北大・理・地球物理,[10] 東北大・理・地球物理,[11] 東北大・理・地球物理

Validation of the geocorona model in comparison with the HISAKI satellite observations

#Koga Ryoichi[1)],Fuminori Tsuchiya[2)],Go Murakami[3)],Masaki Kuwabara[4)],Shotaro Sakai[2,9)],Tomoki Kimura[5)],Kazuo Yoshioka[6)],Jun Kimura[7)],Seiko Takagi[8)],Shingo Kameda[4)]
([1]Graduate School of Environmental Studies, Nagoya University,[2]Planetary Plasma and Atmospheric Research Center, Graduate School of Science, Tohoku University,[3]Institute of Space and Astronautical Science, Japan Aerospace Exploration Agency,[4]Rikkyo University,[5]Tokyo University of Science,[6]Department of Complexity Science and Engineering, The University of Tokyo,[7]Osaka University,[8]Hokkaido University,[9]Department of Geophysics, Graduate School of Science, Tohoku University,[10]Department of Geophysics, Graduate School of Science, Tohoku University,[11]Department of Geophysics/Planetary Plasma and Atmospheric Research Center, Graduate School of Science, Tohoku University

The Earth's exosphere is dominated by hydrogen and helium atoms, and the density of oxygen atoms is also large at altitudes of 500-1000 km, where many space telescopes orbit. Since these atoms emit light due to solar resonance scattering, they are one of the major obstacles to astronomical observations by space telescopes and need to be quantitatively evaluated. On the other hand, it is important to evaluate the atomic density distribution in the lower part of the exosphere to understand the dissipation process of the Earth's atmosphere. We are promoting the LAPYUTA (Life-environmentology, Astronomy, and PlanetarY Ultraviolet Telescope Assembly) project and are developing a model of the geocorona necessary to study the observations of Jupiter's satellites and other celestial bodies. In this presentation, we will report the progress of the model development and its validation using sky observations by the HISAKI satellite from December 2013 to February 2014.

The HISAKI satellite was launched in 2013 and has been performing UV spectroscopic observations of solar-system objects while orbiting at an altitude of 950-1050 km. For altitudes above 1000 km, we extrapolated the above model for O atoms and used Kameda et al. (2017) for H atoms, normalized to connect with the above model. To match the conditions of the model and the observations as much as possible, the parameters of the database used for the model were set to 18h for Local time and 90 for F10.7, the index of solar radio strength. For each angle between the line of sight and the zenith (zenith angle), the column density and surface brightness in the line of sight direction were calculated. On the other hand, only the data from the HISAKI satellite with a local time of 17-19:00 were extracted, and the data were sorted by the zenith angle of 30.

The analysis of the observed data shows that the surface brightness at HI 121.6 nm and OI 130.4 nm is 7.5 k Raleighs (R) and 2.5 R when the zenith angle in the line of sight is 0-30 degrees, and 12.2 kR and 6.3 R for 60-90 degrees, respectively. The HI 121.6 nm observations are a fraction of the model calculations. One of the reasons for this is the multiple scattering of H atoms. We will add this factor to our future calculations. On the other hand, the observed value of OI 130.4 nm is several times larger than the model calculation. Since the density profile of OI 130.4 nm is expected to change significantly at altitudes between 950 and 1050 km, it is necessary to analyze the dependence of the actual observed results on altitude, latitude, and longitude.

地球の外気圏は水素原子及びヘリウム原子が支配的であり、多くの宇宙望遠鏡が周回している 500-1000 km の高度では酸素原子の密度も大きい。これらの原子は太陽光共鳴散乱によって発光するため、宇宙望遠鏡による天体観測の主要な障害の一つとなっており、定量的な評価が必要である。一方で地球大気散逸過程を理解する上で、外気圏下部の原子密度分布を評価することは重要である。私たちは LAPYUTA（惑星科学、生命圏科学、および天文学に向けた紫外線宇宙望遠鏡）計画を推進しており、木星衛星等の天体の観測検討に必要なジオコロナのモデルを開発している。この発表ではモデル開発の進捗とひさき衛星による 2013 年 12 月から 2014 年 2 月の sky 観測結果を用いた検証を報告する。

ひさき衛星は 2013 年から打ち上げられ、高度 950-1050 km を周回しながら、太陽系天体を中心に紫外線分光観測を行っている。2013-2016 年まではターゲット天体から視野を少し外して観測を行う sky 観測も行われていた。O, H 原子の数密度の高度分布の内 500-1000 km の範囲は NRLMSIS-E Atmosphere Model のデータベースを参照した。1000 km 以上の高度では、O 原子は上記のモデルを外挿し、H 原子は Kameda et al. (2017) を上記のモデルと接続するように規格化して使用した。なるべくモデルと観測結果の条件を合わせるため、モデルに使用したデータベースのパラメータは Local time は 18h、太陽電波強度の指数である F10.7 は 90 に設定した。その上で視線方向と天頂がなす角度 (天頂角) ごとに視線方向の柱密度と面輝度を計算した。一方でひさき衛星の local time が 17-19 時のデータのみを抽出し、 天頂角 30° ごとにデータを選別した。

観測データの解析の結果、視線方向の天頂角が 0-30° のとき、HI 121.6 nm、OI 130.4 nm の面輝度は 7.5k Raleighs

(R)、2.5 R、60-90°のときはそれぞれ、12.2 kR、6.3 R となった。これは外気圏を横切る視線方向の距離が異なるためである。HI 121.6 nm の観測結果はモデル計算結果の数分の 1 となった。この理由として H 原子の多重散乱の影響などが考えられるため、この要素を追加した計算を今後行う。一方で OI 130.4 nm の観測結果の値はモデル計算の数倍となった。OI 130.4 nm の密度分布は 950-1050 km の高度で大きく変化することが予想されるため、実際の観測結果の高度や緯度・経度依存性を解析によって明らかにする必要がある。

R009-20
B 会場 ：9/27　AM2 （10:45-12:30）
10:45〜11:00

#鎌田　有紘 [1)], 黒田　剛史 [1)], 小玉　貴則 [2)], 笠羽　康正 [1,3)], 寺田　直樹 [1)]
([1] 東北大学大学院理学研究科,[2] 東京大学大学院総合文化研究科,[3] 東北大学大学院理学研究科　惑星プラズマ・大気研究センター,[4] 東北大学大学院理学研究科

Obliquity-Driven Early Mars Climate Evolution and Valley Network Formation

#Arihiro Kamada[1)],Takeshi Kuroda[1)],Takanori Kodama[2)],Yasumasa Kasaba[1,3)],Naoki Terada[1)]
([1]Graduate School of Science, Tohoku University,[2]Komaba Institute for Science, Graduate School of Arts and Science, University of Tokyo,[3]Planetary Plasma and Atmospheric Research Center, Graduate School of Science, Tohoku University,[4]Graduate School of Science, Tohoku University

We have studied the evolution of surface water environment on early Mars (Kamada et al. 2021 and 2022). Two opposing theories have been proposed to explain these fluvial landforms such as valley networks (VNs) formed 3.8 - 3.6 billion years ago. We evaluated two scenarios, “warm and wet” and “cold and icy”. The “warm and wet” hypothesis proposes that Mars once had a thick atmosphere that caused a global warming enough for liquid water to exist. Conversely, the “cold and icy” hypothesis posits that Mars has always been as cold as it is today.

The long-term variation in obliquity can affect significant influence to both scenarios, as eccentricity and orbital inclination. Changes in obliquity shifted the distribution of solar insolation on early Mars, which critically affected climate dynamics and surface water cycling. Although the evolution of Martian obliquity is characterized by chaotic behaviour, making it difficult to accurately predict the obliquity of early Mars, it’s statistically likely that the obliquity was about 37.62 degrees $\pm$ 13.82 degrees.

Here, we applied possible obliquity cycles to the GCM simulations with full couplings of atmosphere, hydrosphere, and cryosphere. The complicated obliquity variation of early Mars was simply assumed based on a Fourier series with a mean obliquity value of 40 degrees, and long-term oscillation periods of ~10^5 years. We assumed a CO_2/H_2O/H_2 mixed atmosphere with surface pressures of between 1 bar and 2 bar, H_2 mixing ratios of between 0% and 6%, and geothermal heat flux of 55 mW/m^2. We assumed the existence of a northern ocean and lakes in our model with the amount corresponding to a 500 m Global Equivalent Layer (GEL) in the initial state and implemented a pre-True Polar Wander topography to investigate the global water cycle of early Mars before the late Tharsis formation.

We found that long-term variations in the obliquity of Mars have significantly affected the thermal structure of the atmosphere, thereby influencing its climate and the formation of VNs. When the H_2 mixing ratio was lower, periods of higher obliquity led to the formation of ice sheets at lower latitudes. Conversely, during periods of lower obliquity, equatorial ice sheets would melt, and the meltwater would flow into rivers. This pattern of freeze-thaw cycles would have created a dynamic water cycle on early Mars, with changing obliquity driving repeated cycles of ice accumulation and melting, potentially contributing to the formation of the VNs. On the other hand, a higher H_2 mixing ratio in the atmosphere led to a warm, precipitation-dominated climate. The resulting rainfall would have created river systems that formed near the equator during periods of higher obliquity and at higher latitudes during periods of lower obliquity. This constant movement of water would have been a significant driver of erosion, contributing to the formation and development of the VNs. Furthermore, this study has shown that about 50% of the VNs could be attributed to snowmelt streams at a 3% H_2 mixing ratio, while about 70% of the VNs could be explained by rain-fed rivers at a 6% H_2 mixing ratio. These proportions are higher than the estimates made assuming fixed obliquity, indicating that long-term obliquity variations play a significant role in the formation of VNs.

R009-21
B 会場 ：9/27　AM2 （10:45-12:30）
11:00〜11:15

欧州火星探査衛星 TGO/NOMAD で観測された CO・CO_2 の C および O 同位体比

#塩原　輝満恵 [1)],Janecke　H. F.[1,2)], 青木　翔平 [3,4)], 吉田　奈央 [5)], 吉田　辰哉 [1)], 中川　広務 [1)], 村田　功 [1)], 寺田　直樹 [1)], 笠羽　康正 [1)],Liuzzi　G.[6)],Vandaele　A. C.[4)],Trompet　L.[4)],Thomas　I. R.[4)],Villanueva　G. L.[7)],Lopez-Valverde　M. A.[8)],Brines　A.[8)],Patel　M. R.[9)],Faggi　S.[7,10)],Daerden　F.[4)],Erwin　J. T.[4)],Ristic　B.[4)],Bellucci　G.[11)], ロペズ　ジョゼホワン [8)], 上野　雄一郎 [12)], 黒川　宏之 [3)]
([1] 東北大学,[2]Heidelberg University,[3] 東京大学,[4]Royal Belgian institute for space aeronomy,[5] 国立研究開発法人 宇宙航空研究開発機構 JAXA,[6]Scuola di Ingegneria, Universita ` degli Studi della Basilicata,[7]NASA Goddard Space Flight Center,[8]Instituto de Astrofi ´ sica de Andaluci ´ a, Gl

Isotope ratios of C and O in CO and CO_2 on Mars observed by ExoMars-TGO/NOMAD

#Kimie Shiobara[1)],H. F. Janecke[1,2)],Shohei Aoki[3,4)],Nao Yoshida[5)],Tatsuya Yoshida[1)],Hiromu Nakagawa[1)],Isao Murata[1)],Naoki Terada[1)],Yasumasa Kasaba[1)],G. Liuzzi[6)],A. C. Vandaele[4)],L. Trompet[4)],I. R. Thomas[4)],G. L. Villanueva[7)],M. A. Lopez-Valverde[8)],A. Brines[8)],M. R. Patel[9)],S. Faggi[7,10)],F. Daerden[4)],J. T. Erwin[4)],B. Ristic[4)],G. Bellucci[11)],J. J. Lopez-Moreno[8)],Yuichiro Ueno[12)],Hiroyuki Kuwokawa[3)]
([1]Tohoku University,[2]Heidelberg University,[3]The University of Tokyo,[4]Royal Belgian institute for space aeronomy,[5]Japan Aerospace Exploration Agency,[6]School of Engineering, University of Basilicata,[7]NASA Goddard Space Flight Center,[8]Institute of Astrophysics of Andalusia, Glorieta de la Astronomia,[9]School of Physical Sciences, The Open University,[10]American University,[11]National Institute of Astrophysics,[12]Tokyo Institute of Technology

Carbon and oxygen isotope ratios in the Martian atmosphere are important tracers to constrain the atmospheric evolutionary history and origin of organics at the surface of Mars (Jakosky et al., 1994; House et al., 2021). The carbon isotopic ratio can be fractionated by degassing, atmospheric escape to space (e.g., Lammer et al, 2020), and recent photochemical research shows that it is also strongly affected by isotope fractionation effects via photodissociation of CO_2. Theoretical calculations by Schmidt et al. (2013) suggest that the absorption cross-section via CO_2 photodissociation is 200 per mil smaller for CO. Our Mars atmospheric photochemical calculations, which are based on these results, also show that the $\delta\ ^{13}C$ of CO is significantly depleted by about -170 per mil compared to CO_2 (Yoshida et al., 2023). In addition, Schmidt et al. (2013) also showed that oxygen, as well as carbon, is fractionated -100 per mil during the photodissociation of CO_2, and the derivation of oxygen isotope ratio is also expected to be an indicator of photodissociation. The previous observations of carbon isotope ratios are limited to CO_2 ($\delta\ ^{13}C$ = 46+/-4 per mil, $\delta\ ^{18}O$ = 48+/-5 per mil, at the surface; Webster et al.,2013; $\delta\ ^{13}C$ = -3+/-37 per mil, $\delta\ ^{18}O$ = -29+/38 per mil, 70-90 km; Alday et al.,2021), and until recently, the observation of CO isotopic ratios had not been achieved. ExoMars Trace Gas Orbiter (TGO), which started science operations in 2018, has multiple high-spectral resolution spectrometers that carry out solar occultation measurements, which allows us to perform a sensitive measurement of isotopic ratios for CO as well as CO_2 on Mars.

The Atmospheric Chemistry Suite (ACS) on board the TGO observed $\delta\ ^{13}C$ = -160+/-90 per mil and $\delta\ ^{18}O$ = -20+/-110 per mil for Martian Year 34 Ls 166-349 ° and Martian Year 35 Ls = 141-366 °, and altitude range is 10-50 km, respectively (Alday et al., 2023). In Aoki et al. 2023, which is also an initial result of our study, the Nadir and Occultation for MArs Discovery (NOMAD) on board TGO observed a very strong negative carbon isotope fractionation with $\delta\ ^{13}C$ = -263+/-132 per mil for Martian Year 36 Ls = 182-205 ° and altitudes 30-50 km. In this study, we extended the data period of Aoki et al.,2023 to 36 Martian years Ls = 182-359 ° (2022/3/1 〜 2022/12/24), and also attempted to derive oxygen isotopes as well as carbon.

Furthermore, not only for CO, but we start to derive the oxygen isotope ratios ($\delta\ ^{17}O$, $\delta\ ^{18}O$) in CO_2, which serves as a reference for discussion of the fractionation process via photodissociation, targeting the middle and lower atmosphere below 50km. The analysis of this altitude range is very important for the validation of isotope fractionation by CO_2 photodissociation, since, $\delta\ ^{18}O$ at the surface is not consistent with the values above 70 km according to previous studies, and the oxygen isotope ratios in the altitude range between them have not yet been determined. The altitude range and observable period for CO_2 analysis overlap with those for our CO analysis, and there are no examples in previous studies where simultaneous analyses for CO_2 and CO isotope ratio have been conducted at the same altitude. Therefore, the derivation of the CO_2 isotope ratio in this study and the comparison with CO isotope ratios are expected to provide the first observational evidence of CO isotope fractionation in CO_2 photodissociation in the middle and lower atmosphere.

To summarize above, in this study, by using infrared spectral data observed by NOMAD on board TGO, we attempt these two things; 1) to derive the carbon and oxygen isotopic ratios for CO in middle and lower atmosphere and to validate the CO isotope fractionation process suggested by the model, and 2) to derive oxygen isotope ratios for CO_2 in middle and lower atmosphere and to validate the fractionation process of photodissociation observationally by comparison with the CO observation. About 2), we plan to report the initial results in this presentation.

We perform the retrievals within the following spectral ranges: order183-186, full spectral range, (4112-4213 cm^{-1}) for CO, and order117 (2629-2650 cm^{-1}), order132 (2966-2990 cm^{-1}), and order141 (3168-3194 cm^{-1}) for CO_2. For the retrieval, we use a radiative transfer and inversion code, ASIMUT (Vandaele et al., 2006), which uses Optimal Estimation Method (OEM) (Rodgers, 2000) to find the best parameters to fit the data. A-priori profiles of pressure and CO_2 volume mixing ratio in the Martian atmosphere for radiative transfer calculations are obtained from the theoretical predictions by GEM-Mars model (Daerden et al., 2019). For temperature profiles, we used observations from simultaneously obtained CO_2 absorption lines (Trompet et al., 2023) for CO, and the value of GEM-Mars model for CO_2.

We consider the total amount of $^{12}C^{16}O$, $^{13}C^{16}O$, $^{12}C^{18}O$ for CO, $^{16}O^{12}C^{16}O$, $^{16}O^{12}C^{17}O$, and $^{16}O^{12}C^{18}O$ for CO_2 volume mixing ratio along the line of sight as the free parameters and perform the retrievals for each altitude independently.

The following are the data selection conditions and results for CO. For the retrieval value obtained at altitudes of 30-50 km, we did not use values for CO volume mixing ratios below 1000 ppm, whose reliability is under verification, and we only selected the results with a confidence level of at least 3-sigma. About the retrieved isotope ratios, when we take the weighted average from 30 to 50 km in all orbits, the averaged value and the standard derivation are $\delta\ ^{13}C$ = -286+/-175 per mil, $\delta\ ^{18}O$ = -188+/-240 per mil. ☒☒ In addition to the theoretical predictions, the NOMAD data also show strong negative isotope fractionation. Although the standard deviation is large because of uncertainties in the assumed atmospheric temperature, even if we take into account those errors, ^{13}C depletion is suggested, and for $\delta\ ^{18}O$, the weighted mean over this altitude range is negative. For these reasons, we think that the results provide observational evidence that CO isotope fractionation is due to CO_2 photodissociation in this altitude range, as predicted by the model. This result is consistent with the trend observed by the ACS, the CO_2 photolysis is a more reliable process of isotope fractionation in isotope analysis with large uncertainties.

On the other hand, as for CO_2, we are doing a test analysis on 1 orbit. It has been determined that the $^{16}O^{12}C^{16}O$ retrievals are not accurate at this time, and we think this is because the temperature was not accurately defined. We plan to proceed with our analysis with a view to simultaneous temperature retrievals to minimize uncertainties caused by temperature in the future.

火星大気の炭素・酸素同位体比は、火星における大気進化史や表層有機物の起源を制約するための重要なトレーサーとして知られている (Jakosky et al., 1994; House et al., 2021)。大気中の各炭素種の同位体変化は、脱ガスや大気散逸に加え、CO_2 の光解離時の同位体分別効果の影響も強く受けることが近年の光化学研究から明らかになってきた (Lammer et al., 2020 など)。Schmidt et al. (2013) で示された理論計算では CO_2 光解離時の吸収断面積が CO の方が 200 ‰小さいことが示唆された。その結果を元に我々が行なった火星大気光化学計算では、CO の $\delta\ ^{13}C$ が CO_2 と比べおよそ-170 ‰減少するという ^{13}C の著しい枯渇が示された (Yoshida et al.,2023)。また、CO_2 の光解離時には炭素のみならず酸素も-100 ‰の分別が示唆されていることから (Schmidt et al., 2013)、炭素に加えて CO 中の酸素同位体比も光解離の指標となることが期待される。従来の観測研究は CO_2 に限定され、地表面で $\delta\ ^{13}C$ = 46 ± 4 ‰, $\delta\ ^{18}O$ = 48 ± 5 ‰ (Webster et al.,2013) に対して高度 70-90 km で $\delta\ ^{13}C$ = -3 ± 37 ‰、 $\delta\ ^{18}O$ = -29 ± 38 ‰, (Alday et al.,2021) が得られてきたのみであった。2018 年から稼働中の欧州火星探査衛星 ExoMars Trace Gas Orbiter (TGO) により高波長分解能を有する複数の赤外太陽掩蔽分光観測が実現し、CO_2 のみならず CO の同位体比を調べることが初めて可能になった。TGO に搭載される分光器 Atmospheric Chemistry Suite (ACS) では、火星年 34 年 Ls 166 – 349° と火星年 35 年 Ls = 141 – 366°、高度 10-50 km に対して、$\delta\ ^{13}C$ = − 160 ± 90 ‰ , $\delta\ ^{18}O$ = − 20 ± 110 ‰ (Alday et al., 2023) という値が得られた。また、我々の研究の初期結果でもある Aoki et al.,2023 では、TGO に搭載された赤外分光器 Nadir and Occultation for MArs Discovery (NOMAD) で、火星年 36 年 Ls = 182-205°、高度 30-50 km に対して $\delta\ ^{13}C$ = − 263 ± 132 ‰ と非常に強い負の同位体分別が観測された。本研究では Aoki et al.,2023 のデータ期間を火星年 36 年 Ls = 182-359° (2022/3/1 〜2022/12/24) に拡張し、また、新たに酸素同位体を導出することも試みた。

また私たちは CO のみならず、光解離による分別過程の議論の基準となる CO_2 の同位体比についても 50 km 以下の中低層大気をターゲットに、酸素同位体比 ($\delta\ ^{17}O$, $\delta\ ^{18}O$) の導出を開始している。先行研究による地表面の $\delta\ ^{18}O$ と 70 km 以上の値は一致しておらず、その間の高度域での酸素同位体比は未だ明らかにされていないため、本高度域の解析は CO_2 光解離による同位体分別の検証において非常に重要である。また、CO_2 解析高度域は、我々の CO の解析高度をカバーしており、先行研究においても CO_2 および CO の同位体比解析を同高度で行った例は存在しない。したがって、本研究における CO_2 同位体比の導出と CO の同位体比との比較は、中低層大気における CO_2 光解離での CO 同位体分別の初めての観測的証拠となることが期待される。

以上をまとめると、本研究の目的は、TGO に搭載された赤外分光器 NOMAD で得られた太陽掩蔽分光データを用いて、1) 中低層大気 CO 中の炭素・酸素同位体比を導出し、モデル結果が示す CO 同位体分別過程の検証すること、そして、2) 中低層大気 CO_2 中の酸素同位体比を導出し、CO の観測との比較から観測的に光解離の分別過程を検証することである。2) については、初期結果を本発表で報告する予定である。

解析には、CO には NOMAD の観測波長域 order183 から 186 (4112-4213cm^{-1}) の全スペクトル領域を、CO_2 には、order117 (2629-2650 cm^{-1})、order132 (2966-2990 cm^{-1})、および order141 (3168-3194 cm^{-1}) を使用した。リトリーバルには、最尤推定法 OEM (Rodgers, 2000) を用いて観測データに合う最適な変数を調べる放射伝達・反転解析コード ASIMUT (Vandaele et al., 2006) を用いた。この計算では、大気圧と CO_2 体積混合比の初期高度分布には GEM-Mars による予測値 (Daerden et al., 2019) を使用した。温度分布は、CO では同時取得された CO_2 吸収線による観測値 (Trompet

et al., 2023) を使用し、CO_2 では GEM-Mars による予測値を使用した。CO については $^{12}C^{16}O$ と $^{13}C^{16}O$、$^{12}C^{18}O$、CO_2 については $^{16}O^{12}C^{16}O$、$^{16}O^{12}C^{17}O$、$^{16}O^{12}C^{18}O$ の観測視線方向の積算量を変数とし、リトリーバルを各高度で取得されたスペクトルに対して独立に行った。

以下は、CO におけるデータ選定条件と結果である。高度 30〜50 km で得られたリトリーバル結果について、信頼性が検証中である CO 体積混合比 <1000 ppm 以下のデータは使用せず、かつ 3-sigma 以上の信頼度がある値のみを選定した。全高度域を加重平均した結果、同位体比とその標準偏差は、$\delta\ ^{13}C$ = -286 ± 175 ‰、$\delta\ ^{18}O$ = -188 ± 240 ‰となり、モデル予測と同様に大きな負の同位体分別が確認された。仮定した大気温度の不確定性に起因する誤差は大きいが、^{13}C の枯渇は十分示唆される結果となり、$\delta\ ^{18}O$ でも全高度域の加重平均の値は負となっている。この結果はモデル予測で示された CO_2 光解離による CO 同位体分別がこの本高度域で実際に起こりうることを観測的に証明するものである。また、この結果は ACS による観測とも傾向として一致しており、大きな不確定性を抱える同位体解析において、CO_2 光解離による同位体分別の確証性を高めるものとなった。

一方、CO_2 については、1 軌道についてテスト解析を行っている。現時点で $^{16}O^{12}C^{16}O$ のリトリーバルが正確に行えていないことが分かっており、私たちはその原因は温度を正確に定義できていないためであると考えている。温度による不確定性を最小限に抑えるため、今後は温度の同時リトリーバルも視野に入れながら解析を進めていく予定である。

R009-22
B 会場 ：9/27　AM2 （10:45-12:30）
11:15〜11:30

ひさき衛星によって観測された金星酸素・水素大気光の長期変動

#益永　圭 [1)], 能勢　千鶴 [2)], 土屋　史紀 [3)], 笠羽　康正 [4)]
([1] 宇宙研,[2] 東北大・理・惑星プラズマ大気,[3] 東北大・理・惑星プラズマ大気,[4] 東北大・理・惑星プラズマ大気

Long-term variations of oxygen and hydrogen airglow in the upper atmosphere of Venus as observed by Hisaki

#Kei Masunaga[1)],Chizuru Nose[2)],Fuminori Tsuchiya[3)],Yasumasa Kasaba[4)]
([1]Department of Earth and Planetary Science, Graduate School of Science, University of Tokyo,[2]Planetary Plasma and Atmospheric Research Center, Graduate School of Science, Tohoku University,[3]Planetary Plasma and Atmospheric Research Center, Graduate School of Science, Tohoku University,[4]Planetary Plasma and Atmospheric Research Center, Graduate School of Science, Tohoku University

Previous observations have shown that dust storms on Mars transport materials such as water vapor to the upper atmosphere and affect the hydrogen and oxygen escape from the Martian upper atmosphere (e.g., Chaffin et al., 2021, Masunaga et al., 2022). On the other hand, although the atmospheric escape such as hydrogen and oxygen from the upper atmosphere to space has been observed on Venus, the understanding of how materials are transported from the lower atmosphere to the upper atmosphere is not well understood.

Recent observations by the Hisaki telescope have revealed that the total amount of oxygen atoms in the upper atmosphere of Venus fluctuates by several percent with a period of about 4 days (Masunaga et al., 2015, 2017). In particular, model calculations show that on the morning side of Venus, atmospheric gravity waves propagate periodically to the upper atmosphere, inducing periodic transport of oxygen atoms (Nara et al., 2020), suggesting that the 4-day circulating middle atmosphere and the upper atmosphere dominated by day-night convection are coupled through atmospheric waves. In the Venusian middle atmosphere, Akatsuki and other spacecraft have observationally shown that wind speeds and mixing ratios in the Venusian cloud layer show long-term variations on long time scales of hundreds of days to decades (Kouyama et al., 2013, Marcq et al., 2013, Lee et al., 2019). Such long-term variations in the middle atmosphere which is coupled to the upper atmosphere would suggest that similar time-scale variations exist in the upper atmosphere, but long-term variations in the upper atmosphere of Venus on the scale of hundreds of days to years have not yet been investigated.

In this study, we analyzed the long-term dataset of OI 130.4 nm and HI Ly-β airglow of Venus obtained by the Hisaki space telescope for about 10 years. The results suggest that these airglow emissions not only vary with the solar activity but also have its own long-term cycle. We show that the total amount of oxygen and hydrogen atoms in the Venusian upper atmosphere fluctuates over a long period of time, and discuss the mechanisms driving this periodic variation based on past observations of the lower atmosphere.

これまでの観測により、火星では砂嵐等の下層大気で発生する現象が水蒸気などの物質を上層へ輸送し、火星上層大気からの水素・酸素の流出に影響を及ぼすことが示された (e.g., Chaffin et al., 2021, Masunaga et al., 2022)。一方、金星では上層大気から水素・酸素などの大気成分が宇宙空間への流出は観測されているものの、大気下層から上層へ物質がどのように輸送されているのか理解が進んでいない。

近年、ひさき衛星の観測により、金星上層大気中の酸素原子の総量が約 4 日周期で数 % 変動することが明らかになった (Masunaga et al., 2015, 2017)。特に、金星朝側では大気重力波が周期的に上層まで伝搬し、酸素原子の輸送が周期的に引き起こされることがモデル計算により示され (Nara et al., 2020)、4 日循環する中層大気と昼夜間対流が卓越する上層大気が大気波動を介して結合していることが示唆された。金星の中層大気に関しては、あかつき衛星等により金星の雲層における風速や物質の混合比が数百日から数十年という長い時間スケールで長期変動していることが観測的に示された (Kouyama et al., 2013, Marcq et al., 2013, Lee et al., 2019)。上層大気と結合する中層大気にこのような長期変動があれば、上層大気にも同様の時間スケールの変化が存在することが考えられるが、金星上層大気の数百日-年スケールの長期変動についてはまだ調べられていない。

そこで、本研究では、ひさき衛星が約 10 年にわたって観測した金星上層大気の酸素・水素大気光のデータを解析した。その結果、大気光は太陽紫外線強度や太陽活動に伴って変動するだけでなく、独自の長期的な周期を持って変動することが示唆された。本発表では、金星上層大気中の酸素原子や水素原子の総量が長期的に変動することを示し、この周期変動を駆動するメカニズムについて、過去の下層大気の観測をもとに議論する。

R009-23
B 会場 ：9/27　AM2 （10:45-12:30）
11:30〜11:45

#古林　未来 [1)], 鎌田　有紘 [1)], 黒田　剛史 [1)], 黒川　宏之 [2)], 青木　翔平 [3)], 中川　広務 [1)], 寺田　直樹 [1)]
([1] 東北大学大学院理学研究科,[2] 東京大学大学院総合文化研究科,[3] 東京大学大学院新領域創生科学研究科

Global effects of regolith properties on the subsurface ice distribution on Mars using a General Circulation Model

#Mirai Kobayashi[1)],Arihiro Kamada[1)],Takeshi Kuroda[1)],Hiroyuki Kurokawa[2)],Shohei Aoki[3)],Hiromu Nakagawa[1)],Naoki Terada[1)]
([1]Graduate School of Science, Tohoku University,[2]Graduate School of Arts and Sciences, College of Arts and Sciences,[3]Graduate School of Frontier Sciences, The University of Tokyo

The distribution and abundance of subsurface ice on present-day Mars are essential for understanding the environmental evolution of the hydrosphere. Exposed ice following meteorite impacts has been found in recent decades, suggesting the presence of subsurface ice in the shallow layers (Byrne et al., 2009; Dundas et al., 2008, 2014, 2023). Several numerical simulations have investigated the subsurface ice distribution, calculating the water vapor exchange between the shallow subsurface and the atmosphere. Previous studies have shown that surface albedo, thermal inertia, weather variables (e.g., atmospheric water vapor column abundance and atmospheric dustiness), and orbital parameters (e.g., obliquity and eccentricity) play important roles in the subsurface ice distribution (Mellon and Jakosky, 1993; Tokano, 2003; Schorghofer and Forget, 2012; Steele et al., 2017). However, soil properties (e.g., porosity, pore size, and specific surface area of the regolith for adsorption) have received less attention.

Here, we investigated the effects of soil properties on the simulated distribution and abundance of subsurface ice using our Mars General Circulation Model (Kuroda et al., 2005, 2013), coupled with a regolith scheme that has been developed based on Zent et al. (1993), Steele et al. (2017), and Jakosky et al. (1997). The regolith scheme considers the water vapor exchange between the regolith and the atmosphere and phase changes, including adsorption and condensation. Calculations were performed under different conditions of pore size (with globally uniform values of 10 and 100 um, and a globally inhomogeneous distribution diagnosed from thermal conductivity referring to Presley and Christensen, 1971), and porosity (with globally uniform values of 30, 40 and 50%, and a globally inhomogeneous distribution which has defined corresponding to grain size) for 30 years, starting from the initial condition of 3-5wt% of subsurface ice.

First, we found that the globally inhomogeneous pore size distribution increased the contrast of the subsurface ice distribution. The subsurface ice distribution is influenced by ground temperature and geothermal gradient, but also water vapor flux, which is controlled by the Knudsen diffusion coefficient. Pore size, one of the parameters determining the diffusion coefficient, is highly correlated with thermal conductivity. Therefore, the effects of thermal conductivity and pore size tend to overlap. When grain size is taken into account, the range of diffusion coefficients increases by up to an order of magnitude or more. Our results suggest that the setting of a globally uniform pore size of 10 um, which is used by previous studies (Bottger et al., 2005; Steele et al., 2017), would underestimate the amount of subsurface ice in the northern equatorial to mid-latitudes below several meters.

Second, the higher porosity accelerated the convergence of the calculations globally, and subsurface ice decreased in the northern hemisphere but increased in the southern hemisphere. This suggests that the southern hemisphere has a greater potential for subsurface ice accumulations than the northern hemisphere. However, it will adversely affect the amount of atmospheric water vapor if the porosity is inadequate. With a globally uniform porosity of 50%, the atmosphere became too wet. Our results suggest that 35-40% is suitable for near-surface porosity in terms of reproducing the water cycle on Mars.

This study suggests the possible significant influence of soil properties on the subsurface ice distribution. However, the long-term orbital climate forcing should be considered for quantitative discussion of subsurface ice distribution.

R009-24
B 会場 ：9/27　AM2 （10:45-12:30）
11:45〜12:00

#狩生　宏喜 [1)], 黒田　剛史 [1)], 今村　剛 [2)], 寺田　直樹 [1)],Vandaele　Ann Carine[3)]
([1] 東北大,[2] 東京大学,[3] ベルギー王立宇宙科学研究所

A study of the Venusian cloud structure and condensational gas distribution using a 1-D cloud microphysics model

#HIROKI KARYU[1)],Takeshi Kuroda[1)],Takeshi Imamura[2)],Naoki Terada[1)],Ann Carine Vandaele[3)]
([1]Tohoku University,[2]The University of Tokyo,[3]Belgian Institute for Space Aeronomy

Venus is completely shrouded by thick sulfuric acid clouds. The clouds significantly influence the distribution of condensational gas species, including H2O and H2SO4. The distributions of these gases are determined by a delicate balance among the efficiency of condensation into droplets, eddy transport, and chemical production/loss. It is important to understand the distribution of H2O vapor through these cloud-mediated processes because the H2O vapor abundance beneath the homopause regulates the diffusion-limited escape rate of hydrogen (Catling and Kasting, 2017), hence the history of water on Venus. Furthermore, H2SO4 vapor distribution is important for atmospheric chemistry above 80 km altitude, as suggested by Zhang et al. (2010). They argued that sulfur species, including SO, SO2, and SO3, could be generated from H2SO4 vapor provided by the upper haze layer. However, the transport process of these gaseous species and their interaction with the clouds are not well understood above the cloud top altitude.

To investigate Venusian cloud microphysics and its interaction with the background atmosphere, we developed a 1-D microphysics model based on Imamura and Hashimoto (2001). The model takes into account cloud microphysics and vertical transport of gaseous species (H2SO4 and H2O) as well as those of cloud particles. On top of the previous work, we extended the model top altitude from 70 km to 100 km. As a result of this enhancement, the model can now simulate the structure of the upper haze and the distribution of gaseous species above the main cloud layer. We also updated the sulfuric acid production rate profile in accordance with recent photochemical studies (Krasnopolsky, 2013), whose production peak altitude is located 5 km higher (˜66 km) compared to the previous work. Finally, we conducted cloud microphysics simulation using the abovementioned settings under different eddy diffusion profiles above the cloud top altitude (˜70 km).

The resulting cloud structure and the H2SO4 distribution around the cloud deck align closely with previous observations (e.g., Knollenberg and Hunten, 1980; Oschlisniok et al., 2021). The H2O profile above the cloud top agrees well with the past observation (e.g., Fedorova et al., 2009) within an observed range of eddy diffusion profiles. The updated H2SO4 production rate profile improved the H2O profile by altering the time scale of H2O loss due to chemical reactions and condensation. We also found that H2O abundance above the cloud top is highly sensitive to the eddy diffusion profile. Higher eddy diffusion results in an increased H2O abundance above the cloud top, as eddy transport becomes more efficient in supplying H2O compared to losses through chemical reactions and condensation. Furthermore, we observed an increasing concentration of H2SO4 with altitudes above 80 km within a wide range of eddy diffusion profiles, although it remains inadequate to account for the elevated SO2 concentration, as shown by Zhang et al. (2010). In our upcoming presentation, we aim to provide a more detailed investigation to gain a better understanding of the mechanisms that dictate the cloud structure and the distribution of gaseous species.

R009-25
B 会場 ：9/27　AM2 （10:45-12:30）
12:00〜12:15

高速回転球殻内の非弾性流体の熱対流の長時間積分

#佐々木　洋平 [1)], 竹広　真一 [3)], 石岡　圭一 [4)], 榎本　剛 [5)], 中島　健介 [6)], 林　祥介 [2)]
([1] 北海道情報大 情報メディア学部,[2] 神戸大・理・惑星/CPS,[3] 京都大学数理解析研究所,[4] 京都大学大学院理学研究科地球惑星科学専攻,[5] 京都大学防災研究所,[6] 九州大学 大学院理学研究院 地球惑星科学部門

Long-time integration of thermal convection of anelastic fluid in a rapidly rotating spherical shell

#Youhei Sasaki[1)],Shin-Ichi Takehiro[3)],Keiichi Ishioka[4)],Takeshi Enomoto[5)],Kensuke Nakajima[6)],Yoshi-Yuki Hayashi[2)]
([1]Faculty of Information Media, Hokkaido Information University,[2]Department of Planetology/Center for Planetary Science, Graduate School of Science, Kobe University,[3]Research Institute for Mathematical Sciences, Kyoto University,[4]Department of Earth and Planetary Sciences, Kyoto University,[5]Disaster Prevention Research Institute, Kyoto University,[6]Department of Earth and Planetary Sciences, Faculty of Sciences, Kyushu University

The banded structures composed of alternating zonal jets observed in the surface atmospheres of Jupiter and Saturn have attracted many researchers in planetary atmospheric sciences. However, their satisfactory physical understandings have not been obtained yet. In this study, we perform massive parallel numerical experiments treating both small scale convection and planetary scale flows simultaneously, reveal fine structures of turbulent motions which have not yet been resolved by the previous numerical models so far, and try to illustrate dynamical origin of global scale structures of surface flows of Jovian planets.

One of the model categories explaining the surface patterns of the gas giant plants is so called “deep” model, where the concerned fluid motion is assumed as thermal convection in a rapidly rotating spherical shell whose thickness is comparable to the radius of the planet. The early models of this category could produce equatorial prograde flows rather easily, while they were unable to generate alternating jets in mid- and high-latitudes. Heimpel and Aurnou (2007) tried to solve this difficulty by considering a thinner spherical shell model than those used in the previous studies, and argued that the equatorial prograde zonal jets and alternating zonal jets in mid- and high-latitudes can be produced simultaneously when the Rayleigh number is sufficiently large and convection becomes active even inside the tangent cylinder. Since then, substituting the Boussinesq system of Heimpel and Aurnou (2007) with the more realistic anelastic system, several successive studies have been performed to explain the banded structure of the gas giants.

However, in Heimpel and Aurnou (2007) and the succeeding studies, longitudinal symmetries were assumed to reduce the computational domains to be not the whole but some sectorial regions of the spherical shells. Moreover, they introduced hyper viscosity in order to save the numerical resources and to compensate for the model resolutions. Although such an artificial dissipation process may influence the structures of the global flow field, the effects of hyper viscosity have not been examined so far. We have therefore performed, with the Boussinesq system, long-time numerical simulations of thermal convection in a thin rotating spherical shell in the full global domain. As a result, we found that multiple zonal jets in mid- and high-latitudes in each hemisphere merged into a single prograde jet with time, and the banded structure in mid- and high-latitudes disappeared.

We expect the same long-time evolution as that of the Boussinesq system may occur in the anelastic system. Therefore, in this study, we perform long-time numerical simulations of thermal convection in a thin rotating spherical shell in the full global domain with the anelastic system by following the set up of Heimpel et al. (2015), which is the most realistic and highest-resolution simulation of Jovian-type atmospheric circulation using the anelastic system. We focus on whether the banded structure disappears after a long time due to the merger of multiple jets in mid- and high-latitudes. For comparison, we also perform the numerical calculation with the 4-fold longitudinal symmetry, which is adopted in Heimpel et al. (2015). Our results show that a trend toward the merger of alternating jets in the mid- and high-latitudes can be observed, and the kinetic energy is still increasing and has not yet reached a statistical equilibrium. Since the integration time is still 1000 rotations, which is about a half of that of our numerical experiments with the Boussinesq system where disappearance of banded structure was observed, we will continue to carry out time integration and observe the transitions and properties of the banded structure.

木星型惑星 (木星・土星) 表層大気の力学的な特色である縞状パターンはこれまでに多くの大気科学研究者の関心を引いてきたが，これらの特徴を矛盾なく整合的に説明できる満足な力学的描像と理解は得られてはいない．本研究は全球規模から微細規模対流までにわたる空間スケールを統一的にあつかう大規模数値計算を実行し，従来の数値モデルでは表現できなかった微細規模の対流や乱流の構造を解像し，木星型惑星大気に見られる表面流の大規模構造の力学的成因を解明することを目指している．

木星型惑星大気の縞状パターンを説明する有力なモデルカテゴリーの一つは流体層の厚さが惑星半径に匹敵する一連の「深い」モデルである．高速回転する球殻中の熱対流が引き起こす帯状流により表層の縞状構造を説明することを試みるこのモデルでは，赤道域の順行するジェットは容易に生成されるものの，中高緯度の交互に表われるジェットの生成が困難であった．「深い」モデルのこの問題に対して Heimpel and Aurnou (2007) (以下,HA2007) は，球殻の厚さを従来の研究で用いられて来たよりも薄くした数値実験を行い，レイリー数が十分大きく内球接円筒での対流活動が活発な場合に赤道域の順行流と中高緯度の交互に現われる狭いジェットが共存して発現できることを示した．HA2007 ではブシネスク流体を用いていたが，より現実的と思われる非弾性近似を用いての同様な研究が縞状構造生成を説明するべく現在に至るまで続けられている．

しかしながら，これら一連の研究では経度方向に対称性を仮定しており全球の一部のセクター領域の運動しか解いていない．加えて高速回転中の熱対流を解像するために超粘性を導入し水平高解像成分の散逸を人工的に高めている．散逸過程の性質の意図的な変更は生成される流れ場に大きく影響していることが予想されるものの，その検証はきちんとなされていない．そこで我々は HA2007 の設定のもとでの薄い回転球殻内のブシネスク熱対流の長時間数値計算を全球領域で遂行してきた．その結果，時間とともに中高緯度において複数の東西ジェットが融合して 1 本の順行ジェットとなり，中高緯度の縞状構造が消失してしまうことを見出した．

本研究では，非弾性系でもブシネスク系と同様な長期時間発展が起こるのではないかと想定し，非弾性系での最も高解像な計算である Heimpel et al. (2015) の設定での薄い回転球殻内の熱対流の全球領域での長時間数値計算を試みた．中高緯度において複数ジェットが長時間後に融合し縞状構造が消失していくのか否かが注目点である．比較のため, Heimpel et al. (2015) と同様の経度方向 4 回対称性を課した計算も並行して実行した．いずれの場合も初期に赤道域の強い幅広の順行ジェットと中高緯度に交互に向きが入れ換わる複数の幅狭のジェットが出現し，木星型大気の表層パターンに似た縞状の帯状風分布が観察された．時間とともに中高緯度のジェットが融合されつつある傾向がみられ，運動エネルギーはまだ増加しており，統計的平衡状態に達していない．現時点では，ブシネスク系にて縞状構造の消失が観察された半分程度の積分時間である 10000 回転にしか計算が到達しておらず，引き続き時間積分を遂行し，縞状構造の遷移や性質を観察していく予定である．

R009-26
B 会場 ：9/27　AM2 （10:45-12:30）
12:15〜12:30

ファイバーとファイバーカップラーを用いた惑星大気観測用中間赤外ヘテロダイン分光器の開発

#大畑　元 [1)], 中川　広務 [2)], 笠羽　康正 [1)], 村田　功 [3)], 片桐　崇史 [4)], 平原　靖大 [5)], 松浦　祐司 [6)], 山崎　敦 [7)]
([1] 東北大・理,[2] 東北大・理・地球物理,[3] 東北大院・環境,[4] 富山大・工,[5] 名古屋大・環境,[6] 東北大・医工,[7]JAXA/宇宙研

Development of mid-IR heterodyne spectrometer with fibers and a fiber coupler for the observation of planetary atmospheres

#Hajime Ohata[1)],Hiromu Nakagawa[2)],Yasumasa Kasaba[1)],Isao Murata[3)],Takashi Katagiri[4)],Yasuhiro Hirahara[5)],Yuji Matsuura[6)],Atsushi Yamazaki[7)]
([1]Planetary Plasma and Atmospheric Research Center, Graduate School of Science, Tohoku University,[2]Department of Geophysics, Graduate School of Science, Tohoku University,[3]Department of Environmental Studies, Graduate School of Environmental Studies, Tohoku University,[4]Faculty of Engineering, University of Toyama,[5]Graduate School of Environmental Studies, Nagoya University,[6]Graduate School of Biomedical Engineering, Tohoku University,[7]The Institute of Space and Astronautical Science, Japan Aerospace Exploration Agency

Fiber optics enables significant improvements of optical instruments to reduce their size and mass achieving higher efficiency and stability. It also enables the simultaneous measurement of multiple targets that can only be accessed through fibers. All of these are essential for onboard instruments for planetary orbiters, landers, rovers, aircraft, etc. This technology has been widely applied in visible and is beginning to be adopted in near-IR. In mid-IR which also has rich spectral information, the progress was limited by transmission materials for fibers. Recent hollow fiber technology enables to achieve higher transmission efficiency. We have applied this hollow fibers to mid-IR laser heterodyne spectrometer.

Mid-IR laser heterodyne spectroscopy is a method in which the light from the target is mixed with the light from a local oscillator (LO). Its frequency is down-converted to the intermediate frequency. This method can achieve a high wavelength resolution of $\lambda/d\lambda > 1{,}000{,}000$ around 10 μm (in frequency, df $<$30 MHz around 30 THz). This has enabled to resolve planetary wind velocities with a resolution of several 10 m/s and achieved unique results such as the wind changes associated with global dust storms on Mars and the super-rotation of Venus and Titan. However, precise convention of two optical paths is needed, so high-precision optical-axis adjustment with many mirrors makes the spectrometer large and complex., so iIt was unsuitable for instruments aboard spacecraft. We have tried to solve this problem by utilizing a hollow fiber that has high transmittance in the mid-IR region.

In this presentation, we report the feasibility test results of a laser heterodyne spectrometer in the mid-IR region using a hollow fiber and a fiber coupler. (1) For the hollow fiber, transmission efficiencies of $>$85%/m were achieved for both CO2 lasers and quantum cascade lasers, and transmission efficiency of 89.6%/m was achieved for sunlight, i.e., incoherent natural light. It was also confirmed that heterodyne spectroscopy of lights from black body and CO2 laser through fibers using a beam splitter can achieve the same sensitivity as that without fibers (Nakagawa et al., Applied Optics, 2023). (2) For hollow fiber couplers, we have demonstrated that heterodyne spectroscopy of CO2 lasers and quantum cascade lasers with a fiber coupler is as sensitive as the system with a beam splitter (Nakagawa et al., Applied Optics, 2023). In addition, the heterodyne spectrometer using a CO2 laser as the LO showed system noise temperature was the same as the quantum noise limit. System noise temperature was calculated by the Y-factor method, which uses the ratio of spectral power of black bodies that has two different temperatures 673 K and 293 K.

With these results, we have shown for the first time that it is possible to construct the heterodyne spectrometer using fibers and a hollow fiber coupler. Although these results were obtained with a laboratory system, we are now assembling a portable heterodyne spectrometer attached to a telescope. This system will be used for the test observations of the Venusian atmosphere using the Hitomi telescope at Sendai astronomical observatory in July 2023. The observation targets CO2 absorption around 10.3 μm at limb and calculates mesospheric wind velocity in the Venusian atmosphere by Doppler shift.

R009-27
B 会場 ：9/27　PM1 （13:45-15:30）
13:45〜14:00

#Nakagawa Hiromu[1)],Barucci Maria Antonietta[2)],Iwata Takahiro[3)],Nakamura Tomoki[4)],Tsuchiya Fuminori[1)],Reess Jean-Michel[2)],Bernardi Pernelle[2)],Fornasier Sonia[2)],Doressoundiram Alain[2)],Sawyer Eric[5)],Le Du Michel[5)],Piou Veronique[5)],Pons Nathalie[5)],Donny Christophe[5)],Mathe Christophe[2)],Kurokawa Hiroyuki[6)],Matsuoka Moe[7)],Aoki Shohei[8)]
([1] 東北大・理・地球物理,[2] パリ天文台,[3] 宇宙航空研究開発機構・宇宙科学研究所,[4] 東北大・理・地学,[5] フランス国立宇宙研究センター,[6] 東京大学,[7] 産業技術総合研究所,[8] 東京大学・新領域創成科学研究科

Remote sensing of near infrared spectral maps on Phobos, Deimos, and Mars by an imaging spectrometer MIRS onboard MMX

#Hiromu Nakagawa[1)],Maria Antonietta Barucci[2)],Takahiro Iwata[3)],Tomoki Nakamura[4)],Fuminori Tsuchiya[1)],Jean-Michel Reess[2)],Pernelle Bernardi[2)],Sonia Fornasier[2)],Alain Doressoundiram[2)],Eric Sawyer[5)],Michel Le Du[5)],Veronique Piou[5)],Nathalie Pons[5)],Christophe Donny[5)],Christophe Mathe[2)],Hiroyuki Kurokawa[6)],Moe Matsuoka[7)],Shohei Aoki[8)]
([1]Department of Geophysics, Graduate School of Science, Tohoku University,[2]LESIA, CNRS, Observatoire de Paris, Meudon, France,[3]ISAS/JAXA,[4]Department of Earth Science, Graduate School of Science, Tohoku University,[5]CNES, Toulouse, France,[6]The University of Tokyo,[7]The National Institute of Advanced Industrial Science and Technology,[8]Graduate School of Frontier Sciences, The University of Tokyo

Martian Moon eXploration (MMX) is the first sample return mission from the Martian moon, Phobos, planned by JAXA (Kuramoto et al., 2022). The MMX will be launched in 2024, and stay at circum-Mars orbits for 3 years (2025-2028), bringing back samples (>10 g) from Phobos return to Earth in 2029. The MMX infrared spectrometer (MIRS) is an imaging spectrometer onboard MMX, developed by LESIA-Paris Observatory in collaboration with four other French laboratories, collaboration and financial support of CNES and close collaboration with JAXA and Japanese colleagues. MIRS will remotely provide near-infrared (0.9-3.6 micron) spectral maps of Phobos and Deimos containing compositional diagnostic spectral features (Barucci et al., 2021). The derived spectra will be used to analyze the surface composition and to support the landing site selection.

One of the major mission goals is to understand the origin of the two moons, which will provide important constrains on planetary formation and on the material transport in the region connecting the inner and outer solar system. MIRS will acquire spectra of Phobos at a spatial resolution of about 20 m during the Medium altitude survey (at altitude around 60 km) and of Deimos at spatial resolution of 100 m (at a distance of 300 km during the multi-flybys). The high signal to noise ratio (>100 up to 3.2 micron) and the unprecedented spatial resolution achieved by MIRS will contribute to characterize the detailed surface composition material of Phobos and Deimos to investigate the local heterogeneity associated with the different surface morphology. The similarity to carbonaceous chondrites with the possible presence of hydrous minerals (features at 2.7-2.8 micron, water (ice)) and/or organic matter (3.3-3.5 micron) would imply a capture origin, while the presence, even if partially, of high-temperature phase materials representing a mixture from crust and mantle of Martian silicates would indicate a giant impact origin.

Thanks to its unique orbit near the equatorial plane on the quasi satellite orbit (QSOs), MIRS can also offer the first opportunity to probe the atmospheric processes of mesoscale to synoptic scale in the Martian atmosphere, such as horizontal water transport including surface-atmosphere interaction, clouds formation, and dust storm evolution etc. The MMX will have a 7-hr orbit around Mars, allowing to complete a global coverage. The well-controlled scanner system of MIRS enables the wide spatial coverage at low-mid-latitudes by combining with the spacecraft slewing maneuvers in hourly time-scale. These spectra provide the atmospheric species (CO2, H2O, CO) and aerosols (dust and clouds) to reveal the rapid transport processes with relatively high spatial resolution (typically 2-5 km) over a wide coverage. Owing to the unprecedented high-frequent and multi-spectral maps by MIRS on Mars, thousands to million spectra in a single orbit will be obtained, and need to be retrieved in an appropriate time manner.

In this paper, these planned observations, current status of data pipelines, Japanese contributions will be presented, with possible collaborations with other MMX instruments, sample analysis, and with other missions by MAVEN, MEx, and EMM.

R009-28
B 会場 ：9/27　PM1 （13:45-15:30）
14:00〜14:15

OMEGA/Mars Expressによって観測されたMY27-29における火星表面圧力分布の季節変動

#風間　暁 [1,2], 笠羽　康正 [1], 青木　翔平 [2], 中川　広務 [1], 小郷原　一智 [3], 今村　剛 [2], 佐藤　隆雄 [4], 黒田　剛史 [1]
([1] 東北大学,[2] 東京大学,[3] 京都産業大学,[4] 北海道情報大,[5] 情報大,[6] 東北大・理

Seasonal variation of surface pressure distribution on Mars in MY27-29 observed by OMEGA/Mars Express

#Akira Kazama[1,2],Yasumasa Kasaba[1],Shohei Aoki[2],Hiromu Nakagawa[1],Kazunori Ogohara[3],Takeshi Imamura[2],Takao M Sato[4],Takeshi Kuroda[1]
([1]Tohoku University,[2]University of Tokyo,[3]Kyoto Sangyo University,[4]Hokkaido Information University,[5]Hokkaido Information University,[6]Department of Geophysics, Tohoku University

On Mars, dust heats the atmosphere, driving various meteorological phenomena such as thermal tides and global dust storms, but the mechanisms of these phenomena are not understood. Surface pressure is an important physical parameter to understand these meteorological phenomena, however, our current understanding of the global distribution of surface pressure on Mars is limited to specific locations sampled by landers and a few remote sensing observations from orbiters. Unlike single-point lander observations, remote sensing observations can retrieve the spatial distribution of surface pressure and its variability over a wide area. Forget et al. (2007) and Spiga et al. (2007) retrieved surface pressure distribution from the initial observations of the Mars Express (MEx) onboard near-infrared imaging spectrometer OMEGA, conducted from January 2004 to November 2005, and detected fluctuations that were thought to originate from atmospheric gravity waves. Since then, retrievals of surface pressure distribution by remote sensing observations have not been reported, and OMEGA has over three years of analyzable data. Therefore, we aim to retrieve surface pressure from long-term remote sensing observations over the planet and to investigate the generation of thermal tidal waves, atmospheric gravity waves, and global dust storms from surface pressure fluctuations. For that, we first developed a fast and accurate surface pressure retrieval tool from orbiter. We then used the retrieval tool to analyze orbiter data from multiple Martian years to investigate the seasonal variation of surface pressure. In this presentation, we summarize the evaluation of the retrieval tool and report on the seasonal variation of surface pressure distribution during Mars years 27-29.

We used data observed by OMEGA/MEx from January 2004 to March 2010; short wave infrared (SWIR) channel has a wavelength range of 0.93-2.65 μ m and a wavelength resolution of 13 nm, covering three Mars years 27-29 (March 2004 to October 2009).

There are more than tens of thousands of observation points in one orbit, and retrieval of surface pressure requires both high speed and high accuracy. This study uses a fast retrieval method by using a look up table (LUT) (Forget et al., 2007). Two methods were attempted for retrieval: a new method that compares the equivalent width of the CO2 absorption band between the observed and LUT spectra (equivalent width method), and a fitting method that uses all 25 observed spectra within 1.8-2.2 μ m, including the CO2 absorption band (fitting method).

Absolute and relative values of the retrieved surface pressure were evaluated from these two methods. Absolute values were evaluated by comparing them with the surface pressure retrieval results of a previous study (Forget et al., 2007) at three specific sites (Hellas Basin, Cruse Plain, and Terra Meridiani). Absolute differences ranged from -1.2% to +2.7% for the equivalent width method and from -2.3% to -0.1% for the fitting method, both within the error range (˜5%) and in agreement with observations from previous studies. Relative values were evaluated by comparing surface pressures in the same area obtained at close intervals (3 days). The relative accuracy (3 σ) between locations was ˜± 20 Pa (± 2.5%) for the equivalent width method and ˜± 15 Pa (± 2.0%) for the fitting method, both of which were sufficient for the analysis of meteorological phenomena (e.g., fluctuation of thermal tidal wave is expected to be ˜5% at surface pressure), which was the objective of this study.

Therefore, we applied the faster equivalent width method (more than 400 times faster than the fitting method) to about 4300 OMEGA orbits data during Mars years 27-29 and retrieved the seasonal variation of the surface pressure. It was confirmed that in each year, surface pressure increased in the northern hemisphere spring and fall and decreased in the northern hemisphere summer and winter. This is caused by seasonal condensation and sublimation of CO2 into the polar cap and is consistent with observations from multiple landers (Zurek et al., 1992).

Using these data, we are attempting to detect thermal tidal waves by referring to the Mars climate database version 6.1 （Forget et al., 1999; Millour et al., 2018） and separating seasonal and local time variability.

MMX (Martian Moons eXploration), scheduled for launch in FY2024, will be equipped with a near-infrared spectroscopic imager MIRS（Barucci et al., 2021）, which has the same wavelength range and resolution as OMEGA and can observe a wide area at once (˜20x40 deg, more than 80 times the field of view of OMEGA) with time resolution of less than 1 hour. By

applying our retrieval tools to MIRS, we expect to be the first in the world to visualize global surface pressure distribution and variation（Ogohara et al., 2022）.

火星では、ダストによる大気加熱によって、顕著な熱潮汐波や全球を覆う砂嵐などの様々な気象現象が引き起こされているが、それらの発生・発達メカニズムは十分に理解されていない。気象現象を理解する上で地表面圧力は重要なパラメーターであるが、これまでの研究は、着陸機による特定地点と非常に限られた周回探査機からのリモートセンシング観測のみである。リモートセンシング観測は、着陸機の一点観測と異なり、地表面圧力の空間分布やその変動を広域にわたり導出できる。Forget et al. (2007) および Spiga et al. (2007) は、Mars Express（MEx）に搭載されている近赤外分光撮像装置 OMEGA の初期観測データ（2004 年 1 月から 2005 年 11 月）のうち 29 軌道で地表面圧力分布を導出し、大気重力波起源と考えられる変動を検出した。しかしこれ以降は、周回探査機を利用した地表面圧力分布の導出は報告されておらず、OMEGA だけでも 3 火星年（MY）分以上の解析可能データが蓄積されている。

本研究の目的は、長期間のリモートセンシング観測データから地表面圧力を導出し、その変動から熱潮汐波や大気重力波、そして全球を覆う砂嵐のメカニズムを理解することである。これに向けて、周回探査機の観測データから高速かつ高精度な地表面圧力リトリーバルツールの開発を行った。さらに、開発したリトリーバルツールを用いて複数の火星年における周回探査機のデータを解析し、地表面圧力の季節変動を調べた。本発表では、リトリーバルツールの性能を評価するとともに、MY27-29 の地表面圧力分布の季節変動について報告する。

本研究は、OMEGA/MEx の近赤外チャンネル（SWIR: 波長範囲 0.93-2.65 μ m、波長分解能 13 nm）によって観測された MY27-29（2004 年 3 月から 2009 年 10 月に約 8100 軌道の観測）を網羅する 2004 年 1 月から 2010 年 3 月までの観測データを使用した。

1 軌道あたりの観測スペクトルは数万点以上あり、地表面圧力の導出には高速かつ高精度を両立する必要がある。本研究は、Look up table(LUT) を使用（Forget et al., 2007）することで高速にリトリーバルする手法を用いた。リトリーバルには、CO2 吸収帯の等価幅を比較する新しい手法（等価幅法）と、CO2 吸収帯を含む 1.8-2.2 μ m 内の 25 点のスペクトルを比較する従来の手法（フィッティング法）を用いた。

この 2 手法から導出された地表面圧力について、絶対値と相対値の評価を行った。絶対値の評価は、特定 3 地点（ヘラス盆地、クリュセ平原、Terra Meridiani）における先行研究（Forget et al., 2007）の地表面圧力リトリーバル結果と比較することで行った。絶対値の差が、等価幅法では-1.2% から +2.7%、フィッティング法では-2.3% から-0.1% となり、両者とも誤差範囲内（˜5%）で先行研究の観測結果と一致した。相対値の評価は、短期間（3 日）で取得された同一地域の地表面圧力の比較で行った。地点間での相対精度（3 σ）は、等価幅法では˜± 20 Pa(± 2.5%)、フィッティング法では˜± 15 Pa(± 2.0%) となり、両者とも火星気象現象の解析（例：熱潮汐波の振幅で、地表面圧力は˜5% 程度）に十分な結果となった。

そこで、より高速な等価幅法（フィッティング法の 400 倍以上）を、MY27-29 における OMEGA の約 4300 軌道の観測データに適用し、地表面圧力の季節変動を導出した。この結果、地表面圧力は各年で北半球春・秋頃に地表面圧力が上昇し、北半球夏・冬頃に地表面圧力が減少することが全球にわたって確認された。これは季節に応じて CO2 大気が極冠に凝結し、また大気中に昇華することで解釈でき、複数の着陸機による観測事実とも概ね整合的である（Zurek et al., 1992）。これらのデータを用いて、Mars Climate Database ver. 6.1（Forget et al., 1999; Millour et al., 2018）を参照し、地表面圧力の季節変動と地方時変動の切り分けによって、熱潮汐波の検出を試みている。

本手法は、2024 年度に打ち上げ予定の MMX(Martian Moons eXploration) に搭載される近赤外分光撮像装置 MIRS（Barucci et al., 2021）への適用を目指している。MIRS は OMEGA と同等の波長範囲と波長分解能で、1 時間以内の時間分解能で一度に広域（˜20 × 40°、OMEGA の視野の 80 倍以上）な観測が可能である。我々のリトリーバルツールを MIRS へ適用し、世界初の広域表面圧力分布・変動の可視化を実現する（Ogohara et al., 2022）。

R009-29
B 会場 ：9/27　PM1 （13:45-15:30）
14:15〜14:30

金星雲頂に見られるメソスケールの構造の時間発展

#松井　龍郎[1)], 今村　剛[2)], 佐藤　毅彦[3)], 佐藤　隆雄[4)], 山崎　敦[5)]
([1] 東京大学,[2] 東京大学,[3] 宇宙研,[4] 情報大,[5]JAXA/宇宙研

Temporal Evolution of Mesoscale Structures seen at the Venusian Cloud Top

#Tatsurou Matsui[1)],Takeshi Imamura[2)],Takehiko Satoh[3)],Takao M Sato[4)],Atsushi Yamazaki[5)]
([1]Graduate school of Science ,The University of Tokyo,[2]Graduate School of Frontier Sciences, The University of Tokyo,[3]Institute of Space and Astronautical Science, Japan Aerospace Exploration Agency,[4]Hokkaido Information University,[5]The Institute of Space and Astronautical Science, Japan Aerospace Exploration Agency

Venusian cloud images show mesoscale cellular structures at the cloud tops. AKATSUKI's Ultraviolet Imager (UVI) and the 2-μm camera (IR2) take a series of images every two hours, allowing us to see the temporal evolution of the cellular structure. The 365-nm channel of UVI provides the spatial distribution of the unidentified UV absorbers, and the 2.02-μm channel of IR2 provides the cloud top altitude. The purpose of this study is to investigate the origin and mechanism of mesoscale atmospheric dynamics at the cloud tops by analyzing the temporal evolution of cellular structures using 365nm and 2.02 μm images. We extracted 6 sets of continuous observations composed of 8 pairs of 365-nm and 2.02-μm images, and classified them into two groups; one is for cellular structures developing over time and the other for no development. For each data set, we applied a high-pass filter to each image in order to pick out mesoscale structures, and then calculated the correlation coefficient between each 365-nm image and the corresponding 2.02-μm image taken at approximately the same time to evaluate the growth and decay of cloud morphology common to these wavelengths. Correlation coefficients were also calculated between each 365 nm image and the 2.02 μm image taken 2-4 hours before or 2-4 hours after. The results showed that, when the cellular structures are evolving, the correlation coefficients between each 365-nm image and the 2.02 μm image taken 2-4 hours later tend to be higher than those between the pairs taken at the same time. On the other hand, when the cellular structures do not evolve with time, there is no significant difference between the correlation coefficients. This can be interpreted as: the morphology of the unidentified UV absorber observed at 365 nm appears first, and then a similar morphology of the cloud top altitude observed at 2.02 μm develops. We can propose a hypothesis that the spatial distribution of the unidentified UV absorbers causes an inhomogeneous solar heating, which results in an inhomogeneous temperature distribution, and then mesoscale atmospheric motions are caused to create a morphology of the cloud top altitude.

金星探査機あかつきで撮影された金星雲画像には、雲頂にメソスケールのセル状構造が確認されている。あかつきに搭載された紫外線および赤外線カメラは 2 時間おきに連続した画像を撮影しているため、セル状構造の発展の様子を見ることができる。365nm の紫外画像から未同定の紫外線吸収物質の空間分布を、2.02 μmの赤外画像から雲頂高度を得られる。本研究は 365nm 画像と 2.02 μm画像を用いてセル状構造の時間変化を調べることで、雲頂に起こるメソスケールでの大気運動の起源とメカニズムを明らかにすることを目的としている。8 枚の 2 時間おきに連続した 365nm 画像と 2.02 μm 画像 6 日分を、セル状構造が時間経過で発達する日としない日に分類した。それぞれの分類で、画像にハイパスフィルタをかけてメソスケールの構造のみを取り出した後、ある時刻の 365nm 画像と同時刻および数時間ずらした時の 2.02 μm画像の相関係数を計測した。結果は、セル状構造が時間発展していく時には 365nm 画像と数時間後の 2.02 μm画像の相関係数が同時刻での相関係数よりも高くなった。一方でセル状構造が発展しない時にはそれらの相関係数に有意な差は見られなかった。これは波長 365nm で観測する未同定の紫外線吸収物質が先にセル状構造を発展させ、波長 2.02 μmで観測する雲頂高度がそれに付随して後からセル状構造を発展させると解釈できる。得られる一つの仮説として未同定の紫外線吸収物質が空間的に分布していることで太陽光加熱の空間分布とそれによる温度分布を生じ、メソスケールでの大気運動を引き起こすことで雲頂高度に表れていると考えられる。

R009-30
B 会場 ：9/27　PM1 （13:45-15:30）
14:30〜14:45

LIR の長期観測から得られた金星雲上層での平均温度と熱潮汐波の変動

#神山　徹 [1)], 今井　正尭 [2)], 田口　真 [3)], 二口　将彦 [4)], 堀之内　武 [5)], 村上　真也 [6)], 今村　剛 [2)]
[1 産総研,[2 東京大学,[3 立教大・理・物理,[4 東邦大学,[5 北海道大学,[6JAXA

Variations in mean temperature and thermal tides in upper cloud layer of Venus obtained from LIR long-term observation

#Toru Kouyama[1)],Masataka Imai[2)],Makoto Taguchi[3)],Masahiko Futaguchi[4)],Takeshi Horinouchi[5)],Shinya Murakami[6)],Takeshi Imamura[2)]
[1National Institute of Advanced Industrial Science and Technology,[2The University of Tokyo,[3Department of Physics, College of Science, Rikkyo University,[4Toho University,[5Hokkaido University,[6Japan Aerospace Exploration Agency

Recently, there have been several observational evidence of long-term Venusian climate change. For instance, Lee et al (2019) indicated significant variations in UV albedo (more than twice, 20 % to 40 %) and zonal wind speed (more than 30 m s-1) with decadal scale, and Lee et al. (2020) also suggested a 630-day variation in UV albedo. Khatuntsev et al (2023) suggested 12-year variation in zonal wind speed. Since these variations have huge amplitudes and are global scale, they should be worth to be considered for understanding global-scale dynamic momentum/material transportation in Venusian atmosphere.

In this study, we focused on long-term temperature data obtained by Longwave Infrared camera (LIR) onboard Akatsuki, which has observed Venus for more than 7 years, because such variations should exist in temperature of Venusian atmosphere which is a fundamental atmospheric parameter. We divided LIR data into specific emission angle ranges to obtain a vertical profile of temperature by utilizing LIR's sensing altitude dependence on emission angle, then we conducted a sliding window analysis by averaging one Venusian-year LIR data in terms of local time and latitude with a short interval to obtain temporal variations in both mean temperature and thermal-tide structure. From the result, there was a clear quasi-periodical variation in diurnal tide-amplitude in mid-high latitudes whose time scale was 600 − 800 days, while a similar time-scale variation was also confirmed in mean temperature in low-mid latitudes although the amplitude was faint (less than 1 K). Because of the time-scale similarity, the UV albedo variation with a time scale for 630 days might relate these variations.

R009-31
B 会場 ：9/27　PM1 （13:45-15:30）
14:45〜15:00

#郭　祝安 [1)], 今村　剛 [2)], 田口　真 [3)], 神山　徹 [4)], 佐藤　隆雄 [5)]
[(1] 東京大学,[(2] 東京大学,[(3] 立教大・理・物理,[(4] 産総研,[(5] 情報大

Characteristics of Venusian gravity waves inferred from thermal infrared cloud images

#Zhuan Guo[1)],Takeshi Imamura[2)],Makoto Taguchi[3)],Toru Kouyama[4)],Takao M Sato[5)]
[(1]Graduate School of Science, The University of Tokyo,[(2]Graduate School of Frontier Sciences, The University of Tokyo,[(3]Department of Physics, College of Science, Rikkyo University,[(4]National Institute of Advanced Industrial Science and Technology,[(5]Hokkaido Information University

Although Venus is a terrestrial planet sharing similar size and mass with the Earth, the atmospheric circulation of Venus is yet to be fully understood. Above the surface, the sulfuric acid clouds are located at about 48-70 km altitudes, covering the entire surface. At the cloud-top level, the global zonal wind shows predominantly westward with a maximum speed of about 100 m s^{-1}, namely superrotation, which is about 60 times faster than the rotation of Venus. Gravity waves are thought to play crucial roles in the momentum balance of the superrotation.

However, the details of the gravity waves on Venus remain unknown. In this study, we are developing an algorithm to retrieve the amplitude of gravity waves based on the observation from the Longwave Infrared Camera (LIR) on board Akatsuki. Infrared radiation and other physical quantities will be characterized in the presence of gravity waves. Comparing to the analysis of short-vertical wavelength gravity waves using radio occultation data, we anticipate providing a new perspective for studying the gravity waves with longer vertical wavelengths.

In this study, the infrared radiance was calculated based on line-by-line radiative transfer codes following Sato et al.[1]. We adopted temperature and pressure profiles for equatorial regions ($<30^o$) from The International Venus Reference Atmosphere[2] and the cloud particle density model from Haus et al.[3]. The extinction cross-section of cloud particles was calculated by the Mie Scattering model with parameters corresponding to 75% H_2SO_4 aerosol particles. Gaseous absorption includes H_2O, CO_2, CO, SO_2, HF, and OCS. Their vertical profiles were taken from Marcq et al.[4], and spectral line data was taken from the HITRAN2020 database[5].

Responses of the atmosphere to gravity waves were described by the linear theory [6]. The influence of gravity waves on the infrared radiance includes perturbations of temperature and particle density. Given the equatorial regions being studied, perturbations of temperature and particle density were calculated following the linear theory in the absence of the Coriolis force.

LIR observation data containing large-scale stationary waves on Aug. 3rd, 2016, was analyzed. We applied high-pass filtering to the brightness temperature data to highlight the horizontal structure of stationary waves. Using our model, we managed to retrieve the amplitude of the gravity wave and derive the perturbation of other physical quantities associated with the gravity waves.

However, this model still needs to be polished. More precise models simulating processes including radiative damping, eddy diffusion, etc. are needed. The 3D gravity wave structure should be constructed to estimate the meridional energy propagation of gravity waves. Eventually, we aim to estimate the angular moment transported by gravity waves and evaluate the contribution of gravity waves to the global circulation.

Reference:

[1] Sato, T. M., Sagawa, H., et al. (2014). Cloud top structure of Venus revealed by Subaru/COMICS mid-infrared images. Icarus, 243, 386-399.

[2] Seiff, A., Schofield, J. T., et al. (1985). Models of the structure of the atmosphere of Venus from the surface to 100 kilometers altitude. Advanced in Space Research, 5(11), 3-58.

[3] Haus, R., Kappel, D., Arnold, G. (2013). Self-consistent retrieval of temperature profiles and cloud structure in the northern hemisphere of Venus using VIRTIS/VEX and PMV/VENERA-15 radiation measurements. Planetary and Space Science 89, 77-101.

[4] Marcq, E., Bezard, B., et al. (2005). Latitudinal variations of CO and OCS in the lower atmosphere of Venus from near-infrared nightside spectro-imaging. Icarus, 179, 375-386.

[5] I.E. Gordon, L.S. Rothman, et al. (2022). The HITRAN2020 molecular spectroscopic database. Journal of Quantitative Spectroscopy and Radiative Transfer, 277, 107949.

[6] D. C. Fritts, M. J. Alexander (2003). Gravity wave dynamics and effects in the middle atmosphere. Reviews of Geophysics, 41.

R009-32
B 会場 ：9/27　PM1 （13:45-15:30）
15:00〜15:15

金星周回機あかつきの紫外画像から得られた雲頂高度における二酸化硫黄の地方時分布

#岩中　達郎 [1)], 今村　剛 [2)], 青木　翔平 [3)]
[(1] 東京大学大学院 理学系研究科,[(2] 東京大学大学院 新領域創成科学研究科,[(3] 東京大学大学院 新領域創成科学研究科

Local time dependence of Venusian cloud-top sulfur dioxide obtained from Akatsuki UV images

#Tatsuro Iwanaka[1)],Takeshi Imamura[2)],Shohei Aoki[3)]
[(1]Graduate School of Science, The University of Tokyo,[(2]Graduate School of Frontier Sciences, The University of Tokyo,[(3]Graduate School of Frontier Sciences, The University of Tokyo

The distribution of sulfuric acid clouds in the Venusian atmosphere is an important factor that influences the solar energy absorbed by Venus. Understanding how sulfur dioxide, the precursor of sulfuric acid, is transported from the lower layers to the cloud top, where the cloud particles are formed from sulfur dioxide photochemistry, is essential for understanding the climate system of Venus.

The 283-nm channel of the UV imager (UVI) onboard Akatsuki takes images from the orbit around Venus to observe the spatial and temporal distribution of sulfur dioxide. Retrieval of sulfur dioxide distribution from these data sets is important for understanding not only planetary scale but also finer temporal and spatial scale transport of sulfur dioxide. The 283-nm images reflect the amount of sulfur dioxide as an absorber at first, but they also include the effects of sulfuric acid aerosols, unidentified UV absorbers, and carbon dioxide, which is the main component of the atmosphere. That makes quantitative discussions difficult.

In this study, we estimated the volume mixing ratio of sulfur dioxide at the cloud top from 283-nm images taken by UVI using a newly developed radiative transfer code, assuming that all absorption is due to sulfur dioxide. We have retrieved the mixing ratio of sulfur dioxide from about 13000 images in total, spanning the period from 2016 to 2021. The analysis is limited to low latitudes (<40 degrees) to use the same atmospheric model.

From the retrieved maps of sulfur dioxide, we obtained the mean distribution of sulfur dioxide on the local time-latitude coordinates. The mean value of the volume mixing ratio of sulfur dioxide is from 100 to 200 ppb at the cloud top on the dayside, which is consistent with the previous study (Belyaev et al., 2012). We found that the local time variation of sulfur dioxide has a single peak in the afternoon, which is inconsistent with that of Venus Express nadir observation (Marcq et al., 2020) with two peaks both in the morning and afternoon. We examined the influence of unidentified UV absorbers by retrieving the distribution of sulfur dioxide, taking into account the local time-latitude distribution of the imaginary part of the refractive index of cloud particles obtained by Marcq et al. (2022), which represents the contribution of the unidentified absorbers. However, the major structure remained unchanged and still did not agree with their results. On the other hand, our results are qualitatively consistent with the result of a Venus GCM with photochemistry (Stolzenbach et al., 2023). The enhancement of sulfur dioxide in the afternoon is attributed to the vertical transport of sulfur dioxide induced by thermal tides based on the wave structures reproduced by the Venus GCM by Takagi et al. (2018).

金星大気中の硫酸液滴で構成された雲は，金星が吸収する太陽エネルギーに影響する重要な要素である．雲の前駆物質である二酸化硫黄が下層から雲頂高度まで輸送され，光化学的に硫酸へ変化する一連の雲形成プロセスを理解することは，金星の気候システムを理解する上で不可欠である．

雲の前駆物質である二酸化硫黄の空間分布を観測するために，金星周回機あかつきは軌道上から金星ディスクの紫外画像を継続的に撮影している．このような時空間的に高分解能な画像セットから二酸化硫黄の定量を行うことは，惑星規模だけでなく．時空間的に小さい輸送プロセスを理解するのに重要である．283 nm の紫外画像上には，1 次的には二酸化硫黄の量が反映されているが，二酸化硫黄の定量のためには硫酸エアロゾルや大気主成分である二酸化炭素，未同定の紫外吸収物質による太陽紫外光の散乱・吸収を考慮したリトリーバルが必要である．

そこで，本研究ではあかつきが様々な幾何学条件のもとで撮影した紫外画像から，吸収が全て二酸化硫黄によるものであると仮定し，新たに開発した放射輸送コードを用いて雲頂での二酸化硫黄の混合比を推定する手法を開発し，2016 年から 2021 年の期間の約 13000 枚の紫外画像から二酸化硫黄の空間マップを得た．大気モデルの制約から，本研究では解析範囲を緯度 40 度以下に制限し，得られたマップから，昼面の二酸化硫黄の混合比の地方時・緯度分布を導出した．昼面での平均的な混合比は 100 から 200 ppb であり，先行研究の Belyaev et al. (2012) と矛盾のない値であった．一方，地方時方向には午後側で単一の極大を持つ分布であり，これは午前と午後に 2 つの極大を持つ，ヴィーナス・エクスプレスによる直下視分光観測による結果 (Marcq et al., 2020) には一致しなかった．そこで，未同定の紫外吸収物質の効果をモード 1 の雲粒子の消衰係数として，Marcq et al. (2020) によって導出された消衰係数の地方時・緯度分布を用いて再計算を行ったが，主要な構造は変化しなかった．一方で，我々の結果は光化学反応を組み込んだ大気大循環モデルによって得られた分布 (Stolzenbach et al., 2023) と一致した．午後側の二酸化硫黄の極大は，Takagi et al. (2018) が大気大循環モデルによって再現した，熱潮汐波が励起する空気の鉛直変位に起因すると考えられる．

R009-33
B 会場 ：9/27　PM1 （13:45-15:30）
15:15〜15:30

LAPYUTA 計画 (惑星科学、生命圏科学、および天文学に向けた紫外線宇宙望遠鏡) の検討状況

#土屋　史紀 [1)], 村上　豪 [2)], 山崎　敦 [2)], 亀田　真吾 [3)], 鍵谷　将人 [1)], 木村　智樹 [4)], 垰　千尋 [5)], 古賀　亮一 [6)], 木村　淳 [7)], 益永　圭 [2)], 堺　正太朗 [1)], 吉岡　和夫 [8)], 中山　陽史 [3)], 生駒　大洋 [9)], 桑原　正輝 [3)], 成田　憲保 [8)], 小玉　貴則 [8)], 鳥海　森 [2)], 大内　正巳 [8,9)], 田中　雅臣 [1)]
([1] 東北大,[2] 宇宙科学研究所,[3] 立教大,[4] 東京理科大,[5] 情報通信研究機構,[6] 名大,[7] 阪大,[8] 東大,[9] 国立天文台

LAPYUTA(Life-environmentology, Astronomy, and PlanetarY Ultraviolet Telescope Assembly) mission: Current status

#Fuminori Tsuchiya[1)],Go Murakami[2)],Atsushi Yamazaki[2)],Shingo Kameda[3)],Masato Kagitani[1)],Tomoki Kimura[4)],Chihiro Tao[5)],Koga Ryoichi[6)],Jun Kimura[7)],Kei Masunaga[2)],Shotaro Sakai[1)],Kazuo Yoshioka[8)],Akifumi Nakayama[3)],Masahiro Ikoma[9)],Masaki Kuwabara[3)],Norio Narita[8)],Takanori Kodama[8)],Shin Toriumi[2)],Masami Ouchi[8,9)],Masaomi Tanaka[1)]
([1]Tohoku University,[2]ISAS/JAXA,[3]Rikkyo University,[4]Tokyo University of Science,[5]NICT,[6]Nagoya University,[7]Osaka University,[8]The University of Tokyo,[9]NAOJ

The LAPYUTA (Life-environmentology, Astronomy, and PlanetarY Ultraviolet Telescope Assembly) mission is an ultraviolet space telescope scheduled for launch in the early 2030s as an ISAS M-class mission. We will accomplish the following four objectives, which are related to two scientific goals: understanding the ”habitable environment” and the ”origin of structure and matter” in the universe. The first objective focuses on the subsurface ocean environment of Jupiter’s icy moons and the atmospheric evolution of terrestrial planets. In the second objective, we will characterize the atmospheres of exoplanets in the habitable zone by detecting their exospheric atmospheres and estimating the surface environments of the planets. In cosmology and astronomy, we will test whether the structures of present-day galaxies contain ubiquitous Ly α halos and reveal the physical origins of Ly α halos (Objective 3), and elucidate the heavy element synthesis process from observations of ultraviolet radiation from hot gas immediately after neutron star mergers (Objective 4).

In April 2023, the LAPYUTA mission was selected as a candidate for the 6th JAXA M-class mission candidate. Currently, scientific and feasibility studies are underway for a pre-project candidate review scheduled for the fall of 2023. For Solar System objects, in addition to the feasibility study of the water plume ejected from the surface of Jupiter’s moon Europa, we are studying the role of magnetospheric plasmas, which are necessary to understand space weathering of satellite surfaces and dissipation of surface materials. For Venus and Mars, ionospheric imaging studies using carbon ion observations and D/H observations are underway. For exoplanets, in addition to observations of oxygen atoms and carbon ions, we are investigating the runaway water vapor greenhouse that is thought to be common to planets at the inner edge of the habitable zone with surface oceans. Based on conceptual studies of system design and key technologies conducted in 2022, we are updating the design of the telescope and focal plane instruments (spectrometer, imager, and guide cameras). Two major updates are the change of the telescope design from F60 to F32 to meet a field of view requirement of the guide camera, and the implementation of a high dispersion section in the UV spectrograph. The high dispersion section will use an Echelle grating to achieve a spectral dispersion 3 to 5 times higher than that of the medium dispersion section (resolution of 0.02 nm) studied so far. The high dispersion section allows to resolve the absorption line profile of exoplanet atmospheres and to detect exoplanet atmospheres with a shorter integration time. LAPYUTA’s orbit was initially designed as an elliptical orbit with an apogee of 7,500 km and a perigee of 500 km to avoid the influence of the geocorona when observing oxygen and hydrogen atoms, but it has been modified to an apogee of 2,000 km and a perigee of 1,000 km to avoid the influence of the Earth’s radiation belt (especially high energy protons).

LAPYUTA（惑星科学、生命圏科学、および天文学に向けた紫外線宇宙望遠鏡）計画は、2030 年代初頭に ISAS 公募型小型計画での実現を目指す紫外線宇宙望遠鏡計画である。宇宙での「生命生存可能環境」と「構造と物質の起源」の理解を目指し、4 つの科学課題の達成を目的としている。課題 1 では、宇宙で最も詳細な観測が可能な太陽系内天体のうち、木星の氷衛星の地下海環境と地球型惑星の大気進化に焦点を当て、太陽や磁気圏からのエネルギー流入により時々刻々と変化する惑星・衛星大気の観測を通して、惑星大気・衛星表層の環境と進化の知見を獲得する。課題 2 ではハビタブルゾーン内にある系外惑星を対象に外圏大気の広がり検出することによって大気の特徴づけを行い、惑星表層環境の推定を目指す。課題 3,4 の宇宙論・天文学では、銀河周辺物質の構造の観測を通して宇宙構造形成の枠組みで予言されたガスの流入による星形成を検証し (課題 3)、中性子星合体直後の高温ガスの紫外線放射の観測から重元素合成過程の解明 (課題 4) を目標とする。

2023 年 4 月に公募型小型計画の 6 号機候補に選定され、2023 年秋に予定されているプリプロジェクト候補移行に向けた科学検討と現実性検討を進めている。太陽系内天体では、木星の衛星エウロパの表層から噴出する水プルームの検討に加え、衛星表層の変性や表層物質の散逸の理解に必要となる磁気圏プラズマの降込みの科学検討を、金星・火星では、炭素イオンの観測から電離圏撮像 (イオン散逸) の可能性と D/H の観測検討を進めている。系外惑星の検討では、これまで検討してきた酸素原子と炭素イオンの観測に加え、表層に海洋を持つハビタブルゾーンの内縁の惑星が経験すると考えら

れている水蒸気の暴走温室を水素・酸素原子の観測から検出する検討を実施している。これらの科学検討に加え、2022年度に実施した望遠鏡構造や主鏡の検討結果を焦点面装置の設計にフィードバックする作業を進めている。主要な変更点は、系外惑星や暗い銀河を 0.5”程度の高い解像度で観測するためのガイドカメラの視野要求から、望遠鏡を F60 から F32 に変更したことと、紫外分光器に高分散分光部を追加したことの 2 点である。高分散分光部では、分散素子にエシェル回折格子を用いることによって、これまで検討してきた中分散分光 (波長分解能 0.02nm) の 3〜5 倍の高波長分散を実現することよって、系外惑星大気の吸収線プロファイルを分解し、より短い積分時間で大気の検出を可能とするほか、金星・火星大気の D/H 観測での使用を検討している。LAPYUTA の軌道は、酸素原子や水素原子の観測におけるジオコロナの影響を回避するため、当初は遠地点 7,500km、近地点 500km の楕円軌道とすることを検討していたが、地球の放射線帯（特に高エネルギー陽子）による影響を回避するため、現在は遠地点 2,000km、近地点 1,000km に変更する予定である。ジオコロナと放射線帯の影響を定量的に評価し、放射線シールドや望遠鏡構造設計へ反映させる作業を進める。

R009-P01
ポスター 2 ：9/25　AM1/AM2 （9:00-12:30）

飯舘・蔵王観測所を用いた低周波 VLBI 実験

#北　元 [1)], 三澤　浩昭 [2)], 土屋　史紀 [2)], 近藤　哲朗 [4)], 岳藤　一宏 [3)]
([1] 東北工業大学,([2] 東北大・理・惑星プラズマ大気研究センター,([3]JAXA,([4] 所属無し

Low-frequency VLBI observation with Iitate and Zao observatories

#Hajime Kita[1)],Hiroaki Misawa[2)],Fuminori Tsuchiya[2)],Tetsuro Kondo[4)],Kazuhiro Takefuji[3)]
([1]Tohoku Institute of Technology,([2]Planetary Plasma and Atmospheric Research Center, Graduate School of Science, Tohoku Univeristy,([3]JAXA,([4]No Affiliation

The detection and measurement of exoplanet magnetic fields greatly advances our understanding of planets. Planets with atmospheres and magnetic fields, such as Earth and Jupiter, have auroras, which emit radio waves originating from charged particles accelerated in the polar regions. From the information on auroral radio waves, not only the existence of intrinsic magnetic fields can be determined, but also rotation period, surface magnetic flux density, and magnetic moment can be derived, and planetary dynamo numerical experiments can provide insight into the internal structure of the planet. Furthermore, by clarifying various characteristic quantities of different planets, it will be possible to derive scaling laws, such as for the planetary magnetic field or radio emission power. Although there have been many observations of exoplanets using large radio telescopes, only one or two have been detected so far. We have also made observations using GMRT, but no detection has been made.

In previous studies, all circularly polarized components from planetary systems are assumed to be auroral radio waves from planets, but circularly polarized components are also emitted from the main star. VLBI is widely used in the GHz band, but VLBI observations in the MHz band have been not yet established as a stable method due to ionospheric fluctuations. VLBI is also effective for detecting exoplanet radio waves because the sensitivity can be improved by combining a large number of telescopes. Since the frequency of auroral radio waves is proportional to the strength of a planetary surface magnetic field, lower frequencies (several hundred MHz band) are suitable for observing more candidate planets. However, difficulties for observations in the MHz band are ionospheric fluctuations. The amount of delay in the ionosphere is larger at lower frequencies, and the phase rotates significantly in a few minutes, resulting in reduced sensitivity when integrated over a long period of time. Therefore, it is necessary to establish a method to compensate for the electron density fluctuations between the source and the antenna.

To evaluate the instrumental stability and ionospheric variability for future international VLBI observations, we conducted VLBI observations using the Iitate Planetary Radio Telescope (IPRT) at Tohoku University and the radio telescope at the Zao observatory. The baseline length between Zao and Iitate is 44.5 km, and the observation frequency is 325 MHz. Zao is equipped with a dual orthogonal polarization system, and IPRT is equipped with two systems of dual orthogonal polarization components. K5/VSSP sampler was used for data acquisition, and the correlation analyses were performed after the observations. The target was 3C48 passing near the zenith, and a drift scan was performed. 3C48 has an intensity of 42 Jy at P-band and can be regarded as a point source from the VLA calibrator manual. Since the baseline length between Zao and Iitate is approximately the maximum baseline length of the VLA A-configuration, it is also considered as a point source in this observation. The polarization of 3C48 is known to be close to zero above 1 GHz, and is assumed to have the same characteristics below 1 GHz.

The observations were made on September 29, 2021, using K5/VSSP32 sampler with 32 MHz, 8 bit, 1 channel. We successfully detected the fringe from this data. The fringe phase changed slowly during the 100 sec period. Both phase and group delays were examined, and the trends were consistent, indicating that the phase change found here is not of ionospheric origin. In the observation on December 21, 2022, all channels were measured at 32 MHz and 4 bits using K5/VSSP64 sampler. Fringes were also successfully detected except for some channels with no signal. We also conducted three consecutive days of observation from February 8 to 10 in 2023 using K5/VSSP64. From these data, we will investigate the relationship between the fringe phase and the ionospheric electron density.

R009-P02
ポスター 2 ：9/25　AM1/AM2 （9:00-12:30）

系外惑星の大気と磁場の実証に向けたオーロラ電波データ解析手法の確立

#森野　隆盛 [1)], 木村　智樹 [1)],Philippe　Zarka[2)],Laurent　Lamy[2)], 北　元 [3)], 藤井　友香 [4)], 土屋　史紀 [5)],Member of NenuFAR Exoplanet & Stars(LT02)　Key Program[2)]
([1] 東京理科大学,([2] パリ天文台,([3] 東北工業大学,([4] 国立天文台,([5] 東北大・理・惑星プラズマ大気,([6] 東北大・理・惑星プラズマ大気

Development of data analysis method for auroral radio of exoplanets toward demonstration of their atmospheres and magnetic fields

#Ryusei Morino[1)],Tomoki Kimura[1)],Philippe Zarka[2)],Laurent Lamy[2)],Hajime Kita[3)],Yuka FUjii[4)],Fuminori Tsuchiya[5)],Member of NenuFAR Exoplanet & Stars(LT02) Key Program[2)]
([1]Tokyo University of Science,([2]Paris Observator,([3]Tohoku Institute of Technology,([4]National Astronomical Observatory of Japan,([5]Planetary Plasma and Atmospheric Research Center, Graduate School of Science, Tohoku University,([6]Planetary Plasma and Atmospheric Research Center, Graduate School of Science, Tohoku University

Planetary auroras are generated by the collision of electrons in the magnetosphere accelerated along the magnetic field with the atmosphere. If we detect the auroras from the exoplanets, we can demonstrate their magnetic fields and atmospheres, which contribute to understanding the habitability of exoplanets. Auroral radio emissions are circularly polarized waves effectively excited by the precipitating auroral electrons (Wu & Lee et al, 1979). Therefore they are distinguishable from the stellar radio emissions that are generally not circularly polarized. Detection of auroral radio emissions is a promising way to demonstrate the exoplanetary magnetic fields and atmospheres. Since the frequency of auroral radio emissions depends on the magnetic flux density in the source region (Farrell et al, 1999), it is possible to quantify the exoplanetary intrinsic magnetic field from the auroral radio spectrum. The quantified intrinsic magnetic field may constrain the internal convective structure based on the magnetic dynamo theories. The emitted power of auroral radio emission is dependent on the total energy input of the stellar wind to the planetary magnetosphere(Zarka et al., A&A 2018). The auroral radio intensity tells us about the kinetic energy of the stellar wind and its time variability. The exoplanets have been observed using existing radio telescopes. These observation results reported that circularly polarized radio emissions were detected.(e.g.,Turner et al, 2021;Vedantham et al. & Callingham et al,2020). However, we have not been able to determine that they are auroral radio emissions from planetary sources, and further observation, analysis, and detection methods need to be improved. In this study, we attempt to detect exoplanet auroral radio emissions by applying the analysis method of existing radio telescopes used in Turner et al (2021) to NenuFAR (New Extension in Nancay Upgrading LOFAR), a next-generation low-frequency radio telescope currently under construction and performance evaluation. We applied Turner's data analysis method to Jupiter observation data to evaluate whether the analysis method is valid for NenuFAR. As a result, Jupiter's radio emissions could not be detected significantly due to RFI noise. We developed a data analysis method to suppress RFI noise by improving frequency and time integration methods and estimating weak frequency bands of RFI noise through statistical analysis. This has enabled us to suppress the degree of dispersion of the intensity of RFI noise by up to approximately 50%. In the future, we plan to apply this suppression method to the observed data in advance and analyze it using the method of Turner et al (2021) to remove RFI noise and detect Jupiter radio emissions.After the data analysis method is established, we plan to apply it to the observation data of exoplanets.

惑星のオーロラは恒星風、惑星自転、惑星固有磁場等がエネルギー源となり、磁場に沿って加速された磁気圏中の電子と大気が衝突することによって発生する。もし、系外惑星のオーロラの検出ができれば、系外惑星の磁場と大気の存在を実証することができ、生命居住可能性の理解へと繋がる。オーロラは様々な波長で発光するが、その中でもオーロラ電波は顕著に円偏光しており (Wu & Lee et al, 1979)、一般に円偏光を持たない恒星からの電波と区別することができる。また、恒星光に対する相対的な強度が他の波長と比べ強いと考えられる。そのため、オーロラ電波の観測は、恒星のコンタミネーションを除きつつ、系外惑星の磁場と大気を実証する有望な方法である。オーロラ電波の周波数は、惑星の固有磁場強度に依存するため (Farrell et al, 1999)、系外惑星の固有磁場の定量化や、それに基づく内部対流構造推定が可能である。オーロラ電波強度は、惑星磁気圏に入力される恒星風のエネルギー総量と比例関係がある (Zarka et al., A&A 2018) ため、電波強度から恒星風の運動エネルギーやその時間変動の情報を引き出すことができる。今まで、既存の電波望遠鏡を用いて、系外惑星は観測されてきており、円偏光の電波を検出したと主張する結果が報告された (e.g.,Turner et al, 2021;Vedantham et al. & Callingham et al, 2020)。しかし、惑星源のオーロラ電波であると断定することができておらず、さらなる観測や解析・検出方法の改善が必要である。そこで本研究では、現在建造と性能評価が進む、次世代低周波電波望遠鏡 NenuFAR(New Extension in Nancay Upgrading LOFAR) の系外惑星観測データに、Turner et al (2021) で用いられた既存電波望遠鏡の解析手法を応用し、系外惑星オーロラ電波の検出を試みる。本発表では、同解析手法を、まず木星データに適用し NenuFAR による系外惑星オーロラ電波の検出方法の妥当性の検証を行った。その結果、人工電波によるノイズにより、木星電波を有意に検出することができなかった。そのため、周波数・時間積分方法の改善や、統計解析による人工電波の弱い周波数帯の推定を行い、人工電波を抑制するデータ処理方法を開発した。これにより、人工電波の

強度のばらつきを最大約 50% 抑制することができた。今後はこの抑制方法を事前に観測データに適用し、Turner et al (2021) の解析を行うことで、人工電波を除去して木星電波検出を行う予定である。検出手法が確立した後、系外惑星の観測データに適用していく予定である。

R009-P03
ポスター 2 ：9/25　AM1/AM2 （9:00-12:30）

#齋藤　義文 [1)], 笠原　慧 [2)], 横田　勝一郎 [3)], 齋藤　直昭 [4,6)], 浅村　和史 [1)], 西野　真木 [1)], 川島　桜也 [1)], 米田　匡宏 [1,5)]
([1 宇宙研,([2 東京大,([3 大阪大,([4 産総研,([5 京大理,([6CPE 技術研究組合

Development Status of the TRITON: Triple-Reflection Compact Time-Of-Flight Neutral Mass Spectrometer for Lunar Polar Exploration

#Yoshifumi Saito[1)],Satoshi Kasahara[2)],Shoichiro Yokota[3)],Naoaki Saito[4,6)],Kazushi Asamura[1)],Masaki N Nishino[1)],Oya Kawashima[1)],Masahiro Yoneda[1,5)]
([1ISAS/JAXA,([2The University of Tokyo,([3Osaka University,([4AIST,([5Graduate School of Science, Kyoto University,([6CPE

For the purpose of investigating the presence (and amount) of the water (ice) molecules in the regolith 1 to 1.5 m below the lunar surface, a compact neutral particle mass spectrometer is under development. This neutral particle mass spectrometer TRITON (Triple-reflection Reflectron) is designed to be installed on the LUPEX (Lunar Polar Exploration) Moon rover as part of an onboard instrument REIWA(Resource Investigation Water Analyzer). TRITON will perform mass analysis of the neutral gas generated by LTGA(Lunar Thermogravimetric Analyzer) that is also a part of REIWA.

TRITON not only aims to measure the amount of water molecules included in the lunar regolith but also identify the atoms, molecules and their isotopes up to mass number 200 with mass resolution as high as 120. TRITON is a reflectron that is a Time-Of-Flight mass spectrometer. In order to increase the mass resolution as much as possible within the allocated volume, we have decided to modify the standard reflectron by adding a second reflector that enables triple reflections and doubles the flight length. This newly designed triple-reflection TOF mass spectrometer also has an additional function to select the mass range of the measured particles by changing the temporal pattern of the pulsed high voltage applied to the first and second reflectors. This function is useful, for example, to measure minor target gas by reducing the interference from the major gas. The triple-reflection TOF mass spectrometer can be operated also as a standard reflectron by changing the voltage applied to the analyzer. Triple-reflection mode is suitable for high mass resolution measurement and standard single reflection mode is suitable for high sensitivity measurement.

Based on the test results of the Test Model (TM) analyzer, designing Engineering Model (EM) has been mostly completed and fabrication of EM is underway. The testing of EM is scheduled for later this year.

R009-P04
ポスター 2 ：9/25　AM1/AM2 （9:00-12:30）

Kaguya/LRS のオーロラキロメータ放射観測を用いたパッシブレーダーによる月面及び地下構造探査手法の検討

#田中　絵美 [1)], 土屋　史紀 [2)], 熊本　篤志 [3)], 笠羽　康正 [4)], 三澤　浩昭 [5)], 安田　陸人 [6)], 北　元 [7)]
([1] 東北大学,[2] 東北大・理・惑星プラズマ大気,[3] 東北大・理・地球物理,[4] 東北大・理,[5] 東北大・理・惑星プラズマ大気研究センター,[6] 東北大・理・惑星プラズマ大気研究センター,[7] 東北工業大学

Method to explore the lunar surface and subsurface structure by passive radar using AKR observed by Kaguya/LRS

#Emi Tanaka[1)],Fuminori Tsuchiya[2)],Atsushi Kumamoto[3)],Yasumasa Kasaba[4)],Hiroaki Misawa[5)],Rikuto Yasuda[6)],Hajime Kita[7)]
([1]Tohoku University,[2]Graduate School of Science, Tohoku University,[3]Graduate School of Science, Tohoku University,[4]Graduate School of Science, Tohoku University,[5]Graduate School of Science, Tohoku Univeristy,[6]Tohoku university,[7]Tohoku Institute of Technology

Passive radar is an exploration technique using echoes of strong natural radio emissions such as planetary auroral radio waves phenomena that are reflected at the solid surface and the ionosphere of target bodies. The passive radar has been studied for observations of the subsurface structure of Jupiter's icy moons with the JUICE spacecraft [Kumamoto et al. 2016], and applied to auroral kilometric radiation (AKR) to search the lunar ionosphere [Goto et al.,2011]. This study investigates a method to explore the lunar regolith layer and the subsurface structure using AKR observed by the Lunar Radar Sounder (LRS) onboard the lunar orbiter Kaguya. The LRS consists of three subsystems: the sounder transmitter/receiver (SDR), the HF natural wave receiver (NPW), and the VLF waveform receiver (WFC). The LRS-NPW is capable of natural wave observation in the frequency range of 20 kHz to 30 MHz, and the AKR observed by the NPW is used in this study. This study has two purposes. The first one is to explore the subsurface structure of the Moon from dynamic spectra of AKR observed by the LRS-NPW. To detect the lunar subsurface structure, we will use the interference patterns between direct waves of AKR propagating from the Earth and those reflected from the lunar surface and subsurface structures. Since the frequency of AKR (several 10 to several 100 kHz) is lower than active radar sounders (LRS-SDR, 4-6 MHz), it has the potential to explore deeper subsurface structures than active radar sounders. In this study, the dynamic spectrum was modeled by calculating the interference fringes on the radio spectrum at the position of Kaguya. The second purpose is global exploration of the physical properties of the lunar regolith layers, which will allow estimation of the permittivity of lunar surface materials from the surface echo intensity, since the longer wavelength of AKR (the order of 1 km) could reduce the effect of lunar surface irregularities on the surface echo intensity. Therefore, the dielectric constant of lunar surface materials could be estimated from the surface echo intensity. Since the dielectric permittivity obtained from return samples of the Apollo program depends on local characteristics of the Lunar surface, the remote sensing technique will enable to obtain a global survey of the regolith layer material of Moon. For these purposes, a two-layer subsurface structure was assumed, with a relative permittivity of 4.0 for the first layer from the lunar surface, 8.0 for the second layer, and the thickness of the first layer of 1 km. To consider the attenuation of radio waves in the first layer, the loss tangents of 0.01 and 0.003 are assumed. Under the above assumptions, the interference fringes at the position of Kaguya were calculated, and the frequency interval and amplitude of the interference fringes were derived. When the incident angle of AKR to the Lunar surface is 0 degrees, the frequency interval and amplitude of the interference fringes caused by direct and surface-reflected waves are 1.5 kHz and 6.0 dB, respectively. The frequency interval of the interference fringes between the surface and subsurface reflected waves was 75 kHz, and the amplitude was about 0.5 dB for a loss tangent of 0.01 and about 0.8 dB for a loss tangent of 0.003. Since the frequency resolution of LRS-NPW is 6 kHz, interference fringes due to direct-directed and surface-reflected waves cannot be observed if the incident angle is small. The interval of interference fringes increases as the incident angle increases [Kumamoto et al., 2016], and simulation results show that interference fringes can be observed with the LRS-NPW frequency resolution if the incident angle is larger than 79.2degree. Based on these studies, we have completed development of a tool to simulate interference fringes at arbitrary position of Kaguya. We will identify areas on the lunar surface where interference fringes are observed and investigate the subsurface structure of the lunar surface and the permittivity of materials in the regolith layer.

惑星のオーロラ帯を起源とする強い自然電波放射が衛星の表層や電離圏で反射するエコーを利用した探査手法をパッシブレーダーと呼び、木星探査機 JUICE での実施を想定した木星の氷衛星の地下構造探査の検討 [Kumamoto et al.,2016] や、オーロラキロメータ電波 (AKR) を月の電離層探査に適用した研究がある [Goto et al.,2011]。本研究では月周回衛星「かぐや」に搭載された月レーダーサウンダー LRS(Lunar Radar Sounder) が観測する AKR を用いて、月面のレゴリス層とその下の地下構造を探査する手法の検討を行う。LRS はサウンダー送受信部 (SDR)、HF 帯自然波動受信部 (NPW)、VLF 帯波形受信部 (WFC) の 3 つのサブシステムから成っている。LRS-NPW では 20kHz〜30MHz の周波数帯で自然波動観測が可能であり、本研究では NPW が観測する AKR を検討に使用する。

本研究の目的は、2 つある。１つ目の目的は、LRS-NPW で得られた AKR 観測データから、月の地下構造を探査する手法を検討することである。AKR の地下エコーから月の地下構造を探査するため、地球方向から伝搬する AKR の直達波と、月面及び地下構造での反射波の干渉パターンを利用する。AKR の周波数は数 10〜数 100kHz と低周波であり、4-6MHz のアクティブレーダーサウンダー (LRS-SDR) よりも深い地下構造を調べられる可能性がある。本研究では、AKR の直達波と、月面と地下からの反射波により、電波スペクトル上に生じる干渉縞を計算し、観測されたダイナミックスペクトルとの比較を行う。

２つ目の目的は、月のレゴリス層の物性を全球的に探査する手法を検討することである。AKR は波長が 1km スケールとなるため、アクティブレーダーと比べて表面エコー強度が月表面の凹凸から受ける影響が小さくなることから、表面エコー強度から月表面物質の誘電率を推定できる可能性がある。アポロ計画において持ち帰られた「月の石」の分析から得られる誘電率は局所的なものであり、本研究では LRS で得られた観測結果から、月全体のレゴリス層物質のグローバルな調査が可能かどうかの検討を行う。

本研究の検討では、２層の地下構造を仮定し、月面から 1 層目の比誘電率を 4.0、２層目を 8.0、１層目の厚さを 1km と設定した。１層目での電波の減衰については、比誘電率の虚数部から算出される損失角が 0.01 の場合と 0.003 の場合を検討した。以上の仮定のもとで、AKR の直達波、月面での表面反射波、及び地下反射波の３つの電波をかぐやが受信した時に生じる干渉縞を計算し、干渉縞の周波数の間隔 [kHz] と振幅 [dB] を導出した。その結果、入射角が 0 度の時、直達波と表面反射波による干渉縞の間隔は 1.5kHz、振幅は 6.0dB であった。また、月面の表面反射波と地下反射波の干渉縞の周波数間隔は 75kHz、振幅は損失角が 0.01 の場合は約 0.5dB、損失角が 0.003 の場合は約 0.8dB となった。LRS-NPW の周波数分解能は 6kHz なので、入射角 0° となるような (0° E, 0° N) の付近の領域では直達波と表面反射波による干渉縞を十分な分解能で観測できないが、表面反射波と地下反射波の干渉縞は検出できる可能性がある。一方で、AKR の月面への入射角が大きくなると干渉縞の間隔が大きくなり [Kumamoto et al., 2016]、シミュレーション結果から、入射角が 79.2° 以上であれば LRS-NPW の周波数分解能でも干渉縞の観測が可能であることが分かった。

以上の検討をもとに、かぐやの緯度・経度に応じた、任意の入射角での干渉縞シミュレーションを行うツールを完成させ、実際の LRS-NPW 観測データと、シミュレーション結果の比較を通して、干渉縞の観測可能な領域を調査している。今後は、干渉縞が観測可能な月面上の領域を特定し、月面地下構造を調査するとともに、2 つ目の目的に設定したレゴリス層の物質の誘電率を求める検討を行う。

R009-P05
ポスター 2 ：9/25　AM1/AM2 （9:00-12:30）

かぐや低高度観測データを用いた月ミニ磁気圏の荷電粒子・電磁場特性の研究

#荻野　晃平 [1)], 原田　裕己 [1)], 西野　真木 [2)], 齋藤　義文 [2)], 横田　勝一郎 [3)], 笠原　禎也 [4)], 熊本　篤志 [5)], 高橋　太 [6)], 清水　久芳 [7)]
([1] 京都大学大学院理学研究科,[2] 国立研究開発法人宇宙航空研究開発機構,[3] 大阪大学大学院理学研究科,[4] 金沢大学学術創成センター,[5] 東北大学大学院理学研究科,[6] 九州大学理学研究院,[7] 東京大学地震研究所

Characterization of charged particles and electromagnetic fields in lunar mini-magnetospheres based on Kaguya low-altitude data

#Kohei Ogino[1)],Yuki Harada[1)],Masaki Nishino[2)],Yoshifumi Saito[2)],Shoichiro Yokota[3)],Yoshiya Kasahara[4)],Atsushi Kumamoto[5)],Futoshi Takahashi[6)],Hisayoshi Shimizu[7)]
([1]Department of Geophysics, Graduate School of Science, Kyoto University,[2]Institute of Space and Astronautical Science, Japan Aerospace Exploration Agency,[3]Graduate School of Science, Osaka University,[4]Information Media Center, Kanazawa University,[5]Graduate School of Science, Tohoku University,[6]Department of Earth and Planetary Sciences, Kyushu University,[7]Earthquake Research Institute, University of Tokyo

Although the Moon does not have a global magnetic field like the Earth, crustal remanent magnetizations (lunar magnetic anomalies, hereafter LMAs) are nonuniformly distributed over the lunar surface. The interaction between the solar wind and LMAs leads to the formation of mini-magnetospheres. Since the spatial scales of lunar mini-magnetospheres are very small, below several tens of kilometers, direct observations of the lunar mini-magnetospheres are challenging from a typical altitude of lunar orbiters (~100 km). As a result, the plasma environment and electromagnetic field structure in the solar wind-LMA interaction region have not been fully understood. Saito et al. (2012) first reported simultaneous observations of ions and electrons below 30 km altitude based on a single low-altitude path obtained by 'Kaguya'. In this study, we extensively analyze low-altitude data of ions, electrons, magnetic fields, and wave electric fields obtained by Kaguya. By analyzing multiple orbits over a variety of LMAs, we comprehensively characterize the plasma environment and electromagnetic fields in the solar wind-LMA interaction region. Based on the knowledge and questions derived from the currently available low-altitude data, we discuss implications for future low-orbiting or lander missions.

地球のような全球的な磁場が無い月では、局所的な地殻残留磁化（磁気異常）が太陽風と相互作用を起こし、「ミニ磁気圏」と呼ばれる領域を形成している。月ミニ磁気圏の空間スケールは数 10 km サイズと小さく、月周回衛星の典型的な高度（～100 km）では直接探査が難しい。そのため、太陽風と月地殻磁場が相互作用を起こす領域でのプラズマ環境や電磁場構造の全容は未解明であった。Saito et al. (2012) では、月周回衛星「かぐや」の低高度運用時の 1 軌道のデータから、高度 30 km 以下でのイオン、電子同時観測が初めて報告された。本研究では、かぐやが低高度（～数 10 ㎞）運用時に取得した、イオン、電子、静磁場、波動磁場、波動電場のデータを網羅的に解析する。また、粒子・電磁場データ解析を複数軌道、複数磁気異常について拡張することで、太陽風月磁気異常相互作用領域でのプラズマ環境および電磁場特性について包括的に調査する。それにより、現有のかぐや低高度観測データから得られる知見や今後の課題を整理し、将来的な低高度または月面でのプラズマ環境探査検討に活用できると期待される。

R009-P06
ポスター 2 ：9/25　AM1/AM2 （9:00-12:30）

月面天文台：メートル波電波干渉計の概念検討

#土屋　史紀 [1)], 岩田　隆浩 [2)], 山田　亨 [2)], 磯部　直樹 [2)], 関本　裕太郎 [2)], 宮崎　康行 [2)], 宇佐美　尚人 [2)], 井口　聖 [3)], 高橋　慶太郎 [4)], 大西　利和 [5)], 山内　大介 [6)]
([1] 東北大,[2] 宇宙科学研究所,[3] 国立天文台,[4] 熊本大,[5] 大阪公立大,[6] 岡山理科大

A Conceptual Study on Meter-wave Radio Interferometer: Lunar Astronomical Observatory

#Fuminori Tsuchiya[1)],Takahiro Iwata[2)],Toru Yamada[2)],Naoki Isobe[2)],Yutaro Sekimoto[2)],Yasuyuki Miyazaki[2)],Naoto Usami[2)],Satoru Iguchi[3)],Keitaro Takahashi[4)],Toshikazu Onishi[5)],Daisuke Yamauchi[6)]
([1]Tohoku University,[2]ISAS/JAXA,[3]NAOJ,[4]Kumamoto University,[5]Osaka Metropolitan University,[6]Okayama University of Science

Since high-precision observation in the lower frequency range below 10 MHz has not yet been realized, this frequency range is notable as one of the last frontiers for astronomy. This is because the terrestrial ionosphere prevents ground-based observations of radio waves below the ionospheric cutoff. While spacecraft have been used to observe radio waves below 10 MHz, low-frequency radio waves require longer antenna elements, making it difficult to increase the aperture size of radio antennas mounted on a spacecraft. It is also difficult to observe the faint radio waves from planets and celestial objects even in Earth orbit because of interference from solar flares, artificial radio broadcasts, and terrestrial auroral radio emissions. The far side of the Moon is a suitable location for such low-frequency astronomical observations because radio waves from the Earth can always be avoided and radio waves from the Sun can be shielded during the lunar night. One of the major goals of astronomy on the far side of the Moon is the first detection of the 21 cm neutral hydrogen absorption line from the Dark Ages of the universe. Another goal is the radio emission from the central stars with habitable planets and the radio emission from exoplanets, which would provide us with space weather environments of exoplanets and intrinsic parameters of exoplanets such as magnetic field strength, rotation rate, and so on. We report the progress of a conceptual study on a lunar astronomical observatory consisting of a meter-wave radio interferometer on the far side of the Moon. This observatory aims at more than 100 antennas extended to a maximum baseline of more than 100 km, providing a spatial resolution of about 1 arcmin at 10 MHz. We will report on the feasibility study of the first stage pilot probe with three antenna units and scientific observations with the pilot probe including the lunar environment.

R009-P07
ポスター 2 ：9/25　AM1/AM2 （9:00-12:30）

HISAKI 衛星による紫外線観測とハレアカラ T60 による可視光観測を用いたイオプラズマトーラスの朝夕非対称性の時間変化と太陽風応答の統計解析

#近藤　大泰 [1)], 土屋　史紀 [1)], 鍵谷　将人 [1)], 佐藤　晋之祐 [1)], 村上　豪 [2)], 木村　智樹 [3)], 山崎　敦 [2)], 吉川　一郎 [4)], 北元 [5)]
([1] 東北大学・理・惑星プラズマ・大気研究センター,[2]ISAS/JAXA,[3] 東京理科大学,[4] 東京大学,[5] 東北工業大学

The temporal variation and the solar wind response of dawn-dusk asymmetry of IPT observed by HISAKI and Haleakala T60

#Hiroyasu Kondo[1)],Fuminori Tsuchiya[1)],Masato Kagitani[1)],Shinnosuke Satoh[1)],Go Murakami[2)],Tomoki Kimura[3)],Atsushi Yamazaki[2)],Ichiro Yoshikawa[4)],Hajime Kita[5)]
([1]Graduate School of Science, Tohoku University Planetary Plasma and Atmospheric Research Center,[2]Institute of Space and Astronautical Science, Japan Aerospace Exploration Agency,[3]Tokyo University of Science,[4]Tokyo University,[5]Tohoku Institute of Technology

In Jupiter's magnetosphere, since the strength of a dipole magnetosphere is stronger and the rotating speed is faster, the co-rotation electric field is dominant in the inner magnetosphere, including in Io's orbit. The convective electric field is also known to exist in Jupiter's inner magnetosphere (a few percent of the co-rotating electric field), and the origin of convective electric fields has been discussed so far (Nakamura et al., 2023; Murakami et al., 2016; Barbosa & Kivelson; 1983, Ip & Goertz, 1983).

In Jupiter's inner magnetosphere, there are regions consisted of dense plasma from Io's volcanos, forming the Io-plasma torus (IPT). In the region slightly inside the Io orbit, there is a structure called "ribbon" in which Io-originated plasma spreads in the north-south direction along the magnetic field lines. The presence of a convection electric field causes the ribbon position to shift to the dawn side, providing a direct observation of the strength of the convective electric field. Due to the adiabatic change in electron temperature caused by the change in the drift orbit, the temperature is higher in dusk side than in dawn side. If the efficiency of ion excitation by electron collisions depends on the electron temperature, the strength of the convective electric field can be estimated indirectly from the difference in emission intensity between dawn and dusk sides of the IPT.

Schneider et al. (1995) reported a temporal variation of ribbon's radial position using 80 images at 673.1 nm observed by the Catalina telescope. The position fluctuational was asymmetry between the dawn and dusk sides, suggesting the non-uniformity of the electric field structure.

In this study, we analyzed the relationship between temporal variation of the ribbon's radial position in the IPT and the solar wind dynamic pressure to investigate temporal variation and inhomogeneity of the electric field in Jupiter's magnetosphere associated with the solar wind response. We used sulfur ion emission lines (SII, SIII, and SIV in 64.0-77.0 nm) observed by the HISAKI/ EXtreme ultraviolet spectrosCope for ExosphEric Dynamics (EXCEED) and sulfur ion visible images (SII 673.1 nm) obtained by the Visible Imager and SPectrograph with coronagraphy (VISP) with the 60cm aperture telescope (T60) at the Haleakala observatory of Tohoku University. The MHD simulation of the dynamic pressure of solar wind were introduced in Tao et al. (2005).

We analyzed the T60/VISP data observed in December 2014 – May 2017. We define the position of ribbon at a location where the brightest emission at 673.1 nm appears in the IPT. The 1,427 ribbon images are classified into two groups in terms of the dynamic pressure of the solar wind; those during quiet solar wind ($<$0.1 nPa) or disturbed solar wind ($>$0.1 nPa). We investigate the System III longitude dependence of the ribbon's position in the dawn and dusk sides and fit the result with sinusoidal functions. When the solar wind dynamic pressure was quiet, the ribbon's position is fitted with 5.761 $\pm$ 0.042 cos (λ -133 [deg]) [Rj] in the dawn side and 5.587 $\pm$ 0.047 cos (λ -130 [deg]) Rj on the dusk side (λ : System III longitude [deg]; Rj: Jupiter's radius 71,492 [km]). When it disturbed, it is fitted with 5.786 $\pm$ 0.042 cos (λ -147 [deg]) [Rj] in the dawn side and 5.558 $\pm$ 0.049 cos (λ -123 [deg]) [Rj] in the dusk side. The results indicate that there is a dawn-ward shift both in the dawn and dusk sides when the dynamic pressure increases: the shift is derived at 0.025 Rj and 0.029 Rj in the dawn side and the dusk side, respectively. To Estimate the convection electric field strength from this shift, we found that it averaged 2 [mV/m] during quiet, and tended to be larger when solar wind disturbed, which is consistent with the convection electric field strength derived by the HISAKI data: the strength is estimated at 3.8 [mV/m] on average and 8.6 [mV/m] for the particularly stronger solar wind(Murakami et al., 2016).

Next, we investigated the change of the solar wind dynamic pressure and the shift in the ribbon's radial position. We

focused on events in which the solar wind pressure was continuously quiet (<0.05 nPa) for several days and then increased to more than 0.1 nPa. We derive the shift of the ribbon's position in response to the increasing dynamic pressure at every 10 [deg] of the central meridian longitude (CML). The results showed that when solar wind dynamic pressure increases, the ribbon's position tends to shift toward the dawn side in more than 90% of the events in the dawn side, whereas in dusk side, the variation of the ribbon's position were divided into cases where it shifted to the dawn side and the dusk side. This indicates that the response of the convection electric field induced by solar wind dynamic pressure was asymmetric between the dawn and dusk sides of the IPT, during the events. It was also shown that the convection electric field may have a non-uniformity.
may have a non-uniformity.

木星磁気圏では、双極子磁場が強く、自転は速いため、衛星イオ軌道のある内部磁気圏では共回転電場が支配的である。一方、木星内部磁気圏には共回転電場の数 % 程度の対流電場が存在することが知られており、対流電場の起源と大局的な磁気圏構造との関係が議論されている (Nakamura et al., 2023; Murakami et al., 2016; Barbosa & Kivelson; 1983, Ip & Goertz, 1983)。

木星内部磁気圏にはイオ起源のプラズマが濃い領域が存在し、イオプラズマトーラス (IPT) を形成している。イオ軌道より少し内側には、イオ起源のイオン温度が高い領域が存在する。このイオンの発光を地球から観測すると、磁力線に沿って南北方向に広がりをもつシャープな構造が IPT の朝側と夕方側で捉えられる。これを"Ribbon"と呼ぶ。対流電場が存在すると、荷電粒子のドリフト軌道の変化に伴って Ribbon の位置が朝側にシフトするため、対流電場の強さを直接観測する手段となる。ドリフト軌道の変化によって、電子温度が断熱的に変化することで、電子の温度は夕方側で高くなる。電子衝突によるイオン励起効率が電子温度に依存する場合は、IPT の朝側と夕方側の発光強度の違いから間接的に対流電場の強さを推定できる。

Schneider et al. (1995) では、Catalina 望遠鏡 (1.5m) で観測された S Ⅱ 6731Å の 80 の image を用いて、Ribbon の位置が動径方向に時間変化することを報告した。その位置変動は朝側と夕方側で挙動が異なり、電場構造の非一様性を示唆するものであった。しかし、Ribbon 位置の変動の報告例はこの 1 例にとどまっており、Ribbon 位置の変化と太陽風動圧との関係は明らかとなっていない。

本研究では、木星内部磁気圏の電場構造の (1) 太陽風応答と (2) 非一様性を明らかにすることを目的とし、対流電場の強さを直接反映する IPT の Ribbon の動径位置の時間変動と太陽風動圧の関係と、朝側と夕方側の挙動の相違について調べた。解析には、HISAKI/ EXtreme ultraviolet spectrosCope for ExosphEric Dynamics (EXCEED) で観測された硫黄イオンの電子衝突励起輝線 (S Ⅱ, S Ⅲ, S Ⅳ (640-770Å)) とハワイ・ハレアカラ山頂にある東北大の口径 60cm の望遠鏡 (T60) に取り付けられた複数の分光器撮像機で得られた硫黄イオンの可視イメージ画像 (S Ⅱ 6731Å)、太陽風動圧データとしては、Tao et al. (2005) の MHD シミュレーション結果を使用した。

T60 のデータから、硫黄イオン発光強度を南北方向に積分した分布が動径方向に最大となる位置を Ribbon と定義し、朝側、夕方側の Ribbon の動径位置を決定した。2014 年 12 月から 2017 年 5 月の期間に得られた 1427 の image のうち、太陽風動圧が静穏なとき (<0.1nPa) と強いとき (>0.1nPa) で分類し、Ribbon の平均動径位置を導出した。木星の磁気双極子の位置が自転軸からオフセットしていることにより、Ribbon の位置は木星の磁気経度 (system III) により周期的に変化するため、朝側、夕方側のそれぞれの Ribbon の動径位置について、system III 経度を変数とする正弦関数でフィッティングを行った。動圧が静穏な時は、朝側で 5.761 ± 0.042 cos (λ-133°) [Rj]、夕方側で 5.587 ± 0.047 cos (λ-130°) [Rj] であった (λ: System III 経度 [deg]; Rj: 1 木星半径=71,492 [km])。一方で、動圧が強い時は、朝側で 5.786 ± 0.042 cos (λ-147°) [Rj]、夕方側で 5.558 ± 0.049 cos (λ-123°) [Rj] となった。動圧の増大によって、朝側では 0.025Rj、夕方側では 0.029Rj 朝側にシフトすることが初めて明らかになった。このシフト量から対流電場強度を見積もると、静穏な時で平均 2 [mV/m]、 動圧が強い時はそれよりも大きな値を示す傾向が見られた。これは、HISAKI の朝夕発光非対称性から推定された対流電場強度が、平均で 3.8 [mV/m]、動圧が特に強い時で 8.6 [mV/m] であり (Murakami et al., 2016)、対流電場が太陽風動圧により増大することを示した HISAKI の結果を支持するものである。

次に、太陽風動圧の変化量と Ribbon の位置のシフト量について、朝側と夕方側の相違を詳しく調査した。太陽風動圧が静穏 (0.05nPa 未満) である状態が数日間続き、その後 0.1nPa 以上へ上昇したイベントに着目した。Ribbon の位置には System III 経度依存性があるため、経度 10° 毎に分けて Ribbon の位置の変化を評価した。朝側の Ribbon の動径位置は、太陽風動圧の上昇ともに、9 割以上のイベントで朝側に移動する傾向が見られたのに対し、夕方側では朝側と夕方側にシフトする場合に別れる結果となった。これは太陽風動圧に対する対流電場の応答が朝側と夕方側で異なっていることを示しており、対流電場の不均一性を示すものとなった。

R009-P08
ポスター 2 ：9/25　AM1/AM2 （9:00-12:30）

エウロパ大気における発光輝線の探索：地上望遠鏡による可視観測

#高木　聖子 [1)], 鶴海　達大 [2)], 木村　淳 [2)], 太田　峻介 [3)], 松尾　太郎 [3)]
([1] 北海道大学,[2] 大阪大学,[3] 名古屋大学

A search for emission lines in the atmosphere of Europa with ground-based telescope

#Seiko Takagi[1)],Tatsuhiro Tsurumi[2)],Jun Kimura[2)],Shunsuke Ohta[3)],Taro Matuso[3)]
([1]Hokkaido University,[2]Osaka University,[3]Nagoya University

For the Jovian icy moon Europa, telescopic observations have confirmed the existence of atomic sodium and potassium in its tenuous atmosphere [Brown and Chaffee, 1974; Brown, 2001]. Such components are considered to be originated from the surface materials. Spectrographic evidence on the surface acquired from the Galileo spacecraft suggests that hydrated salt minerals, such as magnesium and sodium sulfates, sodium carbonate and their mixtures, are concentrated at the linear features and in the chaotic terrains [e.g., McCord et al., 1999]. Furthermore, recent visible spectroscopic observations by the Hubble Space Telescope suggests the presence of sodium chloride on the surface [e.g., Trumbo et al., 2019]. The following mechanisms have been proposed as the origin of Europa's tenuous atmosphere: (1) sputtering of materials from the surface by energetic particles in the Jupiter's magnetosphere, (2) the impact supply from meteorites and dusts, (3) contamination due to volcanism from nearby Io. However, sodium-to-potassium for the Europa's atmosphere does not simply agree with chemical model of the Europa's ocean and with meteoritic origin. In addition, no positive signal from magnesium and calcium atoms has been reported despite their expected presence [Horst and Brown, 2013]. The search for such materials is crucial not only to understand the chemical information in the present Galilean moons, but also to evaluate the primordial environment, formation process and evolution of the moon.

In this study, we searched for emission lines (400-930 nm) in the atmospheres of Europa from 2018 to 2021 using the spectral imager Multi Spectral Imager [Watanabe et al. 2012] on board the Pirka telescope (the primary mirror is 1.6 m in diameter) of Hokkaido University. Here we will report the investigation.

大気中の原子は太陽光共鳴や電子衝突により励起され、特定波長の輝線を発することから、発光輝線の観測により大気成分の推定が可能である。エウロパにおいては、ナトリウム原子とカリウム原子による発光輝線 (波長 590, 767 nm) が検出されたことから、それらの存在が明らかになった [Brown and Chaffee, 1974; Brown, 2001]。このような大気成分は、天体表面（氷地殻）に存在する物質との関連が示唆されている。エウロパ上には、マグネシウムやナトリウムの硫酸塩や炭酸塩などの水和物といった塩類の存在が木星探査機ガリレオの近赤外分光観測から推測されている [e.g., McCord et al., 1999]。また、表面の褐色化の原因とされてきた塩化ナトリウムの存在もハッブル宇宙望遠鏡の可視分光観測から明らかになった [e.g., Trumbo et al., 2019]。表面に存在が示唆されるそれらの物質は、地下海からの物質表出を伴うと思われる地形に集中して存在することから、岩石質のマントルと接する海底には岩石と液体水との相互作用が行われる環境が存在し、液体水に溶出した塩分が氷地殻に取り込まれ対流運動などに伴って表出、あるいはプルームとして地下海から直接に噴出する内的要因がその起源として考えられている。また、イオの火山活動に起因する木星ナトリウム雲と呼ばれる巨大構造やイオ周辺大気、彗星などからエウロパ表面へともたらされる外的要因も考えられている。エウロパに大気が形成される機構には、塩類の存在が示唆される表面に木星磁気圏の高エネルギー粒子が衝突し、地殻から原子が叩き出される (スパッタリング) 過程や、太陽光加熱により表面物質が昇華する過程が提案されている。マグネシウム原子による発光も予想されたがこれまで検出には至っておらず [Horst and Brown, 2013]、現在検出されているのはナトリウム原子とカリウム原子の発光輝線のみである。このような衛星大気中の発光輝線の検出は、形成時の材料物質やその後の衛星の進化過程、衛星間の物質輸送過程を知る手段である。しかしながら、過去の探査機によるスナップショット的な観測や時間が限られた宇宙望遠鏡による観測で捉えた輝線は僅かであり、衛星における物質調査は不十分と言わざるを得ず、物質の起源や衛星の進化過程について理解は停滞している。

北海道大学大学院理学研究院附属天文台は北海道名寄市にあり、地上望遠鏡 (ピリカ望遠鏡) を所有している。主鏡口径は 1.6 m であり、その大きさは惑星観測用の望遠鏡としては世界最大級である。本研究では、衛星の誕生環境や進化過程を明らかにすることを目的とし、ピリカ望遠鏡に搭載されたスペクトル撮像装置 MSI [Watanabe et al., 2012] を用いて、2018 年から 2021 年にかけて数十夜の多波長撮像観測を行い、エウロパ大気における発光輝線の探索 (400-930 nm) を行った。本講演ではその報告を行う。

R009-P09
ポスター 2 ：9/25　AM1/AM2 （9:00-12:30）

惑星高分散エシェル分光器 ESPRIT の開発と近赤外撮像装置 TOPICS の初期観測報告

#木下　凌太 [1)], 坂野井　健 [1)], 永田　和也 [1)], 大友　綾 [1)], 鍵谷　将人 [1)], 平原　靖大 [2)], 高木　聖子 [3)], 齊藤　大晶 [3)], 内藤　博之 [4)]
[1 東北大理,[2 名古屋大環境,[3 北海道大理,[4 なよろ市立天文台

Development of the infrared echelle spectrograph ESPRIT and initial results of the first light of TOPICS

#Ryota Kinoshita[1)],Takeshi Sakanoi[1)],Kazuya Nagata[1)],Aya Otomo[1)],Masato Kagitani[1)],Yasuhiro Hirahara[2)],Seiko Takagi[3)],Hiroaki Saito[3)],Hiroyuki Naito[4)]
[1Tohoku Univercity,[2Nagoya Univercity,[3Hokkaido Univercity,[4Nayoro Observatory

We report on the first light of the near-infrared imaging system TOPICS (Tohoku Planetary near-Infrared Camera System) using the Pirka telescope at Astronomical Observatory, Faculty of Science, Hokkaido University, and the current status of development of the near-infrared echelle spectrograph ESPRIT (Echelle Spectrometer for Planetary Research In Tohoku University). TOPICS and ESPRIT are being developed to be installed on the telescopes dedicated to planetary observation at the Haleakala summit(3055m), Hawaii. Concerning Jupiter, the largest giant planet in the solar system, plasma originating from Io volcanoes is dominant and accelerated in the co-rotating magnetosphere which causes auroral emission at high-latitudes through ionosphere-thermosphere coupling processes. Therefore, understanding the relationship between Jupiter's aurora, plasma supplied from Io, and plasma transport in the magnetosphere is essential for understanding Jupiter's magnetospheric variability.

TOPICS is a monochromatic imager with an InSb 256 x 256 array detector sensitive to 1-5 μ m, and its development was almost completed at the end of FY2022. The first-light observation was carried out from February 14 to 27, 2023 (Sakanoi et al., see presentation at this conference). On the evening of 26th, K-band (2.2 μ m and 2.3 μ m) and L-band (3.4 μ m and 3.9 μ m) observations of Venus (Vmag=-3.9) and Jupiter (Vmag=-2.0) were successfully made, and Jupiter and Europa were imaged in K-band, indicating that they can be observed well even in Japan. On the other hand, in the L-band, the TOPICS 3.4 μ m narrow-band filter observation had a strong background sky emission of about 6,000 counts in a 10-second exposure. Therefore, the Jupiter's H3+ aurora was not detected from the data analysis of images with an exposure of about 10 minutes. In addition, oblique noise pattern in the image, which was not seen in the laboratory tests, was confirmed, suggesting that noise countermeasures for the driving circuit system are necessary. We plan to perform another observation with TOPICS and the Pirka telescope in the summer of 2023, and we will install TOPICS on the T60 telescope at Haleakala in the winter of 2023. Since the sky background is low at Haleakala even in the L-band, observations of Jupiter's H3+ aurora and thermal radiation from Io volcano are expected to be obtained. We also make simultaneous visible observations (S+673nm and Na589nm) to monitor the gas transport in the vicinity of Io to the magnetosphere.

In parallel, we are developing the near-infrared spectrograph ESPRIT (R˜20,000) covering a wide wavelength range of 1-4 μ m. This adopts a common detector and driver circuit system with TOPICS. Mounting on the Haleakala T60 telescope (F12), the plate scale is 0.3"/pixel and the slit length is 50". With this long slit and wavelength resolution, the entire Jupiter will be captured to derive the Doppler velocity of the H3+ auroral emission lines simultaneously in the northern and southern hemispheres. The echelle grating is Newport #53∗453 (braze angle 71 degrees, groove 31.6/mm, effective size W=130mm x D=23mm). The vacuum chamber consists of an InSb detector (30-35 K), collimator-camera mirrors, and several mechanisms, such as, a two-stage filter turret mechanism (16 positions, including order sorters), a slit exchange mechanism, an image-spectral exchange mechanism, and a grating angle adjustment mechanism. The picomotor of grating angle adjustment mechanism is installed outside the radiation shield because of its specifications. This adjustment mechanism can change the angle of echelle grating with respect to the incident light from 60 to 75 degrees. The required accuracy is an absolute repeatability of less than 0.4 degrees and a stability of less than 1 arcsec/5 minutes (the physical length in the push/pull direction is 0.65 μ m, corresponding to a plate scale of 1/10 pixel, and the Doppler shift of the mission line is 0.5 km/s). A slit viewer camera, a gas lamp for wavelength calibration, and a blackbody for intensity calibration will be mounted outside the vacuum chamber. The dimensions are ˜800x500x400 mm and it weighs about 150 kg.

Currently, the optical system of ESPRIT has been completed and its performance has been demonstrated using visible laser light. The cooling system has also been completed by Kambara (2020) et al. using oxygen-free copper mesh (wire diameter φ 0.23 mm, density 50 mesh/inch), and both the radiation shield (90 K) and detector box (30 K) have been confirmed to be sufficiently cooled. We will carry out tests to verify the operation of the mechanisms mentioned above in the air and cooled vacuum conditions. Further, we plan to perform electrical tests with the InSb detector, and then transfer it to the Haleakala telescope.

本発表では、近赤外撮像装置 TOPICS(Tohoku Planetary near-Infrared Camera System) の北海道大学大学院理学研

究院附属天文台ピリカ望遠鏡によるファーストライト報告と、近赤外高分散エシェル分光撮像装置 ESPRIT（Echelle Spectrometer for Planetary Research In Tohoku University）の開発現況について報告する。これまで、ハワイ・ハレアカラ山頂観測所（3,055 m）の惑星専有望遠鏡を用いて惑星の連続観測を可能とするために、TOPICS と ESPRIT の開発を実施してきた。特に、太陽系最大の巨大惑星木星では、イオ火山を起源とするプラズマは共回転型磁気圏で加速され、電離圏-熱圏結合を通じて極域オーロラ発光を引き起こす。そのため、木星オーロラとイオからのプラズマ供給、ならびに木星磁気圏でのプラズマ輸送との関係を知ることは、木星磁気圏変動現象の理解に本質的である。

TOPICS は、1 – 5 μmに感度をもつ InSb256 × 256 アレーを検出器とする単色イメージャーである。2022 年度末にほぼ開発が完了し、2023 年 2 月 14 - 27 日までピリカ望遠鏡に設置してファーストライト観測を実施した（坂野井他、本学会発表参照）。特に 26 日の晩では、金星（Vmag=-3.9）と木星（Vmag=-2.0）の K バンド（2.2 μ m、2.3 μ m）、および L バンド（3.4 μ m、3.9 μm）の観測に成功し、 K バンドで木星およびエウロパが撮像され、国内でも十分に観測可能なことが分かった。一方 L バンドでは、TOPICS の 3.4 μ m 狭帯域フィルター観測の場合、背景スカイ発光が 10 秒露出で約 6000 カウントあった。このため、木星観測では露出約 10 分の画像の解析では H3+ オーロラは検出されなかった。また、東北大の実験室では見られなかった画像中の斜めノイズが確認され、駆動回路系のノイズ対策が必要であることがわかった。今後、TOPICS は、2023 年夏にピリカ望遠鏡による木星赤外観測を再度実施し、2023 年冬にハレアカラの T60 望遠鏡に設置する計画である。ハレアカラでは、L バンドにおいてもスカイ背景光は低いため、木星 H3+ オーロラ発光や、イオ火山火口の熱輻射の観測の実現が期待される。これとほぼ同時の可視観測（S+673nm、Na589nm) からイオ近傍〜磁気圏のガス輸送を捉え、イオ火山ガスが木星磁気圏に及ぼす影響を明らかにする。

これと並行して、近赤外分光器 ESPRIT の開発を進めている。ESPRIT は、TOPICS と検出器と駆動回路が共通のエシェル分光器（分解能は 20,000）であり、1-4 μ m の広波長範囲をカバーする。ハレアカラ T60 望遠鏡（F12）に取り付けた場合、プレートスケールは 0.3”/pix, スリット長は 50”である。この広視野スリットと波長分解能により、木星全体を同時に捉え、南北半球の H3+ オーロラ発光のドップラー速度を導出する。エシェル回折格子は Newport #53∗453（ブレーズ角 71 度、溝 31.6/mm、有効サイズ W=130mm × D=23mm）である。真空チャンバ内には、InSb 検出器（30-35K)、コリメーター-カメラミラー、2 段フィルターターレット機構（16 ポジション、オーダーソーター含む)、スリット交換機構、画像-分光切り替え機構、グレーティング角度調整機構が設置されている。この機構のうち、グレーティング角度調整機構に使用するピコモーターのみ、要求仕様のために冷却部外に設置される。この調整機構により、入射光に対するエシェルの角度を 60 度から 75 度まで変えることができる。これに要求される精度は、絶対繰返し精度 0.4 度以下、安定度 1arcsec/5 分以下（プッシュ/プル方向の物理的長さが 1/10 ピクセルのプレートスケールに相当する 0.65 μ m、これに対応する輝線のドップラーシフトは 0.5km/s）である。また、真空チャンバ外には、スリットビューワーカメラと波長校正用ガスランプ、および強度校正用黒体炉が搭載される。装置の寸法は˜800x500x400 mm、重さは約 150kg である。

現在、ESPRIT は、光学系が完成し、可視レーザー光を用いて性能が実証されている。また、冷却系についても Kambara(2020) らにより、無酸素銅メッシュ（ワイヤー径φ 0.23 mm、密度 50 mesh/inch）を用いて自作した熱パスが完成し、ラジエーションシールド (90K)、検出器ボックス (30K) ともに十分冷却することが確認されている。今後の試験により、2 段フィルターターレット機構、スリット交換機構、画像-分光切り替え機構、グレーティング角度調整機構の大気中および真空中冷却時の試験を行い、動作を検証する。この後、TOPICS の電気系回路を用いた検出器駆動試験を実施し、ハレアカラ望遠鏡に移設する計画である。

R009-P10
ポスター 2 ：9/25　AM1/AM2 （9:00-12:30）

#Matsuoka Ayako[1)],Dougherty Michele[2)],Brown Patrick[2)],Auster Hans-Ulrich[3)]
[(1 京都大学 理学研究科,[(2Imperial College London,[(3Institut fur Geophysik und extraterrestrische Physik, Technische Universitat Braunschweig

Magnetic field experiment at Jupiter icy moons (JUICE J-MAG) and in-flight sensor alignment calibration

#Ayako Matsuoka[1)],Michele Dougherty[2)],Patrick Brown[2)],Hans-Ulrich Auster[3)]
[(1Graduate School of Science, Kyoto University,[(2Imperial College London,[(3Institut fur Geophysik und extraterrestrische Physik, Technische Universitat Braunschweig

The magnetometer (J-MAG) is one of the core instruments on the JUICE spacecraft and is critical for examining prime scientific objectives of the mission. Firstly, we are expecting to gain an understanding of the interior structure of the icy moons of Jupiter, specifically those of Ganymede, Callisto and Europa. We will be able to obtain the knowledge of the depth at which the liquid oceans reside beneath their icy surfaces. We are also interested in the configuration of internal magnetic fields and the induced magnetic fields arising within these oceans. Secondary, the magnetic field drives the plasma processes within the Jupiter system. Magnetic field observations allow for a better interpretation of dynamical plasma processes, auroral phenomena and various current systems within the Jovian magnetosphere.

Defined J-MAG science targets result in a requirement to determine accurate knowledge of the sensing orientation by two fluxgate sensors, MAGIBS and MAGOB, on the spacecraft. Due to the long MAG boom it is not possible to meet J-MAG's alignment requirement by mechanical stability alone. To evaluate the alignment error of the sensing direction, the spacecraft includes two orthogonal coils mounted around its body. The coils can be driven with a current which produces a measurable magnetic field vector at the fluxgate sensors. This signal can then be used by the fluxgates to track the variation in the sensor alignment. In the presentation we show the results of an analysis using an alignment recovery technique that was developed for the Kaguya mission, applied to the specific case of JUICE, considering the relative positions of the fluxgate sensors with respect to JACS.

We derived equations to calculate the directions of the measurement axes in the frame fixed to the spacecraft, namely alignment angles, from the measurement results of reference magnetic fields generated by JACS. The errors of the alignment angle estimation and their dependence on measurement noise as well as inaccuracy of the coil current intensity are examined. Based on the quantitative results, the requirements to the JACS design and operation to satisfy the requests to the alignment accuracy are determined.

R009-P11
ポスター 2 ：9/25　AM1/AM2 （9:00-12:30）

#佐藤　晋之祐 [1)], 土屋　史紀 [1)], 堺　正太朗 [2)], 笠羽　康正 [1)],Nichols　Jonathan[3)], 木村　智樹 [4)], 安田　陸人 [1)]
([1] 東北大学 惑星プラズマ・大気研究センター,[2] 東北大学 理学研究科地球物理学専攻,[3]School of Physics and Astronomy, University of Leicester,[4] 東京理科大学 理学部物理学科

Analyzing Brightness of Europa's Auroral Footprint with the HST/STIS Dataset Taken in 2014 and 2022

#Shinnosuke Satoh[1)],Fuminori Tsuchiya[1)],Shotaro Sakai[2)],Yasumasa Kasaba[1)],Jonathan Nichols[3)],Tomoki Kimura[4)],Rikuto Yasuda[1)]
([1]Planetary Plasma and Atmospheric Research Center, Tohoku University,[2]Department of Geophysics, Graduate School of Science, Tohoku University,[3]School of Physics and Astronomy, University of Leicester,[4]Department of Physics, Faculty of Science, Tokyo University of Science

Satellite auroral footprints at Jupiter's upper atmosphere are the signature of the electromagnetic interaction between the Galilean moons and the Jovian magnetosphere. Wannawician et al. (2010) revealed that brightness of the Io footprint (IFP) aurora at far-ultraviolet (FUV) wavelength depends on the System III longitudes (λ_{III}) of Io, yet the same variation has not been found at the Europa, Ganymede, and Callisto footprints (EFP, GFP, and CFP, respectively) (e.g., Clark et al., 2002; Bonfond et al., 2013a; Bonfond et al., 2017a, Bhattacharyya et al., 2018). Our study aims to confirm if the brightness of the EFP auroras changes with the System III longitude of Europa as previously found at the IFPs.

Power generated through the moon-plasma interaction depends on the plasma density and magnetic field at the moon and propagates as the Alfven waves along the field lines into Jupiter's ionosphere to accelerate electrons. Hess et al. (2010) estimated the power generated at Io and found that it peaks twice when Io crosses the plasma torus equator at λ_{III} ~110 [deg] (the first peak) and 290 [deg] (the second peak), which corresponds to the peak brightness of the IFP auroras observed at the same longitudes (Wannawichian et al., 2010). This model would also be applicable to the EFPs, but the small number of detected EFP auroras and the low signal-to-noise ratio prevented further discussion of the longitudinal dependence.

We have investigated the variation of the EFP auroral brightness using FUV images taken in 2014 and 2022 by the Space Telescope Imaging Spectrograph (STIS) on the Hubble Space Telescope (HST) with the F25SRF2 filter (130 – 174 nm). In the northern hemisphere, we found that the first peak brightness of the EFP auroras appears when Europa is at λ_{III} ~135 [deg], which is longitudinally shifted from the expected longitude λ_{III} ~110 [deg], although this longitudinal shift is not notable in the IFP auroras according to the analysis by Wannawichian et al. (2010). On the other hand, we have not confirmed the second peak at λ_{III} ~290 [deg] so far, even though the EFP aurora at λ_{III} ~290 [deg] is expected to be brighter than the local minima at λ_{III} ~20 [deg] and 200 [deg] according to the power generation model at Europa as an application of Hess et al. (2010)'s model. The EFP auroras are detected in a range of $82 < \lambda_{III} < 198$ [deg] in the northern hemisphere, although the dataset we use covers wider λ_{III} ranges ($82 < \lambda_{III} < 278$ [deg]) and includes the instantaneous footprints expected by the JRM33 magnetic field model (Connerney et al., 2022) inside the HST's field of view. We have not identified what controls the detectability of the EFP auroras.

As a future work, we will try to reveal (a) why the first peak of the EFP aurora is longitudinally shifted from the model estimation and (b) why the second peak is not detectable in the dataset we use. We expect that comparing satellite footprint auroras of Io, Europa, Ganymede, and Callisto will provide a great opportunity to gain universal understandings of the electromagnetic interaction between the Galilean moons and the Jovian magnetosphere.

R009-P12
ポスター 2 ：9/25　AM1/AM2 （9:00-12:30）

望遠鏡観測を用いた天王星大気の輸送速度の推定

#天田　耕太郎 [1)], 高木　聖子 [1)], 高橋　幸弘 [2)], 佐藤　光輝 [3)]
([1] 北大理学院,[2] 北大・理・宇宙,[3] 北大・理

Estimations of the atmospheric transport velocity of Uranus using telescope observations.

#Kotaro Amada[1)],Seiko Takagi[1)],Yukihiro Takahashi[2)],Mitsuteru SATO[3)]
([1]Faculty of Science, Hokkaido University,[2]Faculty of Science, Hokkaido University,[3]Faculty of Science, Hokkaido University

Uranus is a planet that orbits at an inclination of 98 degrees to its orbital plane. As of June 2023, the only close observations of Uranus were made during the flyby observation by Voyager-2 in 1986. Apart from that, ground based observations have been ongoing using telescopes. In 2007, Uranus passed through the vernal equinox, and since 2014, a polar cap resulting from methane condensation has been observed in the northern polar region[Toledo et al., 2018]. Also, in observations conducted at the H-band (1.6 μ m), bright localized cloud regions have been identified on Uranus, which appear brighter than other areas[Sromovsky et al., 2015].

天王星は公転面に対し地軸が 98 ° 傾いた状態で公転する惑星である。2023 年 6 月現
在、過去の接近観測は 1986 年のボイジャー 2 号によるフライバイ観測のみであり、
この他は望遠鏡により観測が続けられている。2007 年に春分点を通過し、2014 年からは北極域にメタン沈降に起因する極冠が観察されている [Toledo et al., 2018]。また、H-band(1.6 μ m) における観測では他の部分よりも明るい局所雲領域が確認されている [Sromovsky et al., 2015]。

ハッブル望遠鏡 (HST) による雲頂模様のトラッキングから帯状風の最高速度は南北 60 ° 付近でそれぞれ約 250 m/s と推定されている。この帯状風速度は、深部において天王星磁場および惑星間磁場 (IMF) との相互作用が示唆されているが、観測装置のマシンタイム制約により深部大気における実際の輸送形態は判明していない [Soyuer et al., 2021]。

本研究では、北海道大学が所有する 1.6 m ピリカ望遠鏡のカセグレン焦点に搭載された撮像装置 MSI, 及び分光装置 UVS を用いて天王星の継続観測を行い、天王星大気成分であるメタンとアンモニアによる吸収量を用いて各高度における大気輸送速度の推定を行う。

2021 年 12 月から 2022 年 12 月の観測では、MSI で波長域 530 - 760 nm の波長域での分光撮像を行い、アンモニア吸収波長 552 nm とメタン吸収波長 619 nm における吸収量変化と天王星の周期より輸送速度を推定した。この結果、メタン吸収波長では [Soyuer et al., 2021] と同様の速度が推定されたが、アンモニア吸収波長においては速い速度が算出された。

2023 年 7 月以降の観測では、天王星に見られる局所雲の移動速度から大気成分の鉛直・経度方向における移動速度を推定することを目的とする。このため、MSI と UVS の並行観測を行い、従来よりも空間分解能・波長分解能を上げた解析を行う予定である。本発表では、この新たな観測方法における試験観測の結果についても取り上げる。

R009-P13
ポスター 2 ：9/25　AM1/AM2 （9:00-12:30）

水星の日中連続観測などに向けたハワイ・ハレアカラ東北大 60cm 望遠鏡に搭載する補償光学装置の開発

#吉野　富士香 [1)], 鍵谷　将人 [1)], 笠羽　康正 [1)]
([1] 東北大・理・惑星プラズマ大気研究センター,[2] 東北大・理・惑星プラズマ大気研究センター,[3] 東北大・理・惑星プラズマ大気研究センター

An adaptive optics system of Tohoku 60cm telescope at Haleakala observatory for daytime monitoring of Mercury's sodium exosphere

#Fujika Yoshino[1)],Masato Kagitani[1)],Yasumasa Kasaba[1)]
([1]Planetary Plasma and Atmospheric Research Center, Graduate School of Science, Tohoku University,[2]Planetary Plasma and Atmospheric Research Center, Graduate School of Science, Tohoku University,[3]Planetary Plasma and Atmospheric Research Center, Graduate School of Science, Tohoku University

We report on the development of a visible adaptive optics (AO) instrument for Tohoku 60cm telescope (T60) at Haleakala Observatory in Hawaii. The current goal is to join the ground-based support observation for the ESA-JAXA joint Mercury mission BepiColombo on the orbit in 2025˜2028.

The summit of Haleakala on Maui island (3,040 m) is one of the suitable site for monitoring the variable solar-system bodies due to clear sky and good seeing. T60 is equipped with a fiber-field-integrating instrument and a visible high-dispersion spectrograph with a wavelength resolution of 50,000, and contributes to continuous observations of solar-system objects mainly by remote control. Mercury, one of the targets of this development, has an exospheric atmosphere due to alkali metals. The resonant scattering emission of sodium D-lines (589.0 nm and 589.6 nm) is particularly bright and its distribution and velocity field can be observed from the ground by high dispersion spectroscopy. In the Mercury's magnetosphere the typical time scale of the variability expected from the interaction with the solar wind is as short as a few minutes. Ground-based observations have shown that the north-south ratio of the Na exospheric emission has a time scale of several tens of minutes, which is consistent with the time scale of the emission response due to the sputtering of magnetospheric particles, one of the factors that generate the Na exospheric atmosphere. There are also several global-scale emission patterns in the Na exosphere, but with previous observations using a slit scanning technique, it takes about an hour of scan data is required to create a global Mercury emission distribution. Therefore, observations that capture spatial variations on the scale of several tens of minutes have not been performed. Therefore, we are aiming to obtain global areal spectroscopic data with an integration time of about 5 minutes by using the high-resolution spectrograph (R=50,000) with an integral fiber unit installed on T60. However, for Mercury, which is an inner most planet with a maximum separation angle of only about 20 degrees from the Sum, we can only observe Mercury from the ground after sunset or before sunrise for a maximum of about one hour. In order to capture spatial-temporal variations of a few tens of minute time-scale, we need stable continuous observations that can resolve the disk not only at low altitudes just after sunset and just before sunrise, but also during the daytime when atmospheric fluctuations near the ground surface are large (seeing 2"˜5") due to surface heating caused by solar radiation, although at high altitude. Continuous observation is needed to enable disk decomposition even during the daytime.

Our visible AO system for T60 consists of a 12x12 140-element MEMS deformable mirror (Boston Micromachine) and a Shack-Hartmann wavefront sensor (TIS DMK33UX287 and Thorlabs MLA300-7AR). The size of each AO element is 12 cm on the primary mirror, which divide the primary mirror into 5x5. The test system has been installed at the Cassegrain focus of T60 in March 2022, and we developed and evaluated the AO control software remotely from Japan. The method for wavefront compensation calculation is mode-specific control by expanding the wavefront into Zernike modes. In this method, stable closed-loop AO control at 900 Hz was achieved for natural stars up to 4.4 mag. In a nighttime test observation of a 1.0-mag star, an FWHM of 1.4 " was achieved under natural seeing of 2.9 ". In a daytime test observation of a 1.0-mag star, an FWHM of 3.2 " was achieved under natural seeing of 4.3 ". In order to achieve a spatial resolution of 1", the wavefront sensor will be refurbished to increase the number of specular divisions for the purpose of sensing wavefront errors on a smaller spatial scale in June 2023.

In this presentation, we will report on the results, evaluation, and prospects of these test observations, including those after the refurbishment.

東北大学ハワイ・ハレアカラ観測所 60cm 望遠鏡 (T60) に搭載する可視補償光学 (AO) 装置の開発状況について報告する。本開発は、日欧合同 BepiColombo 水星探査機の周回観測 (2025˜2028) に対する地上観測支援を直近の目標としている。

マウイ島ハレアカラ山頂（海抜 3,040m）は、晴天率が比較的高くシーイングもよいため、連続的なモニター観測を要請される太陽系天体の変動観測に適した観測所のひとつである。ここに設置された T60 はファイバー視野集積装置と波長分解能 50000 の可視高分散分光器を備え、遠隔操作によって主に太陽系天体の継続的観測に寄与している。本開発の適用対象の１つである水星は、アルカリ金属による外圏大気の存在が知られ、特に中性ナトリウムの共鳴散乱発光 (589.0

nm および 589.6nm）が明るく地上からの高分散分光によりその分布と速度場の観測が可能である。地球と比較して小さい水星磁気圏では、太陽風との相互作用により期待される変動の典型的な時間スケールが数分程度と短い。地上観測により、Na 外気圏の発光の南北比が数 10 分の時間変動をすることがわかっており、これは Na 外圏大気の生成要因の一つである磁気圏粒子のスパッタリングによる放出応答時間のスケールと一致している。また Na 外気圏にはいくつかの全球規模の発光パターンがあるが、これまでの地上観測のスリットを用いた分光観測では、水星全球の発光分布を作成するには 1 時間ほどのスキャンデータの積分が必要になる。そのため、数 10 分スケールの全球規模の空間変動をとらえた観測は行われてない。そこで我々は T60 のファイバー視野集積装置と高分散分光器を用いることで、積分時間 5 分ほどで全球の面分光データを取得することを目指している。しかし、内惑星で太陽最大離角が 20 度程度の水星では、日没後・日出前に地上から観測できる時間は最大でも 1 時間程度で、低空ないし日中に観測するためシーイングが大きく、全球平均での議論に留めざるを得ない。数 10 分程度の時空間変動をとらえるには、日没直後・日の出直前の低高度に加え、高高度ではあるが日照による地表加熱に伴って地表面付近の大気ゆらぎが大きい（シーイング 2”~5”）日中でもディスク分解できるような安定した連続観測が必要である。日中の荒れたシーイングを補正しうる補償光学（AO）を、高時間分解能で長期モニタリング可能な T60 へ適用することは、BepiColombo 探査機との協調観測において重要なポイントとなる。本開発は、昼間の水星に対して空間分解能 1 “を達成するような AO を実現することを目標としている。

開発中の T60 用可視 AO システムは、12x12 の 140 素子の MEMS 可変型鏡 (Boston Micromachine 社) と Shack-Hartmann 波面センサ (TIS 社 DMK33UX287 と Thorlabs 社 MLA300-7AR) を用いた構成をとり、Windows PC を用いて最大 900 Hz の閉ループ制御を実現した。波面センサのサブ開口は 60cm 主鏡上で 12 cm であり、主鏡を 5x5 に分割する。昼間の水星 (視直径 5”-12”) に適応させるため、波面センサのサブ開口は視野角 32”とし、隣り合うサブ開口の背景光が重ならないように視野絞りを設置した。

このシステムを 2022 年 3 月からハワイ現地の T60 のカセグレン焦点に設置し、遠隔制御により AO 制御ソフトの開発と評価を行ってきた。波面補償計算には、波面センサの出力から Zernike モード 15 項に展開した波面誤差を導出し、事前に校正した可変形鏡出力を制御する手法を用いた。夜間では、4.4 等級までの対象で安定した閉ループ制御を実現しており、1.0 等級の恒星に対する試験では波長 590 nm でシーイング 2.9”(FWHM) の条件下で AO 動作時 1.4”を達成した。背景が明るくまたシーイングが厳しい昼間では、同じく 1.0 等級の恒星を対象にしたとき、シーイング 4.3”の条件下で AO 動作時に 3.2”を達成している。2023 年 6 月には、空間分解能 1 ”を目指すため、波面センサの鏡面分割数を 15x15 に増やす改装を行う。60cm の主鏡上で 4cm になる。これにより、より小空間スケールの波面誤差センシングが可能となるが、スポットの SN が下がるというデメリットもある。その上で、7 月以降には水星をターゲットとした試験観測を行う想定である。本講演では、この改装後を含む試験観測の結果・評価および今後の展望を報告する。

R009-P14
ポスター 2 ：9/25　AM1/AM2 （9:00-12:30）

MGS 探査機の長期間電離圏磁場観測に基づく火星電離圏 ULF 波動の特性と長期トレンドの調査

#今田　馨 [1)], 原田　裕己 [1)]
(1 京大・理,(2 京大・理

Investigation of Characteristics and Long-Term Trends of ULF Waves in the Martian Ionosphere: MGS Observations

#Kaworu Imada[1)],Yuki Harada[1)]
(1Graduate School of Science, Kyoto University,(2Graduate School of Science, Kyoto University

The solar wind directly interacts with the low-altitude plasma environment of Mars because the planet lacks a global intrinsic magnetic field. Waves that are left-hand polarized with a frequency similar to the local proton cyclotron frequency in the spacecraft reference frame are called proton cyclotron waves (PCWs), and they could have a long-term impact on the Martian ionosphere. For instance, several events have been reported in which the Mars Atmosphere and volatile EvolutioN (MAVEN) spacecraft observed upstream PCWs driving (”ringing”) new compressive magnetosonic waves in the ionosphere with an ultralow frequency (ULF) close to upstream proton gyrofrequency (Collinson et al., 2018; Fowler et al., 2018, 2021). In particular, the event reported by Fowler et al. (2018) strongly suggests that PCWs-driven waves in the ionosphere heat planetary heavy ions such as O^+ and $O_2{}^+$, contributing to ion escape to space. Romeo et al. (2021) determined the PCW occurrence rate based on the MAVEN spacecraft observations over almost three Martian years, and the results show that it is about 20% during the southern summer (L_s [degree]=[215, 315]). In addition, Fowler et al. (2021) visually identified the presence of compressive magnetosonic waves with a frequency below 0.1 Hz at altitudes below 1,000 km for 101 orbits of the MAVEN spacecraft from August 7, 2020 to August 22, 2020 (L_s [degree]=[253, 263]), and in 28% of the total orbits the waves were present. Considering these previous studies, the occurrence of upstream PCWs and the resultant ringing process are not uncommon, and its long-term impact on planetary ion heating and ionospheric dynamics may not be negligible. However, no statistical characterization has been made for the properties and spatial distribution of PCW-driven waves in the ionosphere.

In this study, we characterize them based on magnetic field data from April 1999 to November 2006 obtained by the magnetometer on board the Mars Global Surveyor (MGS) spacecraft. The MGS spacecraft was placed into Mars orbit in September 1997 and by March 1999 its orbit had transferred through aerobraking to a sun-synchronous orbit with an orbital inclination of 92.96 degrees and an average altitude of 378 km (Albee et al., 2001). The MGS spacecraft possesses an onboard magnetometer that provides vector magnetic field measurements with a sampling frequency of up to 16 Hz (Acuna et al., 1992, 1998), and therefore the PCW-driven waves in the ionosphere at an ultralow frequency can be detected. We calculate power spectral densities (PSD) based on magnetic field data observed at a quasi-constant altitude for about eight years and develop an algorithm that can automatically detect ULF waves from PSD at each time. Based on the results of the automatic detection of ULF waves, we investigate periodicities and long-term trends corresponding to the solar rotation period, solar cycle, and Martian year in the occurrence rate of the waves, statistical characteristics of the wave amplitude, and spatial distributions of the wave occurrence attributed to crustal magnetic field magnitude.

火星は非磁化惑星であるため、火星-太陽風相互作用が低高度のプラズマ環境に直接、大きな影響を及ぼしうる。バウショックの上流で発生する、衛星系で局所的なプロトンサイクロトロン周波数に近いピークを持ち、左回りの楕円偏波の波動はプロトンサイクロトロン波動 (PCW) と呼ばれており、長期的に電離圏に影響を及ぼしうると考えられる現象である。例えば、上流で発生した PCW が電離圏に新たな圧縮性の ULF 磁気音波を駆動する (ringing) 現象を Mars Atmosphere and Volatile EvolutioN (MAVEN) 探査機が観測したイベントがいくつか報告されている (Collinson et al., 2018; Fowler et al., 2018, 2021)。特に、Fowler et al. (2018) で報告されたイベントは、駆動された電離圏波動が惑星由来の重イオン加熱とそれに伴う散逸に寄与していることを強く示唆するものである。Romeo et al. (2021) は PCW の上流での発生率を MAVEN 探査機の 3 火星年にわたる観測データから推定し、南半球の夏の季節 (L_s = 215° − 315°) では、およそ 2 割となることを報告している。また、Fowler et al. (2021) では 2020 年 8 月 7 日から 2020 年 8 月 22 日までの期間 (L_s = 253° − 263° に対応) に観測された MAVEN 探査機の 101 軌道分の電離圏観測データに対して、高度 1,000 km 以下の領域に 0.1 Hz 以下の圧縮性の磁気音波が存在するかどうかを目視で確認している。その結果として全体の 28% の軌道で波動が存在していたという。これらの先行研究を踏まえると、上流で PCW が発生することと、それが電離圏に圧縮性の磁気音波を駆動することは珍しい現象ではなく、惑星イオン加熱や電離圏ダイナミクスへの長期的な寄与は無視できない可能性がある。しかし、現在まで PCW が駆動した電離圏波動の特性や空間分布に対する統計的な特徴づけは行われてこなかった。

本研究ではこの課題に対して、Mars Global Surveyor (MGS) 探査機が 1999 年 4 月から 2006 年 11 月までの期間に観測した電離圏磁場データの解析によってアプローチをする。MGS 探査機は 1997 年 9 月に軌道投入され、エアロブレーキングを行うことで 1999 年 3 月までに軌道傾斜角 92.96°、平均高度 378 km、14:00/2:00LT を通る太陽同期軌道に遷

移した (Albee et al., 2001)。また、探査機は最大サンプリング周波数が 16 Hz の磁力計 (Acuña et al., 1992, 1998) を搭載しているので、研究対象となる ULF 磁気音波を観測できると考えられる。本研究では、一定高度でおよそ 8 年間観測された磁場データに対して周波数解析を行い、適切なアルゴリズムを開発することによって各時刻において波動の自動検出を試みる。また、波動の自動検出結果から、発生率の周期変動 (太陽自転周期、太陽活動周期、火星年) の有無や、波動の統計的特性 (振幅)、空間分布 (地殻磁場の強弱による発生率の違いなど) を調査する予定である。

R009-P15
ポスター 2 ：9/25　AM1/AM2 （9:00-12:30）

初期の火星・地球大気における太陽高エネルギー粒子照射による複数種アミノ酸から構成されるペプチドの非生物合成

#櫻井　悠貴 [1)], 木村　智樹 [1)], 小林　憲正 [2)], 鳥越　秀峰 [1)], 寺田　直樹 [3)]
([1] 東京理科大学,[2] 横浜国立大学,[3] 東北大学

Abiotic synthesis of peptides from amino acids driven by the SEPs in early Martian and terrestrial atmospheres

#Yuki Sakurai[1)],Tomoki Kimura[1)],Kensei Kobayashi[2)],Hidetaka Torigoe[1)],Naoki Terada[3)]
([1]Tokyo University of Science,[2]Yokohama National University,[3]Department of Geophysics, Graduate School of Science, Tohoku University

The origin of amino acids, peptides, proteins, and their precursors is the most important issue for elucidating the origin and evolution of life on planets with the atmosphere and ocean. It has been theoretically predicted that these prebiotic substances are synthesized abiotically from atmospheric molecules by any energy injections: e.g., lightning discharge, solar ultraviolet photon, and Solar Energetic Particles (SEPs). Many laboratory experiments have been conducted for the abiotic synthesis of prebiotic substances from the atmosphere by various energy injections [e.g., Miller, 1953]. Most of these laboratory experiments have used mildly reduced (CO or CO_2, H_2O, N_2) and strongly reduced (CH_4, H_2O, NH_3) atmospheres as early Mars and Earth atmospheres. Proton irradiation experiment simulated the solar energetic particle (SEP) injections produced amino acids and their bound macromolecules called tholins [Sagan and Khare, 1979] from both the mildly and strongly reduced atmospheric molecules [Kobayashi et al., 1989]. Although only the amino acids and tholins were synthesized in the previous studies, the creation of peptides through the amino acid joining and abiotic evolution to synthesize the protein have not been evaluated yet.

Here we focus on the sulfur dioxide gas, which is abundant around the volcanoes on ancient Mars and Earth and highly reactive for the chemical process in the atmosphere. With the assumption that the sulfur-containing amino acids as well as the non-sulfur-containing amino acids were abiotically synthesized from the volcanic atmosphere, we evaluated the abiotic synthesis of peptides from these mother substances based on the laboratory plasma irradiation experiment. We irradiated a powder sample of non-sulfur-containing amino acids composed of 74.6% glycine, 19.9% alanine, and 5.49% serine, and a sample with sulfur-containing amino acids (cysteine) composed of 73.3% glycine, 19.6% alanine, 5.39% serine, and 1.77% cysteine by hydrogen ions at 10 keV with a beam current of 7 μ A. By the high-performance liquid chromatographic analyses, we detected macromolecular organic compounds only from the sulfur-containing amino acid sample. The N-terminal amino acid sequence analyses of the macromolecular compounds showed that the detected macromolecules contained multiple peptide bonds, indicating that the peptide-like compound was synthesized in the sample. These results suggested that the peptides were abiotically synthesized in the atmosphere around the volcanoes on ancient Mars and Earth. We are just ongoing to extend the structural analyses of the peptide-like compounds and the abiotic syntheses of peptides and proteins by the plasma irradiation of atmospheric molecules containing sulfur.

Kobayashi, K, Tsuchiya, M., Oshima, T., and Yanagawa, H.: 1990, Origins of Life and Evolution of the Biosphere 20, 99-109.
Miller, S. L.: 1953, Science 117, 528.
Sagan, C. and Khare, B. N.: I971, Science 173,417.
Sekine, Y.:2012, Jour. Geol. Soc. Japan, Vol 118, No.10, 650-663.

大気や海洋を有する惑星において、生命の発生に必要なアミノ酸やタンパク質の起源は未解明である。タンパク質を構成するペプチド、アミノ酸や、その前駆体の起源を解明することは、生命の起源や発生条件の理解をする上で最重要の課題である。これらの生命前駆物質が、大気へのエネルギー入射により大気分子から非生物的に合成されたとする説があり、様々な初期惑星大気とエネルギーの組み合わせで非生物的合成実験が行われてきた [e.g., Miller, 1953] 。初期の火星や地球の大気は主に弱還元型（CO または CO ☒, H ☒ O, N ☒）と強還元型（CH ☒, H ☒ O, NH ☒）の 2 種類が提案されているが、いずれの場合も太陽高エネルギー粒子 (Solar Energetic Particles, SEPs) を模した陽子照射により大気分子からアミノ酸や、構造が一定でないソリンと呼ばれる高分子の物質 [Sagan and Khare, 1979] が生成されることが分かっている [Kobayashi et al., 1989] 。しかし、先行研究ではアミノ酸とソリンの合成までにとどまっており、アミノ酸結合によるペプチド形成や、タンパク質への非生物的進化は未検証である。

そこで本研究は、初期の火星・地球の火山周辺に豊富に存在し、反応性の高い含硫気体に注目した。元素として硫黄を含むアミノ酸が、他のアミノ酸と同様に SEPs により大気中で非生物的に合成されたと仮定し、それらを母物質としたペプチドの非生物的合成をプラズマ照射実験で検証した。実験室において初期の火星・地球大気から生成されるアミノ酸組成（グリシン 74.6%、アラニン 19.9%、セリン 5.49%）を模した粉体サンプルと、含硫アミノ酸（システイン）を含む粉体サンプル（グリシン 73.3%、アラニン 19.6%、セリン 5.39%、システイン 1.77%）へ、水素分子イオン（10 keV, 7 μ

A）を照射した。高速液体クロマトグラフィー分析の結果から、含硫アミノ酸を含む照射サンプルのみから、アミノ酸より高分子の物質が検出された。また、高分子物質の N 末端からのシーケンス解析結果より、生成した高分子はペプチド結合を複数持つことがわかった。このことから、含硫アミノ酸はアミノ酸同士の結合を促進し、ペプチドライクなポリマーを形成することが明らかになった。これらは、初期火星・地球の火山付近の大気中において、ペプチドが SEP により非生物合成されていることを示唆する。今後は、ペプチドライクなポリマーの構造分析や、硫黄を含む大気分子への照射実験により、ペプチドやタンパク質の非生物合成に取り組む予定である。

R009-P16
ポスター 2 ：9/25　AM1/AM2 （9:00-12:30）

#柿沼　希泉 [1)], 今村　剛 [1)], 青木　翔平 [1)], 野口　克行 [2)],Kleinboehl Armin[3)]
([1] 東京大学大学院,[(2] 奈良女子大,[(3]NASA

Mid-latitude disturbances in the Martian atmosphere studied with MRO MCS data

#Nozomi Kakinuma[1)],Takeshi Imamura[1)],Shohei Aoki[1)],Katsuyuki Noguchi[2)],Armin Kleinboehl[3)]
([1]The University of Tokyo,[(2]Nara Women's University,[(3]NASA

Similarly to the Earth, baroclinic waves are thought to play a significant role also on Mars in determining the climate at mid-to high-latitudes. It is known that baroclinic waves with zonal wavenumber1,2, and 3 are dominant and they become the strongest from autumn to winter in the northern hemisphere (Barnes, 1981). In addition, baroclinic waves are thought to have a connection with the meridional transport of substances in the Martian atmosphere, such as dust and water ice particles. Images taken by Mars Orbiter Camera onboard Mars Global Surveyor (MGS) revealed the possible relations between baroclinic waves and the transport of dust (Wang et al., 2005). However, previous studies considered the behavior of the waves below the 18Pa level with low vertical resolution (~10km) data set (Banfield et al., 2004). The propagation at higher altitudes has not been investigated yet. Also, the relations between baroclinic waves and the transport processes of dust and water ice particles have not been studied quantitatively.

To characterize the behavior of baroclinic waves in high altitudes, we have investigated the meridional distribution of the amplitude of the baroclinic waves and how it changes with a time resolution of 1 Martian day by using Mars Reconnaissance Orbiter (MRO) Mars Climate Sounder (MCS) limb observation data. This has a higher vertical resolution (~5km) than the data used in previous studies of baroclinic waves. To clarify how baroclinic waves have an influence on the transport processes of dust and water ice particles, we examined how the zonal distributions of dust and water ice particles vary with time and latitude and their correlations to the propagation of traveling waves seen in the temperature distribution. The retrieved data of temperature, dust opacity, and water ice opacity in MY30 within a pressure range from 200 to 1 Pa, corresponding to the altitude range from about 10 to 55 km above surface, are used in our survey. After dividing the data into time intervals with a length of 1 Martian day and subtracting the seasonal trend, fluctuations of temperature, dust opacity, and water ice opacity are analyzed. Then, we computed the amplitudes of zonal wavenumber 1-3 for each pressure surface. To examine the way of the propagation of dust and water ice particle distributions, Hovmoller diagrams were made for each substance, and we compared them with the propagation of the traveling waves.

Our results show that waves with zonal wavenumber 1 become dominant at mid-to high-northern latitudes during the perihelion season in high altitudes. Large amplitudes of zonal wavenumber 2 were also seen on several days. The region where a large amplitude appears was consistent with the region of a large temperature gradient. This result indicates that the large amplitude of traveling waves in high altitudes occurs due to baroclinic instability. Also, some zonal propagations of water ice particle distributions were seen at the same region during the same season as the propagation of traveling waves. The correlation coefficients between the zonal distributions of temperature and water ice opacity were found to be negative in most days. This result denotes a possible connection between baroclinic waves and transport of water ice particles.

R009-P17
ポスター 2 ：9/25　AM1/AM2 （9:00-12:30）

#西野　真木 [1)], 原田　裕己 [2)], 関　華奈子 [3)],Halekas　Jasper[4)],Espley　Jared[5)],Dibraccio　Gina[5)]
[(1] 宇宙機構,[(2] 京大・理,[(3] 東大理・地球惑星科学専攻,[(4]University of Iowa,[(5]NASA

Strong bulk plasma acceleration in the Martian magnetosheath under low Alfven Mach number solar wind

#Masaki Nishino[1)],Yuki Harada[2)],Kanako Seki[3)],Jasper Halekas[4)],Jared Espley[5)],Gina DiBraccio[5)]
[(1]Japan Aerospace Exploration Agency,[(2]Graduate School of Science, Kyoto University,[(3]Department of Earth and Planetary Science, Graduate School of Science, University of Tokyo,[(4]University of Iowa,[(5]NASA

The magnetosheath environment around Mars is a key for understanding interactions between the solar wind, the ionosphere, and the induced magnetosphere. The dependence of the magnetosheath plasma on the solar wind Alfven Mach number (M_A) has been studied statistically, while no detailed study of very low M_A events at Mars has been conducted yet. Here we report MAVEN observations of strong bulk plasma acceleration in the magnetosheath near the ionopause around the terminator under the low M_A solar wind condition (M_A~2-3). In these events, the solar wind speed was about 400 km/s and decelerated to 250 km/s at the bow shock, while the speed of the accelerated flows in the magnetosheath was as high as 550 km/s. The interplanetary magnetic field was of the Parker spiral configuration, and the accelerated flows were detected in the -E hemisphere and almost perpendicular to the local magnetosheath magnetic fields. The accelerated flows around the Martian ionopause may be a counterpart of those found in the terrestrial magnetosheath under the low M_A solar wind condition; that is, the strong acceleration may be attributed to both magnetic pressure gradient and tension force. We will discuss the possible effect of the low M_A solar wind on the Martian atmospheric escape in the -E hemisphere, where snowplows can play a substantial role under the typical M_A values.

R009-P18
ポスター 2 ：9/25　AM1/AM2 （9:00-12:30）

#侯　成澤 [1)], 今村　剛 [2)], 杉山　耕一朗 [3)]
[(1] 東京大学,[(2] 東京大学,[(3] 松江高専

Numerical modeling of mesoscale dynamics around enormous mountains on Mars

#CHENGZE HOU[1)],Takeshi Imamura[2)],Koichiro Sugiyama[3)]
[(1]The University of Tokyo,[(2]Graduate School of Frontier Sciences, The University of Tokyo,[(3]National Institute of Technology, Matsue College

The Tharsis Montes on Mars is a vast volcanic plateau, boasting four enormous volcanoes, named Ascraeus Mons, Pvconis Mons, Arsia Mons, and Olympus Mons. On the western flank of Arsia Mons, an elongated, luminous cloud of water ice extending over 1500 kilometers was observed by Mars Express orbiter using its Visual Monitoring Camera (VMC). This spectacular weather event underscores the complexity of the atmospheric circulation in this region, where mesoscale phenomena induced by the massive mountainous terrain are thought to be key contributors.

As exploratory research, we started by revisiting observations and numerical simulations of these mesoscale phenomena in the Tharsis Montes region, as documented in prior studies. This review allows us to succinctly outline the characteristic atmospheric circulation in this area. Following this, we utilized numerical simulations to predict the role of these enormous mountains in influencing atmospheric circulation from an idealized experimental perspective. Next, we delve into simulating with real topography. The insights gleaned from this approach will not only advance our understanding of Mars's atmospheric dynamics but also offer valuable context for future explorations of this region.

R009-P19
ポスター 2 ：9/25　AM1/AM2 （9:00-12:30）

#中村　勇貴 [1)], 関　華奈子 [2)], 堺　正太朗 [3)], 寺田　直樹 [4)]
([1] 東大理・地球惑星科学専攻,[2] 東大理・地球惑星科学専攻,[3] 東北大・理・地球物理,[4] 東北大・理・地球物理

Development of a photochemical model for the impacts of solar energetic particles on prebiotic chemistry on early Mars

#Yuki Nakamura[1)],Kanako Seki[2)],Shotaro Sakai[3)],Naoki Terada[4)]
([1]Department of Earth and Planetary Science, Graduate School of Science, University of Tokyo,[2]Department of Earth and Planetary Science, Graduate School of Science, University of Tokyo,[3]Department of Geophysics/PPARC, Graduate School of Science, Tohoku University,[4]Department of Geophysics, Graduate School of Science, Tohoku University

Understanding the effects of solar energetic particles (SEPs) on the atmospheric chemistry on early Mars is of astrobiological interest, because the precipitation of SEPs into the early Martian atmosphere could have facilitated the prebiotic chemistry. The flare observations of solar-type G stars by Kepler mission suggested that our Sun should have been much more active, and intense SEP events could have hit the planetary atmospheres repeatedly 4 billion years ago (e.g., Lingam et al., 2018). Such recurrent SEP events in the past and high efficiency in the production of amino acids suggested by previous laboratory experiments (Kobayashi et al., 2023). SEPs are therefore considered as one of the key energy sources for prebiotic chemistry on early Mars.

In this study, we developed a photochemical model on the early Martian atmosphere to investigate the contribution of SEPs to production of HCN and H2CO, which are known as the precursors of amino acids and ribose. To take into account the production of hydrogen atom via water cluster ion chemistry properly, we have investigated the dependence of hydrogen atom production rate as a function of the ionization rate. We found that the production rate of hydrogen atoms per one ion pair production reaches unity below the hygropause altitude in CO2-dominated Martian atmosphere, which falls sharply above the hygropause. Application of the parameterization of the production of hydrogen atoms during SEP events to the early Martian neutral atmospheric chemistry will also be presented.

References:

Lingam, M., Dong, C., Fang, X., Jakosky, B., and Loeb, A. (2018). The Propitious Role of Solar Energetic Particles in the Origin of Life, The Astrophysical Journal, 853:10, doi:10.3847/1538-4357/aa9fef.

Kobayashi, K., Ise, J.-i., Aoki, R., Kinoshita, M., Naito, K., Udo, T., Kunwar, B., Takahashi, J.-i., Shibata, H., Mita, H., et al. (2023). Formation of Amino Acids and Carboxylic Acids in Weakly Reducing Planetary Atmospheres by Solar Energetic Particles from the Young Sun, Life, 13, 1103, doi:10.3390/life13051103

R009-P20
ポスター 2 ：9/25　AM1/AM2 （9:00-12:30）

MAVEN NGIMS 観測による火星超高層大気（電離圏）における大気種の振る舞い

#長田　章嗣 [1),Liu　Huixin[2), 中川　広務 [3)
(1 九大・理・地惑,(2 九大・理・地惑,(3 東北大・理・地球物理

Atmospheric Species Behavior in the Martian Upper Atmosphere (Ionosphere) : MAVEN NGIMS Observations

#Noritsugu Nagata[1),Huixin Liu[2),Hiromu Nakagawa[3)
(1Department of Earth and Planetary Sciences, Faculty of Science, Kyushu University,(2Department of Earth and Planetary Science, Graduate School of Science,Kyushu University,(3Department of Geophysics, Graduate School of Science, Tohoku University

The current extremely thin Martian atmosphere is primarily caused by atmospheric escapes into space. Understanding the process of atmospheric escape is important to get insights both of the current and the past Martian atmosphere.

The causes of atmospheric escape are broadly categorized into internal (e.g., dust storms, atmospheric gravity waves) and external (e.g., solar winds, coronal mass ejections) forcing. The ionosphere, which we focus on in this study, is an ionized layer due to photoionization within the thermosphere starting from an altitude of 120 km. Due to its charged nature, the ionosphere plays an important role in understanding of atmospheric escape. Unlike neutral particles, ionized particles, namely ions, cannot be explained only by simple physical processes. It is required to consider the impacts of external forces due to their charged signatures.

Several previous studies have primarily focused on neutral species in the Martian thermosphere, and it leads a limited understanding of ions in the ionosphere. Therefore, in this study, we examine the difference in the behavior of atmospheric species in the Martian upper atmosphere by analyzing observational data from NGIMS (Neutral Gas and Ion Mass Spectrometer) onboard MAVEN (Mars Atmospheric and Volatile EvolutioN) spacecraft. Specifically, we compare the behavior of ions in the ionosphere with the previous studies, e.g. England et al. (2017), which mainly focused on neutral species in the thermosphere.

In the future study, we aim to extend the discussion into the effects of the Martian locally crustal magnetic fields and external forcing on ions in the ionosphere, and atmospheric escape.

現在の非常に薄い火星大気は、主に宇宙空間への大気散逸が原因とされる。大気の散逸について知ることは現在のみならず、過去の火星大気を知る上でとても重要である。

大気が散逸する原因は主に、内的（ダストストーム、大気重力波等）、外的（太陽風、コロナ質量放出等）強制によるものであり、本研究で注目する電離圏（高度 120 km からの熱圏内に含まれる、光電離を受け電離状態にある層）は電荷を持つという性質上、大気散逸の理解において非常に重要である。電離状態の粒子、すなわちイオンは電荷を帯びており、中性粒子のように単純な物理過程のみでは説明出来ず、外的強制による影響を加味する必要がある。

過去の研究では熱圏中性粒子に着目したものが多く、電離圏のイオンについての知見が不足している。そこで本研究では MAVEN (Mars Atmospheric and Volatile EvolutioN) 探査機の NGIMS (Neutral Gas and Ion Mass Spectrometer) による観測結果を用いて、火星の超高層大気の大気種による振る舞いの違いに着目する。具体的には、England et al. (2017) 等の熱圏の中性粒子に関する先行研究と電離圏のイオンとの比較を行う。

本研究では、将来的に火星の局所的な地殻磁場や外的強制による電離圏のイオン、大気散逸への影響へと議論を展開していきたい。

R009-P21
ポスター 2 ：9/25　AM1/AM2 （9:00-12:30）

複数探査機観測に基づく尾部イオン散逸の供給源の研究

#竹内　直之 [1)], 原田　裕己 [2)]
[(1] 京大,[(2] 京大・理

Probing sources of the tailward ion escape based on the multiple spacecraft observations

#Naoyuki Takeuchi[1)],Yuki Harada[2)]
[(1]Kyoto University,[(2]Graduate School of Science, Kyoto University

It is thought that Mars had a warm climate and liquid water on its surface about 4 billion years ago while at present its surface is far colder and drier. Such an environmental change requires the removal of greenhouse gasses such as carbon dioxide, and the loss of the Martian atmosphere can be partially explained by the ion escape from Mars. Since the tailward ion escape accounts for the majority of the ion escape from Mars, identifying the sources of the escaping ions can provide us with clues to understand the mechanism of the ion escape and, ultimately, the environmental change Mars had experienced.

In this study, we focus on the nightside ionosphere as a candidate for the main source of the tailward ion escape, and investigate how the density of the nightside ionosphere affects the tailward ion escape rate. Since it is difficult to simultaneously observe two distant regions by a single spacecraft, we use two spacecraft: Mars Atmosphere and Volatile EvolutioN (MAVEN) and Mars Express (MEX). We analyze data from the Mars Advanced Radar for Subsurface and Ionosphere Sounding (MARSIS) of MEX and the Suprathermal and Thermal Ion Composition (STATIC) of MAVEN when they observe the nightside ionosphere and the tail region, respectively, roughly at the same time, thereby deriving the density of the nightside ionosphere and the tailward ion flux.

約 40 億年前の火星には温暖な気候で表面に液体の水が存在していたと考えられているが、現在の火星は遥かに寒冷で乾燥している。このような火星の環境変化が起きるためには二酸化炭素のような温室効果ガスが取り除かれる必要があり、そのプロセスの一部を火星からのイオン散逸により説明できる可能性がある。火星のイオン散逸において尾部からの散逸は大きな割合を占めているため、その供給源がどこにあるのかを明らかにすることはイオン散逸の機構、ひいては火星の環境変化を理解する手がかりとなりうる。

本研究では、火星の尾部イオン散逸の供給源として夜側電離圏に注目し、夜側電離圏の密度の高低が尾部からのイオン散逸率にどのような影響を与えるのかを調査する。火星の夜側電離圏と誘導磁気圏尾部の関係を調べる上で、単一の探査機で遠く離れた二つの領域を同時に観測することが難しいため、複数の探査機のデータを用いる。Mars Express の MARSIS が夜側電離圏、MAVEN の STATIC が尾部をそれぞれおよそ同じ時期に観測しているデータを収集し、電離圏密度と尾部イオンフラックスを導出してそれらの間にどのような関係性があるのかを調査する予定である。

R009-P22
ポスター 2 ：9/25　AM1/AM2 （9:00-12:30）

#佐藤　隆雄 [1)], 佐藤　毅彦 [2,3)], 村上　真也 [2)]
([1] 情報大,[2] 宇宙研,[3] 総研大

Stability and variability of Venusian cloud top altitude from the complete set of dayside images taken by Akatsuki IR2

#Takao Sato[1)],Takehiko Satoh[2,3)],Shinya Murakami[2)]
([1]Hokkaido Information University,[2]Institute of Space and Astronautical Science, Japan Aerospace Exploration Agency,[3]The Graduate University for Advanced Studies, SOKENDAI

Venus is completely shrouded by optically thick clouds of sulfuric acid that are located between ˜47 and 70 km. The clouds play significant roles in the chemistry, dynamics, and energy balance of the atmosphere. The cloud tops have been investigated through imaging, spectroscopy, and polarimetry in a broad range of wavelengths, from UV to mid-infrared, as well as in-situ measurements. For example, Ignatiev et al. (2009) studied the cloud top altitude from the depth of CO_2 absorption band at 1.6 micron acquired by VIRTIS onboard Venus Express. They found that the cloud tops decreased poleward of 50 deg and this depression coincided with the eye of the polar vortex.

Sato et al. (2020) described the dayside cloud top structure of Venus as retrieved from 93 images acquired at a wide variety of solar phase angles (0-120 deg) using the 2.02-micron channel of the 2-micron camera (IR2) onboard the Venus orbiter, Akatsuki, from April 4 to May 25, 2016. Since the 2.02-micron channel is located in a CO_2 absorption band, the sunlight reflected from Venus allowed us to determine the cloud top altitude corresponding to a unit aerosol optical depth at 2.02 micron. First, the observed solar phase angle dependence and the center-to-limb variation of the reflected sunlight in the region equatorward of 30 deg were used to construct a spatially averaged cloud top structure characterized by cloud top altitude z_c, Mode 2 modal radius $r_{g,2}$, and cloud scale height H, which were 70.4 km, 1.06 micron, and 5.3 km, respectively (Hereafter, this retrieval process is referred to as Step I). Second, cloud top altitudes at individual locations were retrieved on a pixel-by-pixel basis with an assumption that $r_{g,2}$ and H were uniform for the entire planet (Step II). The latitudinal structure of the cloud top altitude was symmetric with respect to the equator. The average cloud top altitude was 70.5 km in the equatorial region and showed a gradual decrease of ˜2 km by the 45 deg latitude. It rapidly dropped at latitudes of 50-60 deg and reached 61 km in latitudes of 70-75 deg. The average cloud top altitude in the region equatorward of 30 deg showed negligible local time dependence, with changes up to 1 km at most.

In this study, we applied the method described above to the complete set of 2.02-micron images (a total of 374 images taken from December 11, 2015, to October 29, 2016) to better understand the latitudinal, local time, and temporal variations in cloud top altitude of Venus. After the publication of Sato et al. (2020), parameters to represent the sensitivity of radiance to the detector temperature was revised and a method for identifying saturated pixels of IR2 image was updated. In addition, the spectroscopic line parameters used for radiative transfer model were also replaced by the latest HITRAN2020 database. In the retrieval process, the complete set of 2.02-micron images was grouped into a few subsets allocated on the basis of the solar phase angle dependence. Then, Step I was applied to each subset. The cloud top structure derived from a subset including the images used in Sato et al. (2020) was found to be robust to these updates. In this presentation, we present initial results of this follow-up analysis regarding the cloud top altitude of Venus using IR2 images.

R009-P23
ポスター 2 ：9/25　AM1/AM2 （9:00-12:30）

#佐藤　毅彦 [1)], 佐藤　隆雄 [2)], 今村　剛 [3)]
([1] 宇宙研,[2] 情報大,[3] 東京大学

Aerosol properties in the ”enormous cloud cover” of Venus as inferred from photometrically improved IR2 night-side data

#Takehiko Satoh[1)],Takao M Sato[2)],Takeshi Imamura[3)]
([1]Institute of Space and Astronautical Science, Japan Aerospace Exploration Agency,[2]Hokkaido Information University,[3]Graduate School of Frontier Sciences, The University of Tokyo

A very abrupt change of cloud opacity seen in the night-side disk of Venus, which we call Enormous Cloud Cover or ECC for short, was imaged by Akatsuki/IR2 and Venus Express/VIRTIS-M (Peralta et al., 2020). Similar phenomena were repeatedly recorded also by the ground-based instruments since the beginning of the night-side observations (Allen and Crawford, 1984), suggesting this phenomenon is not uncommon in the Venus atmosphere and may include essential dynamical implication. We perform radiative transfer (RT) analyses of ECC with comparison to Background Cloud (BC) to understand how aerosol properties change from BC to ECC.

To improve the photometric accuracy, needed especially for the extremely-low radiance region (ECC), an alternative method to clean the IR2 1.735- and 2.26-um data has been developed (named RSS202). The new method uses an over-exposed (12.97 s) 2.02-um image, recorded between the 2.26- and 2.32-um images, to cancel the contamination from the dayside. Acquisition of the 2.02-um image was introduced when the observing program suite was updated in June 2016 after which ECC was observed with IR2 in five occasions. The RSS202-processed data are validated against those processed with the original RSS method (Satoh et al., 2021). The correlation plot of the RSS radiance and the RSS202 radiance appears linear, indicating good consistency between two methods and the robustness of results with the data.

We will present the results of RT analyses and discuss the variation of BC-to-ECC changes for different occasions. The variability will give us clues to understand the mechanism of this prominent phenomena in the Venus clouds.

R009-P24
ポスター 2 ：9/25　AM1/AM2 （9:00-12:30）

金星の下層雲の形成におけるケルビン波の役割

#今村　剛 [1)]
(1 東京大学 新領域創成科学研究科

Role of a Kelvin wave in the formation of Venusian lower clouds

#Takeshi Imamura[1)]
(1Graduate School of Frontier Sciences, The University of Tokyo

Venus is completely shrouded by sulfuric acid clouds, which are thought to play major roles in the climate system of the planet. The main cloud deck extends from about 48 km up to ~ 70 km, and can be subdivided in three layers according to the extinction coefficient and the particle population. The upper cloud, which is located in the stably-stratified atmosphere around 58-70 km altitudes, is thought to be mostly photochemical origin. The middle cloud located around 50-58 km will be maintained by the condensation of H2SO4 vapor transported from below by convection. The lower cloud, which is located around 47-50 km and is highly variable, is not well understood in terms of the origin and the microphysical properties. Using near-infrared window wavelengths, large opacity variations have been observed, and those variations are thought to occur mostly in the lower part of the cloud layer. A notable feature is a planetary-scale dark cloud propagating with a period of 4.9-5.5 days, which was first discovered by ground-based observations (Crisp et al. 1991). The IR2 camera onboard the Venus orbiter Akatsuki observed this phenomenon more in detail, and found that a planetary-scale cloud discontinuity that spans in the north-south direction characterizes the propagating structure (Satoh et al. 2017; Peralta et al. 2020). The relatively large amplitude near the equator and the zonal propagation faster than the background atmosphere indicate that the cloud opacity variation is basically induced by a Kelvin wave. A Venus GCM reproduced a 5.5-day periodicity in the thickness of the lower cloud driven by a Kelvin wave with a zonal wavenumber of unity (Ando et al. 2021). Nevertheless, the observed sharp discontinuity was not reproduced in the previous models. In this study, the nucleation of cloud droplets in oscillating winds associated with a Kelvin wave is studied using a simplified microphysical model, and the role of the wave in the formation of the lower cloud and the conditions for the appearance of the sharp discontinuity are discussed.

R009-P25
ポスター 2 ：9/25　AM1/AM2 （9:00-12:30）

#須川　天万 [1)], 田口　真 [1)]
[(1] 立教大・理・物理,[(2] 立教大・理・物理

Image analysis of the polar vortices of Venus observed by Akatsuki/LIR

#Temma Sugawa[1)],Makoto Taguchi[1)]
[(1]Department of Physics, College of Science, Rikkyo University,[(2]Department of Physics, College of Science, Rikkyo University

Atmospheric temperature at the cloud tops of Venus around an altitude of 65 km decreases with latitude, but it is known that there are high-temperature regions near the poles and cooler regions around them. The high-temperature regions rotate around the poles, and called as the polar vortices, where zonal wavenumber 0, 1 and 2 shapes of the temperature distribution predominate [Garate-Lopez et al., 2013; Sato et al., 2014]. Previous studies have derived a rotation period of about -2.8 to -3.2 days and about -2.2 to -2.5 days for the northern and southern polar vortices, respectively, but the cause of the difference in the rotation periods of the northern and southern polar vortices is unknown [Schofield et al., 1983; Garate-Lopez et al., 2013]. There are also few observational investigations of the relationship between the atmospheric dynamics in mid- and low-latitudes and the thermal structure of the polar regions. A long-term variation of the polar phenomena has not yet been investigated.

The Venus orbiter Akatsuki has been orbiting around Venus since December 2015. Longwave Infrared Camera (LIR) is one of the cameras onboard Akatsuki, still obtaining images of brightness temperature around the cloud-top altitudes every day as of June 2023. Since Akatsuki is orbiting in an almost equatorial plane, LIR can capture both northern and southern polar vortices from a far distance in the elongated elliptical orbit. In this study, the dynamics of the polar vortices is studied by analyzing LIR data obtained from December 7, 2015 to June 17, 2023. Periods and center positions of the rotation of the polar vortices were derived. The derived values may contain biases due to lack of brightness temperature distributions in the region where LIR cannot observe. The errors in the derivation were evaluated by simulation in which an image data that simulate the brightness temperature distribution obtained by LIR was created from an infrared image data obtained by VEx/VIRTIS and analyzed using the same method. The results were compared with the periods and center positions derived from the full images of the polar vortex. Comparison of the periods and center positions of northern and southern polar vortices and their long-term variation are discussed.

R009-P26
ポスター 2 ：9/25　AM1/AM2 （9:00-12:30）

電波掩蔽法を用いた金星赤道域における熱潮汐波の鉛直構造に関する観測的研究

#安藤　紘基 [1)], 野口　克行 [2)], 今村　剛 [3)], 高木　征弘 [1)], 杉本　憲彦 [4)], 松田　佳久 [5)]
([1] 京都産業大学,[2] 奈良女子大学,[3] 東京大学,[4] 慶應義塾大学,[5] 東京学芸大学

Vertical structure of the thermal tides in the equatorial region shown by Akatsuki radio occultation

#Hiroki Ando[1)],Katsuyuki Noguchi[2)],Takeshi Imamura[3)],Masahiro Takagi[1)],Norihiko Sugimoto[4)],Yoshihisa Matsuda[5)]
([1]Kyoto Sangyo University,[2]Nara Women's University,[3]The University of Tokyo,[4]Keio University,[5]Tokyo Gakugei University

It is thought that the angular momentum transport due to the thermal tides is one of the most likely mechanisms how the Venusian atmospheric super-rotation is generated and maintained. Recently, Akatsuki LIR measurements clarified the horizontal structure of the thermal tides at the cloud top level. Akatsuki UVI measurements quantified the angular momentum transport due to the thermal tides in the latitudinal direction at the cloud top level from the local time distribution of the horizontal wind and indicated that the super-rotation is maintained by the accumulation of the angular momentum due to the thermal tides in the equatorial region. However, the vertical structures of the thermal tides have not been investigated observationally. Thus, it is difficult for us to examine the validity of the theoretical studies about the thermal tides. One of the most useful methods to investigate the vertical propagation characteristics of the thermal tides is radio occultation technique because it enables us to retrieve a vertical temperature profile with high measurement accuracy of ˜0.1 K and high vertical resolution of ˜1 km.

We analyzed the Akatsuki radio occultation data and focused on the vertical structures of the thermal tides in low-latitudes because the orbit of Akatsuki is equatorial one. The number of temperature profiles at the latitudes of 0 – 30 degrees is 45, and the local time-height distribution of the temperature deviation from zonal mean was obtained. And then, we detected zonal wavenumber-1 and -2 components from it. As a result, the phase of the diurnal tide little varies in the vertical direction, implying that the non-propagating mode is dominant. On the other hand, the phase of the semi-diurnal tide tilts toward the earlier local times above (below) the altitudes of 50 – 55 km with increasing (decreasing) altitude. This implies that the semi-diurnal tide propagates upward (downward) direction from these altitudes. In addition, the amplitude of the semi-diurnal tide has a small maximum around 45 km. These features shown by the radio occultation measurements are qualitatively consistent with the Venus GCM. In this presentation, we are going to show the results obtained by the Akatsuki radio occultation measurements and discuss the impacts of the thermal tides on the Venusian atmospheric super-rotation quantitatively.

金星大気スーパーローテーションの生成メカニズムの一つとして、雲層の太陽光加熱により励起される熱潮汐波に伴う角運動量輸送が理論的に有力視されている。従来の熱潮汐波理論によれば、熱潮汐波は太陽の動きと同方向、すなわち東向きの角運動量を雲層からその上下に輸送し、一方で雲層内では角運動量保存則によって大気は西向きに加速されると考えられている。特に、雲層から下向きに伝播する熱潮汐波は、地面摩擦を介した大気と固体部分の角運動量交換に寄与しスーパーローテーションの生成・維持に本質的な役割を果たすと考えられている。

これまで、雲頂から上の熱潮汐波構造については、電波掩蔽観測や赤外分光観測による研究が為されている。近年では、あかつきに搭載された中間赤外線カメラ（LIR）によって、雲頂高度における熱潮汐波の水平構造が明らかになった。また、あかつきの紫外イメージャ（UVI）で得られた雲頂における水平風速の地方時分布から熱潮汐波に伴う南北方向の角運動量輸送量が定量され、雲頂付近のスーパーローテーションは熱潮汐波により低緯度に角運動量が集積されることで維持されている可能性が示された。しかし、雲層から下の高度領域における熱潮汐波の鉛直構造についての観測はなく、熱潮汐波理論の妥当性について検証できていない。本研究では、あかつき電波掩蔽観測のデータを用いて、金星低緯度（0 ☒– 30 ☒）における気温擾乱の地方時-高度分布を導出し、そこから高度ごとに東西波数 1（一日潮）と 2（半日潮）成分をそれぞれ抽出した。その結果、一日潮と半日潮の振幅は同程度であった。また、一日潮は位相の高度変化が小さく、非伝播モードが卓越している様子が見られ、半日潮は高度 50-55km から上（下）の高度領域では高度が上がると（下がると）位相は朝側に傾くことが分かった。これは半日潮が高度 50-55km を境に上下に伝播していることを示すと共に、世界で初めて雲層から下に伝播する熱潮汐波を捉えた可能性がある。さらに、半日潮の低高度側の振幅は高度 45km 付近で極大を持つこともわかった。金星大気大循環モデル AFES-Venus と比較したところ、観測とモデルで熱潮汐波の振幅や位相の分布は定性的に良く整合していた。本発表では、あかつき電波掩蔽観測の結果を示すと共に、観測とモデルの比較から熱潮汐波が金星大気スーパーローテーションに及ぼす影響についても定量的に論ずる。

R009-P27
ポスター 2 ：9/25　AM1/AM2 （9:00-12:30）

電波掩蔽観測データを用いた金星の雲層内対流と大気重力波の統計解析

#杉浦　美優 [1)], 今村　剛 [2)], 安藤　紘基 [3)]
[(1] 東京大学,[(2] 東京大学,[(3] 京産大

Statistical study on the cloud-level convection and the atmospheric gravity wave on Venus

#MIyu Sugiura[1)],Takeshi Imamura[2)],Hiroki Ando[3)]
[(1]The University of Tokyo,[(2]The University of Tokyo,[(3]Kyoto Sangyo University

On Venus at 50-70km altitude, there is a thick cloud layer composed of H_2SO_4 and H_2O. Around the cloud base, the clouds absorb infrared radiation from the lower atmosphere and then the atmosphere is heated. On the other hand, the atmosphere near the cloud top is cooled by the emission of infrared radiation to space. This drives convection in the middle cloud layer. Then, by convection, atmospheric gravity waves are generated in the stable layer. Atmospheric gravity waves propagate vertically and transport momentum between distant altitude regions, so they play important roles in atmospheric dynamics.

In previous studies, the latitudinal and the local-time dependence of the convective layer thickness and the gravity wave activity were suggested. Unlike Earth, observations of Venus Express and Akatsuki radio occultation showed that the convective layer is thicker at higher latitudes (Tellmann et al. 2009; Ando et al. 2020). As the solar heating in the upper cloud layer decrease, convection will be enhanced at high latitudes(Imamura et al. 2014). Similarly, convection is expected to be stronger on the night side than on the dayside. Then, larger amplitude gravity waves are expected to be generated.

In this study, we analyze the Akatsuki and Venus Express radio occultation data by using FSI (Full Spectrum Inversion), which has a higher vertical resolution than GO(Geometrical Optics) and can solve the multiple pass problem, to study statistically the correlation between the convective layer thickness, stability in the stable layer, and amplitude of gravity waves.

金星の高度 50-70km 付近には濃硫酸から成る分厚い雲層が存在する。雲底付近では雲が下層大気からの赤外放射を吸収することで雲層下部が加熱される一方、雲頂付近では宇宙空間への赤外放射によって大気が冷却されるため、高度 50-55km で鉛直対流が生じる。この対流によって励起される大気重力波は鉛直方向に伝播し離れた高度間で運動量を輸送するため、金星の大気大循環を考える上で重要である。

先行研究では、金星大気における対流層の厚さとそれに伴う大気重力波活動の緯度依存性やローカルタイム依存性が示唆されている。金星では地球とは逆に、高緯度ほど対流層が厚くなっていることが Venus Express やあかつきの電波掩蔽観測によって示されている (Tellmann et al. 2009; Ando et al. 2020)。これは、雲頂付近での太陽光加熱が小さくなるので、高緯度で対流が強化されることに起因する考えられている (Imamura et al. 2014)。同様にして、対流は昼側より夜側で強くなると予想されている。その結果、より振幅の大きい大気重力波が励起されるとみられる。

本研究では、Venus Express やあかつきの電波掩蔽観測データを、幾何光学より高い鉛直分解能を実現できる電波ホログラフィーの一種である Full Spectrum Inversion (FSI) 法を用いて解析して高度 60-85km 付近における微細スケールの大気重力波まで抽出する。そして、重力波振幅と対流層の厚さや大気安定度との相関関係について統計的に調べる。